A Thesis for the Degree of Doctor of Philosophy

Control of colloidal stability and bioavailability of lipid nanoparticles for oral delivery of food bioactives

식품수준 생리활성물질의 경구 운반을 위한 지질나노입자의 콜로이드 안정성과 생체이용률 조절

August, 2016

Choongjin Ban

Department of Agricultural Biotechnology

College of Agricultural and Life Sciences

Seoul National University

농학박사학위논문

Control of colloidal stability and bioavailability of lipid nanoparticles for oral delivery of food bioactives

식품수준 생리활성물질의 경구 운반을 위한 지질나노입자의 콜로이드 안정성과 생체이용률 조절

지도교수 최 영 진

이 논문을 박사학위논문으로 제출함
2016 년 8 월

서울대학교 대학원
농생명공학부
반 충 진

반충진의 박사학위논문을 인준함
2016 년 8 월

위 원 장 _____ (인)

부위원장 _____ (인)

위 원 _____ (인)

위 원 _____ (인)

위 원 _____ (인)

Abstract

Lipid carrier system capable of the controlled release for encapsulated bioactive materials has attracted an interest for the bioavailability increase and the targeted delivery of the bioactives in many industrial fields (foods, cosmetics, and pharmaceutics) for a long time. However, there was still no system as a perfect solution having both efficient functionality and economic feasibility. Lipid nanoparticle (LNP) system, including solid lipid nanoparticle and nanostructured lipid carrier, was invented as a novel strategy for substitution of conventional lipid carrier systems such as emulsion and liposome, with a little modification (the use of solid lipids) from the emulsion. LNPs have various merits for using physiological lipids, protecting from the outside stress, enhancing the oral bioavailability, modulating the release profile of core materials, and enabling the bulk production. Accordingly, despite many efforts of food scientists for applying LNPs to foods, it was not adopted in foods yet due to unsolved problems in terms of colloidal or storage stability. In this research, the LNP production process was optimized to enhance the stability, and flavonoid-loaded LNPs were developed to improve the bioaccessibility of the flavonoids based on the optimum process, then the uptake pattern of LNP-incorporated curcumins into the blood was controlled on the basis of modulating the lipid-water interfacial property. In detail, 6 min postsonication during the cooling process after the size reduction step of melted lipid droplets can diffuse self-assembled/solo emulsifiers onto the LNP surface, and the addition of 30 wt % oil into

the solid lipid phase ameliorated the LNP colloidal stability resulting from the crystallinity reduction of solid lipid matrix. Additionally, under the simulated *in vitro* gastrointestinal tract (GIT), bioaccessibility values of quercetin, naringenin, and hesperetin encapsulated in LNPs prepared using 3.5 wt % fully hydrogen canola oil, 1.5 wt % squalene, 1.083 wt % soybean lecithin, and 0.583 wt % Tween 20 were increased 11.71-, 5.03-, 4.76-fold than those of the native-formed flavonoids, respectively. Lastly, because the mimicked GIT hydrolysis of LNPs covered with various PEGylated emulsifiers was controlled by the LNP designs in aspects of the PEG length, the emulsifier concentration, and the lipid type, the plasma residence of curcumin encapsulated in the PEGylated LNPs would be successfully extended or shortened as the designs under the *in vivo* rat model for oral administration. In summary, these results suggest that LNP systems developed in this study can satisfy enough an expectation of manufacturers and customers as a food-grade lipid delivery system. In conclusion, this study could serve as a basis for further research that aims to develop delivery systems for foods and pharmaceutics.

Key words: lipid nanoparticle (LNP), bioactive material, colloidal stability, bioavailability, controlled release

Student Number: 2011-23529

Contents

List of Tables

List of Figures

Chapter I. Literature Review: Lipid Nanoparticles (LNPs) as a Delivery Carrier for Orally Ingested Food Bioactives

I-1. Introduction

Food, which supplies water, energy sources, and nutrients, is one of the most essential things for human being. In this regard, balanced diet of foods is a key factor of human health and well-being. Unfortunately, eating habits of modern people are easy to stray into unbalanced diet of foods, due to overeating specific nutrient and the lack of time. This unbalanced diet has brought many people chronic diseases such as cancers, diabetes, cardiovascular diseases, etc. Thereby, biological activities of many bioactive molecules have naturally attracted a lot of attentions for the possibility to prevent or cure these diseases (1). Needs for foods containing the bioactives have been also increased because of their functionality.

In general, bioactive molecules extracted from plants, microbes, and animals occur at low concentration. Hence, concentration of the bioactive materials should be artificially increased to produce foods fortified in the functionality. However, low bioavailability of the bioactives has been constantly reported despite the increase of the ingested concentration, resulting from their pH, ion, and light sensitivity, low water-solubility, poor permeability into circulatory system, autoxidation and avid metabolism during gastrointestinal tract (GIT) digestion (2). What is worse, because the satisfaction on sensory factors, such as taste, flavor, texture, and appearance,

is also important for the food in an aspect of the preference in addition to the function of foods, the unwanted changes (bad odor and taste; undesirable mouthfeel and appearance) by the increased concentration of bioactives could make consumers unwilling to purchase.

Encapsulation is well known as a strategy to overcome the stability and bioavailability problems, which is frequently used in pharmaceutics and cosmetics (3). Emulsions, liposome, micelle, hydrogel, nanoparticle, etc. are usually utilized as carrier systems to encapsulate drugs or valuable materials (4, 5). These carrier systems can be also used in food industry, but they should be appropriately modified to be adopted in foods. Realistically, since foods are not high value products as compared with drugs and cosmetics, the cost for encapsulating bioactive materials should be reduced by using inexpensive ingredients and low energy cost processes for a reasonable price of food products, of course, organoleptic properties of foods adding the encapsulated bioactives should not be bad. Moreover, encapsulation technology in foods keeps aloof from the use of particular ingredients such as organic solvents. Thereby, many encapsulation technologies are hard to utilize in foods, unlike an emulsion which is a conventional carrier system applied in foods. However, emulsion system for encapsulating bioactives also has problems in terms of the colloidal stability (flocculation, coalescence, Ostwald ripening, and creaming) (6) and the stability of the core materials (oxidation and efflux by

an exchange of materials through the interface) (7, 8). In this regard, nevertheless many food scientists have striven to overcome these problems and develop novel carrier systems, there are not a satisfactory solution yet (9).

Solid lipid nanoparticles (SLNs) were introduced in 1991 represent an alternative carrier system to traditional colloid carriers for pharmaceutics, and were realized by simply changing the liquid lipid (oil) of the emulsions by a solid lipid, which means lipids being solid at room and body temperatures (10, 11). The solid lipid of SLNs can militate to the encapsulation as some advantages, e.g. protection of incorporated materials against chemical degradation and more flexibility in controlling the compound release (12). In 2002, nanostructured lipid carriers (NLCs), which was prepared using the mixture of solid lipid and oil, were introduced to enhance the limited drug loading capacity and storage stability of SLNs (13). Lipid nanoparticles (LNPs), as a concept including SLNs and NLCs, do not only have the strength of emulsion but also a potential to overcome the hurdle of emulsion, due to the use of physiological ingredients and solid lipid matrix. Accordingly, food scientists have paid an attention to the advantages and made an effort to develop LNP system adapted for foods, but the adaptation of LNPs in foods is still incomplete. Therefore, this review provided the insights into general features of LNPs and considerations to apply in foods and described a perspective of LNPs in food industry.

I-2. General Features of Lipid Nanoparticles

I-2-1. Ingredients

Conventional ingredients of LNPs were lipids, emulsifiers, and water. Whereas SLNs were prepared using solid lipids, lipids of NLC were composed of the solid lipids and oils (liquid state lipids at room and body temperature). Whatever solid or liquid, the term of lipid is used in a broader sense, and includes mono-/di-/triacylglycerides, steroids, waxes, etc. All classes of emulsifiers, conventionally used in emulsion system, can be utilized to stabilize LNP system including nonionic/ionic emulsifiers, proteins, etc. An overview of the generally used ingredients is provided as shown in Table I-1. In many cases, the multiple use for lipids and emulsifiers was identified due to its synergetic effects in terms of the colloidal stability of LNPs, the high payload for core materials, and the possibility of controlled drug release (14). Anyway, all ingredients composing LNPs should be physiologically usable materials, which is a clear advantage of LNPs. The choice of the ingredients relies on the purpose of LNPs, i.e. the administration routes (oral, intravascular, epidermal, ocular, pulmonary, etc.).

Table I-1. Lipids, Oils, and Emulsifiers used for Preparation of Lipid Nanoparticles

Ingredients	Lists	Literature
Lipids	Triacylglycerides	
	Trilaurin (Dynasan® 112)	(15−17)
	Trimyristin (Dynasan® 114)	(18−23)
	Tripalmitin (Dynasan® 116)	(18, 24−26)
	Tristearin (Dynasan® 118)	(18, 20)
	Mono- and diacylglycerides	
	Glyceryl monostearate (Imwitor® 900)	(20, 25, 27, 28)
	Glyceryl palmitostearate (Precirol® ATO 5)	(20, 22, 25, 29−32)
	Glyceryl behenate (Compritol® 888 ATO)	(15, 16, 20, 22, 25, 28, 33)
	Mono-, di-, and triacylglycerides mixture	
	Witepsol® H 35	(21, 34)
	Witepsol® W 35	(28, 35)
	Witepsol® E 85	(21, 22, 36)
	Fatty acids	
	Palmitic acid	(22, 30, 37, 38)
	Stearic acid	(22, 30, 37, 39−41)
	Waxes	
	Bee wax	(42, 43)
	Cetyl palmitate (Precifac® ATO)	(25, 34, 44)
	Other lipids	
	para-Acyl calix arenes	(45, 46)
	Monostearate monocitrate diacylglyceride (Acidan N12)	(39)
Oils	Caprylic- and capric-triacylglycerides (Miglyol® 812, Labrafac® CC, Labrafac® lipophile)	(19, 20, 22, 24, 33, 36, 44)
	Castor oil	(25, 33)
	Soybean oil	(22, 23, 25, 47)
	Olive oil	(22, 25)
	Corn oil	(22, 38)
	Oleic acid	(22, 43)
	Squalene	(31, 32, 48)
	α-Tocopherol	(26, 49)
Emulsifiers	Polysorbates (Tween® 20, Tween® 60, Tween® 80)	(19, 20, 28−30, 34, 42)
	Poloxamers (Pluronic® F68, Kolliphor® HS15)	(15, 16, 18, 20, 28, 34, 37)
	Caprylcaproyl polyoxylglycerides (Labrasol®)	(44, 50)
	Polyglyceryl-3-methylglucose distearate (Tego® Care 450)	(36, 44)
	Lauryl polyoxylglycerides (Gelucire® 44/14)	(51, 52)
	Polyacrylic acids (Carbopol® 934P)	(19, 49)
	Sorbitan esters (Span® 40, Span® 60)	(30, 53)
	Soybean or egg lecithin (Lipoid® S75, Lipoid® E80)	(15, 16, 21, 29, 42, 47)
	Hydrogenated soybean phosphatidylcholine	(26, 31, 32)
	Sodium dodecyl sulfate (SDS)	(23, 40)
	Sodium cholate (SC)	(23, 37, 43)
	Polyoxyethylene monostearate	(17, 41)

I-2-2. Production Methods

Methods for LNP preparation are similar to the emulsion preparation. In addition, techniques used in emulsion production can be also applied in LNP production. Table I-2 is an overview of the LNP production techniques including top down and bottom up methods. High pressure homogenization (HPH) is a representative method for LNP preparation. In the HPH, since the fluid with very high velocity is pushed through a narrow gap (a few microns) resulting from the high pressure (100−2000 bar), the size of droplets and particles in the fluid be reduced after the gap passing due to high shear stress and cavitation (12). Advantages of the HPH are known for the possibility of high lipid content process and an ease of scaling up (54), and disadvantage of HPH is high energy consumption. HPH method is divided into hot and cold HPH techniques. Both the hot and cold techniques are initiated as dissolving/dispersing bioactive molecules in the melted lipid. In the hot HPH, followed by the dissolving/dispersing, the size of the melted lipid droplets is reduced with maintaining the temperature above melting temperature (T_m), and is finally solidified by cooling down below the T_m. However in the cold HPH, solidification of lipid phase including the bioactives is performed prior to the size reduction at the temperature below T_m and grinding procedure (50−100 microns) of the solidified lipid is conducted between the solidification and the size reduction. The hot HPH brings out smaller particle

sizes and a narrower size distribution compared to the cold HPH. In contrast, the cold HPH is appropriate for encapsulating temperature sensitive materials rather than the hot HPH.

Sonication method by ultrasound LNPs is also a common process for preparing LNPs and is frequently used in the lab-scale production because of its convenience for installation and handling. Sound energy generated from a sonicator gives the cavitation and shear stress to the lipid droplets. Despite an ease of the installation and handling, this method is difficult to apply in the industrial field, due to the demand of high content of emulsifiers and the possibility of the bioactive degradation by contact with a sonication source.

Membrane contractor has advantages for continuous production of the uniform-sized LNPs, which can influence good quality on colloidal stability of LNPs after production. However, because the quality of LNPs fabricated using this method intensively depends on the membrane condition, the spoilage of membrane, such as blockages, can deteriorate the produced LNP quality. Therefore, membrane handling is very important to produce good LNPs.

Microemulsion technique is based on the dilution of microemulsion. The microemulsion prepared with stirring of the mixture of lipids, emulsifiers, and water at the temperature above the T_m of lipids is dispersed (from 25- to 50-fold) into cold water (2−3°C) under stirring (55). No energy requirement

is an advantage of this technique. However, this technique requires additional filtration procedures, additionally achievable lipid concentration is comparatively low due to the dilution. Meanwhile, electro-spray technique as a method for LNP production utilizes a strong electric field, thereby a lot of energy consumption, moreover, its productivity for LNPs is too low as compared with other methods.

Solvent emulsification/evaporation method is divided into emulsification and evaporation steps. The emulsification step is performed using homogenization of the mixture of the water, the emulsifiers, and the organic phase containing lipids and water-immiscible organic solvents (e.g. cyclohexane), and subsequent evaporation step is conducted under stirring. In the evaporation of organic solvents, lipids is precipitated in the organic phase, then LNP is finally produced. In this regard, LNPs produced using this technique have smaller particle size and narrower size distribution as compared with other producing methods. In addition, another advantage is an avoidance of any thermal stress. On the other hands, the residue of organic solvents can induce toxicological problems, and relatively low achievable lipid content (about 0.5−2.5 wt %) is also a clear disadvantage. Beside, some researches related with the burst release problems of the bioactives loaded in LNPs produced by this method have been reported (56).

Phase inversion was introduced as a method for preparing NLCs (57). The mixture of lipids, emulsifiers, and water is heated and cooled for 3 cycles under stirring, which is diluted with cold water causing the phase inversion of emulsion and the breaking, resulting in NLC. In this technique, because maintaining time at the temperature above T_m is shorter than other melted-emulsification techniques such as hot HPH, sonication, etc., thermo-labile bioactives can be encapsulated in LNPs without the degradation. However, it is cumbersome to apply in industry fields and it cannot assure good stability of LNPs.

Table I-2. Methods used for Preparation of Lipid Nanoparticles

Classification	Lists	Literature
Top down technology	High pressure homogenization (HPH)	(58, 59)
	Sonication	(18, 60)
	Membrane contactor	(61, 62)
	Microemulsion technique	(63, 64)
	Electrospray technique	(65, 66)
Bottom up technology	Solvent emulsification/evaporation	(66, 67)
	Phase inversion	(68, 69)

I-2-3. Sterilization and Secondary Processes after the Production

Filtration, γ-irradiation, and steam treatment are normally used to sterilize LNPs. The filtration sterilization of colloid systems is not applicable to particles over 0.2 μm, which requires high pressure process (12). This method do not induce the changes of LNP characteristics in terms of physicochemical stability and the drug release kinetics. On the other hand, there are some reports that γ-irradiation and heating techniques deteriorate the processed LNPs with regard to LNP aggregation, degradation of core materials, etc. During γ-irradiation, free radicals could be generated in sample system due to the high energy of γ-rays, which may undergo secondary reactions with the incorporated materials or modify the characteristics of LNP matrix. Moreover, this degradation is accelerated in the presence of oxygen in the hydrated LNP samples. Steam treatment is a conventional sterilization technique, which is applied in many various industrial fields. Heat energy from the steam would melt solid particles to liquid droplets and elevate the energy level of LNP dispersion, thereby increase the posibility of coalescence among the molten droplets. What a worse, the elevated temperature by the steam leads to dehydration of the ethylene glycol chains in a PEGylated emulsifier such as poloxamers, Tween, etc., which can eliminate the steric hindrance by the ethylene glycol chains (12). As a result, LNPs would be aggregated and their size would be increased. Therefore, additional actions should be required to overcome this problem. For example, the combinational use of

ionic emulsifier such as lecithin, cholate, and phosphatidyl-choline or the specific formulation of lipid matrix can help this problem overcoming (39, 70).

The produced LNPs as a colloid system in aqueous circumstance are easy to degrade and aggregate due to their hydrolysis and Ostwald ripening. Lyophilization can prevent these problems as a strategy for LNP storage and help LNPs easily transforming and applying as various dosage forms such as powders, pellets, tablets, or capsules. However, the lyophilization may also induce the additional stability problems. During the transformation from dispersion to power by lyophilization, the freezing out effect results in changes of osmolarity and pH. Additionally, during the transformation from powder to dispersion by rehydration, the aggregation among the rehydrated LNPs can be instantaneously occurred because of momentary low water content and high osmotic pressure. In this regard, there are some prerequisites to lyophilize intactly LNPs. First one is the low level lipid content of the LNP dispersion. Generally, LNPs containing the lipid content over 5% should be diluted for successful lyophilization (12). The dilution of LNP dispersion will decrease direct contact of lipid particles and increase sublimation velocities and the specific surface area (71). Second, cryoprotectors can hold the place where prevent the contact among discrete LNPs and also serve as a kind of pseudo hydration shell (72−74). In many cases, trehalose is known as the most effective cryoprotector for LNP lyophilization (75, 76). In addition, the injection time of cryoprotectors is also important, e.g. prior to

homogenization. Third, appropriate freezing rate is one of the prerequisites for good LNP lyophilization (16, 76).

Spray drying is scarcely utilized to make aqueous LNPs to powdered LNPs and is economically superior to the lyophilization. Despite its merit in terms of the economic feasibility, the hurdle related to the aggregation and the partial melting of LNPs could be inherent due to the use of high temperatures and shear forces. The use of high melting lipids, the addition of carbohydrates, and low lipid content can preserve the particle size of LNPs during spray drying (77).

I-2-4. General Characteristics

I-2-4-1. Colloidal Stability

Mechanisms for problems with regard to the stability of colloid systems are well known as flocculation, coalescence, and Ostwald ripening, which can be problems themselves and also induce subsequent problems such as creaming, sedimentation, or gelation. These mechanisms and problems can be also applied in the hydrated LNP systems with a little difference. Colloidal stability of LNPs depends on the characteristics of the dispersed phase (i.e. lipids), the interface (i.e. emulsifiers), and the continuous phase (i.e. water). As previously mentioned in the ingredient section, the lipid phase of LNPs could be composed of solid state lipids such as mono-/di-/triacylglycerides, fatty acids, waxes, and other lipids. Among these solid lipids, some lipids such as triacylglycerides and fatty acids have their specific polymorphic forms after the crystallization. Because almost techniques for LNP production have a lipid melting process, the cooling process following the melting could favor the crystallization of the melted triacylglycerides and fatty acids. Generally, it is known that the α-polymorphic form of the lipids could not induce the shape changes of LNPs, but the β-polymorphic form change the LNP shape from the sphere to the rod or angular shapes (Figure I-1a) (78). This shape transition makes the bare lipid surfaces called the hydrophobic patches. In an aqueous circumstance, LNPs having the hydrophobic patches naturally aggregate each other to hide the patches exposed to the water, which cause the particle size increase, creaming, or sedimentation of the LNPs.

In a worse case, gelation phenomenon is observed due to the networks among LNPs by the hydrophobic interaction through the patches. In addition, during the cooling process, some lipid crystals formed in a melted lipid droplet can penetrate the interface of the melted droplet and pierce other droplets, which results in the partial coalescence among the LNPs (79). There are some strategies to prevent the deterioration for the colloidal stability of LNPs by the lipid crystallization, which are the utilization of amorphous solid lipids and the mixing among dissimilar lipids such as the mixture of solid lipids and oils.

Characteristics of the interface between lipid phase and aqueous phase critically affect the colloidal stability of LNPs. Accordingly, emulsifiers positioned at the interface of LNPs dominate properties of the interface and influence the stability. The hydrophobic part of emulsifier as an amphiphilic substance covers the lipid surface of LNPs and the hydrophilic part is hydrated in the water environment, which results in the hydration of the emulsified lipid particles. While emulsifiers prevent the coalescence and Oswald ripening of emulsion system and also reduce the surface tension of oil droplets, in the LNP system, emulsifiers at the interface just hydrate the LNP and prevent the collision among LNPs because of the disappeared surface tension after the solidification during the production. If emulsifiers are absent or wispy on the LNP interface, the collision among LNPs directly means the LNP aggregation. In contrast, the high surface load of emulsifiers could assure good stability of LNPs (Figure I-1b). Increase of molecular weight of the hydrophilic part also gives a good

stability to LNPs due to the steric hindrance effect by the emulsifier. Moreover, ionic emulsifiers on the LNP interface make the repulsion of the identically charged lipid particles due to their electrostatic repulsion action. Meanwhile, physicochemical properties of continuous phase (i.e. water) such as ion concentration, pH, and protein concentration could also trigger the LNP aggregation (Figure I-1c). Divalent metal ions and proteins in the water could intermediate between lipid particles and induce the aggregation of the charged LNPs. Since the ionic emulsifiers have an inherent isoelectric point, their charges could disappear by changing the pH in LNP system resulting in the LNP aggregation. Consequently, the lipid/emulsifier type selection, their contents, and the ion/proton concentration of water phase could determine whether to prevent or accelerate the deterioration of LNPs in aspects of the colloidal stability.

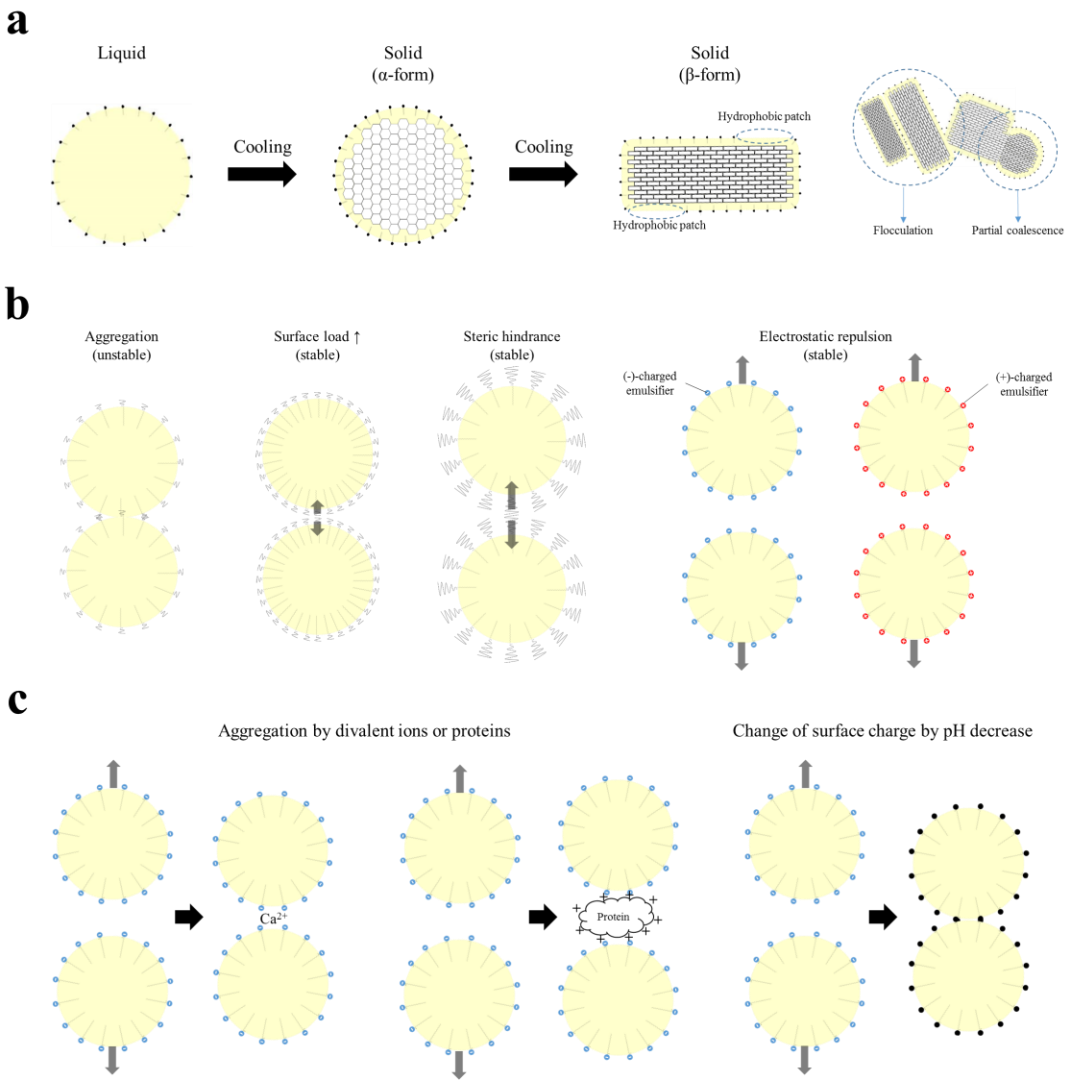

Figure I-1. Pictorial representations of mechanisms for deterioration and enhancement in terms of colloidal stability of the lipid nanoparticles (LNPs). (a) Transformation of LNP polymorphism and shape induced during the cooling process and aggregation among unstable LNPs; (b) enhancement of LNP colloidal stability by using more emulsifiers, high molecular weight emulsifiers, and ionic emulsifiers; and (c) LNP aggregation induced by divalent metal ion, protein, and pH change.

I-2-4-2. Loading and Release of Bioactive Materials

LNP is a simply modified system from emulsions, replacing liquid lipids (oils) of the emulsion with solid lipids. This slight modification can give distinctive characteristics to LNPs and some advantages to load core materials in the solid lipid matrix, which is described as shown in the pictorial representation of Figure I-2a. Core materials incorporated in emulsion and liposome have the high degree of freedom due to the fluidity of oil and empty space, respectively. Therefore, the incorporated materials can migrate close to the interface between lipid and water phases, be influenced by light/radicals/ions in the water, and even run out of the emulsion or liposome through the interface. Moreover, the radicals and ions in the water can also come into the interior space of emulsion or liposome, then degrade the incorporated materials and lipids. On the other hand, the solid lipid matrix in LNPs restricts the activity of core materials and also plays as a barrier against the influx from the water, which can symbolize the protectability of LNP system (80).

Solidified triacylglycerides and fatty acids crystallize to α-, β´-, or β-forms and triacylglycerides/fatty acids in SLN matrix favor the transform to the β-form with passing time because the β-form is the most stable in terms of energy. Since the β-formed lipids aggregate together and build compact structures with perfect crystals, there is little room for the incorporated materials in solid lipid matrix (Figure I-2b). What a worse, the β-formed lipids during storage expulse more and more the incorporated materials from the matrix (21). Thus, mixture of various solid lipids has

been used to improve the payload for a number of core materials and the storage stability resulting from the imperfect structures assembled with various crystals of the various solid lipids (14). Furthermore, the NLC prepared using solid lipids and oils was invented to enhance more the payload and the storage stability. It has been known that there are three types of NLCs, the imperfect type (like SLNs produced using the solid lipid mixture), the amorphous type, and the multiple (oil in fat in water, O/F/W) type (13, 81). Each different type among the three of NLCs can be obtained to control the producing way and the composition of the lipid mixture. Concept of NLCs in the type I is similar to that of the imperfect structured SLNs using the lipid blend. Lipid matrix of NLCs in the type II is solid state but not crystalline, i.e. amorphous stated solid lipid. This can be obtained by blending especial lipids (hydroxyoctacosanyl-hydroxystearate and isopropylmyristate). The characters of the solid state and the amorphous state of lipid matrix was verified by NMR and DSC analyses (82, 83). Lipid phase of NLCs in the type III is divided to solid lipid (fat) and oil nano-compartment phases. In the high melting production of NLCs, a use of increased oil content until a certain level results in the type I or II NLC, but the use over the certain level in the oil content can generate the oil parts immiscible in solid matrix. Because hydrophobic bioactives are generally more soluble in the oil than in solid lipids, the most of the bioactives encapsulated in the type III NLCs could exist in the oil compartments, which affords the best payload for the bioactives among the three types. However, too much use of oils and high shear applied during the cooling process can

separate oil droplets from solid matrix of the NLCs, and even induce the partial coalescence between the droplets and the NLCs (79). Therefore, adequate choices of formulation and processing are required to produce successfully the type III NLC.

LNP system has an advantage for flexibility in controlling the release of incorporated compounds. However, this advantage could be disappear due to high melting production. During the heating process for the high melting production, more bioactive materials loaded in LNPs can solubilize into water phase through the interface due to the increased temperature of the water (Figure I-2c). Further cooling process induces the supersaturation of the materials in the water, which results in the partition back of the materials into lipid phase. Furthermore, some bioactives in the lipid core firstly solidified during the cooling migrate to the outer lipid layer not yet solidified, because of superior capacity of liquid lipids for solubilizing the bioactives. As a result, the bioactive enriched shell is unintentionally built in the outer layer of LNP, which cause the burst release problem of the incorporated bioactives. The burst release problem is getting worse by increasing the heating temperature and the emulsifier concentration (i.e. reducing the size of LNPs). Therefore, using the low temperature and the adequate emulsifier content for LNP production is recommended to improve this burst release problem (81).

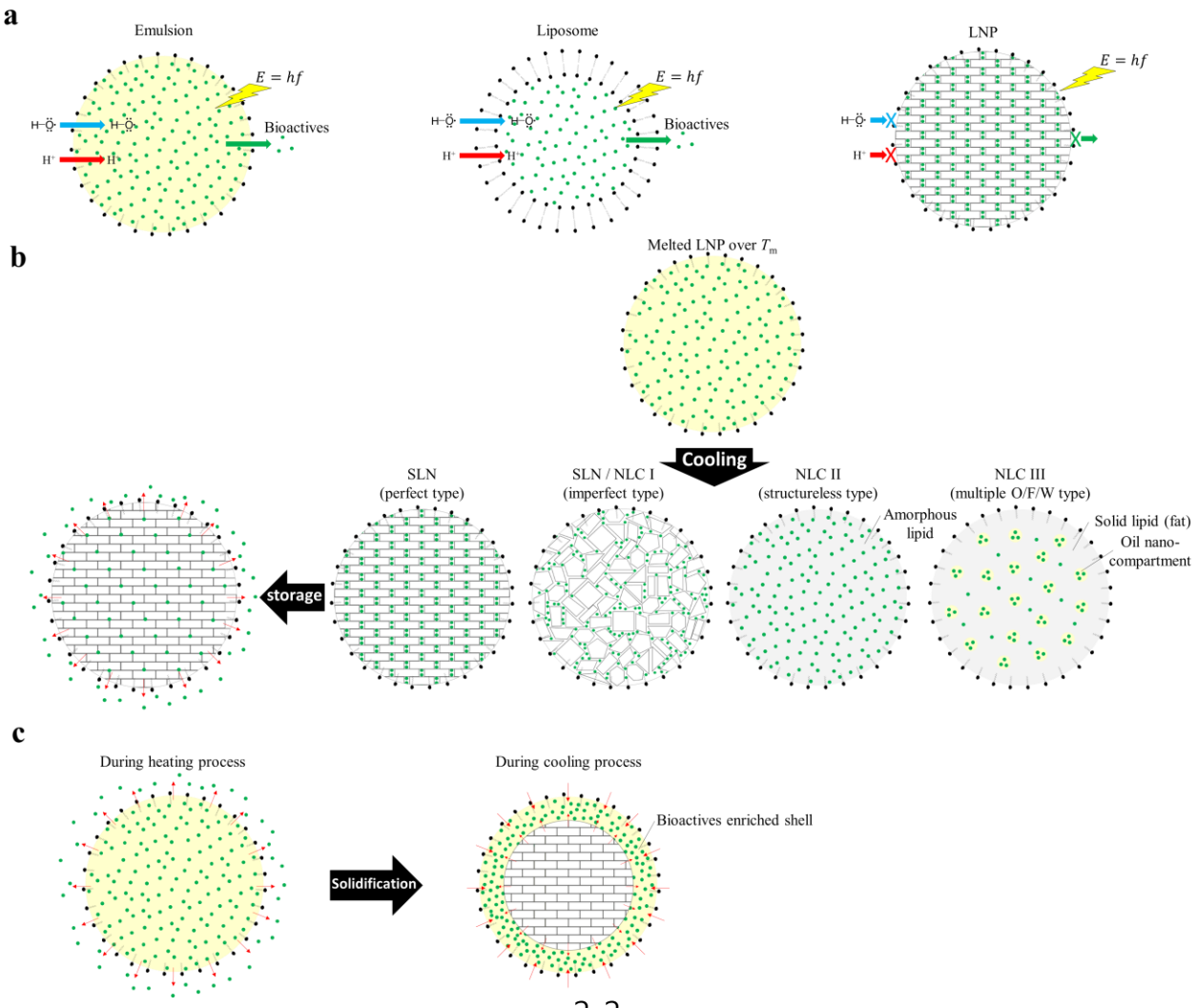
a
Emulsion
$E = hf$
Bioactives
Liposome
$E = hf$
Bioactives
LNP
$E = hf$
b
Melted LNP over T_m
Cooling
SLN
(perfect type)
SLN / NLC I
(imperfect type)
NLC II
(structureless type)
NLC III
(multiple O/F/W type)
Amorphous lipid
Solid lipid (fat)
Oil nano-compartment
storage
c
During heating process
Solidification
During cooling process
Bioactives enriched shell

Figure I-2. Pictorial illustrations for (a) the protectability of the lipid nanoparticle (LNP), (b) types of the solid lipid nanoparticle (SLN) and the nanostructured lipid carrier (NLC), and (c) reason of the LNP burst release problem.

I-2-4-3. Toxicity

LNP system is made from physiological materials which is degradable in the body. In this regard, administered or injected LNPs are well tolerable in living systems. Although the safety regarding toxicity of emulsifiers should be considered as ever, this issue is also applied in other carrier systems such as emulsions and liposomes. In an assumption of the safety of emulsifiers used for LNP production, there would be no problem for oral/transdermal administrations and intramuscular/ subcutaneous injections of LNPs. However in an intravenous injection of LNPs, the increase of LNP size, i.e. the aggregation and gelation, or the presence of large-sized particles can bring out big problems, because diameter of fine capillaries in the body is ~9 μm. The injection of LNPs containing the large-sized particles over the capillary diameter or the aggregation/gelation in the capillaries will be a danger of capillary blockage, which could even result in death by fat embolism (12). Therefore, the particle size and the colloidal stability should be carefully dealt in the intravenous injection of LNPs. On the other hands, except the possibility of the dangerousness regarding the particle size, it has been reported that LNP system is less toxic than other carriers such as polystyrene or various polymeric nanoparticles (84, 85). As a results, the LNP system can be regarded as a low toxic carrier on a par with the emulsions at least.

I-2-5. Applications and Administration Routes

Emulsion system is universally utilized for oral administration for foods and pharmaceutics, parenteral/rectal/nasal/pulmonary/ocular administrations for pharmaceutics, and transdermal administration for pharmaceutics and cosmetics. Likewise, LNP system can be also used in food, pharmaceutical, and cosmetic fields through various administration routes under the use of excipients approved by the regulatory authorities. At the beginning, LNP system was developed for targeting the oral and parenteral purposes and almost research activities for LNP development was focusing on the administrations for pharmaceutical uses (81). Ironically, a fist product (Nanobase®, Yamanouchi) has been introduced as a topically applied moisturizer in the cosmetic field to the Polish market (86), which may be attributed to an easiness of applying LNPs in creams or gels and a difficultness of certifying the safety of LNPs in terms of the oral and parenteral administrations. However, because LNP system has an indisputable merit as a bioactive carrier in an industrial field, many products using the LNP have been developed and released in pharmaceutical and cosmetic markets up to date (87, 88). On the other hands, so far as known, there is no LNP-using product launched in food industry despite the efforts of many food scientists.

Orally administered LNPs undergo various stress by enzymes, changes of pH and ionic strength, proteins, and biological surfactants in GIT. In particular, because physiological lipids composing the LNPs are degradable by lipases, controlling the lipolysis of LNPs by lipases is the most important point to increase the amount of the

uptake of incorporated bioactives and prolong the remaining time of absorbed bioactives in the body. LNPs ingested as traditional dosage forms (tablets, capsules, powders, solutions, and pellets) are exposed to the mouth environment for a little while at first. Lingual lipase in the mouth can hydrolyze the LNP, nonetheless, the LNPs would not be nearly influenced by the lipase due to the shortness of remaining time in the mouth. In stomach, acidity and high ionic strength make a favorable condition for the LNP aggregation and gastric lipase can degrade the LNPs. In small intestine as an organ absorbing the ingested LNPs, pancreatic lipase can finally hydrolyze the LNPs with helping of colipase, bile salts, and phospholipids, and the residues of hydrolyzed LNPs are incorporated in the micelles mixed with bile salts and phospholipids. Next, the mixed micelles containing the bioactives are absorbed into enterocytes, and fatty acids and monoglycerides loaded in the micelles are reassembled as tryglycerides in the enterocyte, transformed to chylomicrons with apoproteins, and then transported into the lacteal (12, 89, 90). Some strategies for accelerating and preventing the lipase access to the LNP interface have been already introduced, which are the use of cholic acids and nonionic emulsifiers, respectively (91). Using these strategies, many researchers has been reported the *in vivo* results of the increased bioavailability and prolonged plasma levels of orally administered bioactives contained in LNPs (92, 93).

Purposes of LNPs for parenteral administration are the increase of mean residence time of encapsulated bioactives in blood stream and the delivery targeting

specific organs. Achievement of these goals depends on the stealth function of LNPs covered by PEGylated emulsifiers. As generally known, polyethylene glycol (PEG) molecules over 2 kDa are not detected by immune system in the body and eliminated from the body for a long time (94). In this regard, the PEGylated LNPs can elevate the mean residence time of the bioactives encapsulated in the LNPs. Besides, the PEGylated emulsifiers combined with antibodies or aptamers binding the specific antigens on the surface of target organ give a target selectivity to LNPs (95). Accordingly, many successful examples in parenteral administration of LNPs have been suggested to deliver the bioactives (96, 97).

LNPs can be fabricated as very high concentrated system using the high melting homogenization technique and there is no need for further steps to form cream or gel in transdermal application. This merit of LNPs has attracted an attention of pharmaceutical and cosmetic companies. Moreover, LNPs have outstanding UV reflecting properties due to their solid state and a clear advantage over existing UV protective system (UV blockers or TiO_2) in aspects of skin penetration and potential of skin toxicity due to the use of physiological ingredients (12), plus excellent moisturizing effect due to their nanometer size (81). For these reasons, many products using the LNP system have been released to cosmetic market. Besides, good ability of the LNP as a capsule can offer the possibility to apply in the strategy for encapsulating perfumes.

I-3. Consideration for Applying Lipid Nanoparticles to Food Industry

I-3-1. Regulation for Using Ingredients

In general, LNPs for peroral administration are produce from excipients accepted by the regulatory authorities−e.g. excipients with a GRAS (generally recognized as safe) status by FDA (Food and Drug Administration)−or ingredients already used in products on the food and pharmaceutical markets (87). The restriction for using food-grade excipients is commonly less cumbersome compared to the use of excipients for pharmaceutics. In an assumption of using cacao butter as a solid lipid for LNP production, it is directly acceptable for foods but not for pharmaceutics. Whereas the safety for utilizing the excipient within a certain concentration should be prove by using toxicity data in the latter case, there is no need to convince the safety of the cacao butter in foods. Of course, there are also restrictions for using the maximum concentration of some excipients in foods such as polysorbates, polyethylene glycols, etc. Nonetheless, all bioactives, lipids, emulsifiers, and polymeric stabilizers used in food industry can be exploited to prepare food-grade LNP system. Another crucial point for producing the LNPs in food industry is the qualification of production lines, which include both production lines for the materials used in LNP preparation and the LNP preparation. Fortunately, LNP production technologies are mostly similar to the technologies for emulsion production using the lines already validated in food industry. Table I-3 is an overview of researches for

LNP system encapsulating food-grade bioactive materials, which convince a superior merits of LNP system for the food-grade bioactives. Therefore, it seems that a priority for the LNP production in food industry is no corruption in taste, flavor, and texture rather than the regulations relating excipients and production lines or the confidence relating the superiority of LNPs in foods.

Table I-3. Food-Grade Bioactive Molecules Encapsulated in Lipid Nano-particles

Classification	Lists	Literature
Carotenoids	Astaxanthin	(98, 99)
	β-Carotene	(38, 100)
	Lutein	(30, 101)
	Lycopene	(102)
	all-trans Retinoic acid	(103, 104)
Vitamin C	Ascorbyl palmitate	(105, 106)
Vitamin E	α-Tocopherol	(26, 107)
Vitamin K_1	Phylloquinone	(108)
Flavonoids	Daidzein	(109, 110)
	Genistein	(111, 112)
	Hesperetin	(89, 113)
	Luteolin	(114, 115)
	Myricetin	(116)
	Naringenin	(89)
	Quercetin	(117, 118)
Hormones	Melatonin	(119)
	Progesterone	(120, 121)
Etc.	Resveratrol	(93, 122)
	Chlorogenic acid	(123)
	Coenzyme Q10	(35, 124)
	Curcumin	(111, 125)
	ω-3 Fatty acids	(101, 126)
	Ferulic acid	(107, 127)
	Rosmarinic acid	(128)

I-3-2. Colloidal Stability in Food System

Foods are composed of various materials including water, salts, carbohydrates, lipids, proteins, etc. and their pH spectrum is broad, which influence the colloidal stability of LNPs contained in foods. As previously shown in Figure I-1c, salts, proteins, and pH changes can promote the aggregation of LNPs in some cases. Therefore, conditions of target foods, which want to use the LNP system, should be known prior to LNP fabrication. For instance, when the target food has high ionic strength and pH 5 conditions, single use of ionic emulsifiers such as lecithin and casein could be not good at colloidal stability of the LNPs, because isoelectric points of whey protein isolate and casein are generally known as pH 5.0 (129) and 4.6 (130), respectively. If producers want to use these emulsifiers at any cost, they should utilize the emulsifier mixture containing the ionic emulsifiers and specific nonionic emulsifiers in a proper ratio, in order to give a stable state to the LNPs in the target foods by a steric hindrance. In general, LNPs emulsified by nonionic emulsifiers over a certain molecular weight are not influenced by surrounding environment such as ionic strength and pH condition, and the surface load of the emulsifiers on LNPs also affects the colloidal stability. As a result, food producer should reasonably choose the type, ratio, and concentration of emulsifiers in terms of the colloidal stability of the LNP system.

I-3-3. Delivery Target of Bioactive Materials among Digestive System

Ingested LNPs containing bioactive materials have no choice but to undergo digestion process through digestive system including mouth, stomach, and small intestine. For oral administration, a unique route to absorb the LNP-encapsulated bioactives into the blood is the small intestine. Therefore, if LNP system is designed to deliver the loaded bioactive compounds into enterocytes and then the blood, the LNPs should mainly release the compounds in small intestinal circumstance. This release can be achieved by using emulsifiers to prevent the lipid degradation from lingual/gastric lipases and by using lipids to be well absorbed as mixed micelles resulting from the action of pancreatic lipases, bile salts, and phospholipids, as discussed in the administration route. Furthermore, if purpose of LNP design is just a simple increase of bioavailability of the bioactives, a strategy for blocking LNP aggregation in stomach would be not required no more. In contrast, for controllable releasing the bioactives, the strategy is essential because LNP interfacial condition right after an entrance into small intestine should be expectable. At least, the LNP aggregation in the stomach should be imagined by using *in vitro* data. In a different case, i.e. in other target of the bioactive such as mouth or stomach, lipid matrix and interface of LNPs should be planned to be degraded in a condition of mouth (body temperature, neutral pH, amylases, and lingual lipases) or stomach (acidic pH, high ionic strength, pepsins, and gastric lipases). Consequently, the type, ratio, and

concentration of LNP ingredients should be concerned about what the target organ of bioactive materials encapsulated in LNPs is.

I-3-4. Choice of the Production Methods

Solvent emulsification/evaporation and phase inversion for LNP production are reluctant techniques in food industry because of their organic solvent using. Microemulsion and electrospray methods are not suitable to fulfill the scale up LNPs production due to the limitation of their manufacturing output. Sonication method has a problem of the bioactive degradation by contact with a sonication source. LNP production using membrane contractor is difficult of real-time monitoring and managing the membrane condition. On the other hands, HPH method is easy to scale up and is already used to fabricate emulsion system in food industry. In addition, HPH technique is capable of producing LNPs at high lipid content without deterioration like a size increase. Therefore, the HPH could be the most proper to apply in industrial field production for foods. After the production using the HPH, LNP can be utilized as intact or transformed into the dispersion by diluting, the gel by concentrating, and the powder/pellet by drying, according to the purpose of usage.

I-3-5. Storage Stability

For successful storage of LNPs, the powdered form (i.e. lyophilized or spray-dried form) of LNPs is the most suitable but it is not only one for good storage. It was reported that highly concentrated condition can maintain the storage stability of LNP suspension for 180 days without the increase of particle size (81). As observed in Figure I-3a, LNPs using low lipid content freely diffuse, collide each other, and may aggregate with collided particles, whereas highly concentrated LNPs are easily unable to move and just border each other through the emulsifier film between the particles. After diluting the stored LNPs, while the highly concentrated LNPs are intactly redispersed into the water, the low concentrated one has the increased particle size as compared with that before the storage. Therefore, LNPs should be powdered or high concentrated for successful storage. Since too high concentration of lipid phase induces the increase of particle size of LNPs even in the production using HPH technique, a strategy for LNP production in the highly concentrated condition is required (81), which is presented as observed in Figure I-3b. Additional lipid phase including surfactants is put into the firstly prepared LNP system and the lipid-added LNP system is processed again using HPH technique. The highly concentrated LNP system can be finally obtained by repetition of this processing. Meanwhile, blocking the light and maintaining the temperature below crystallization temperature of lipid matrix are also important for LNP storage.

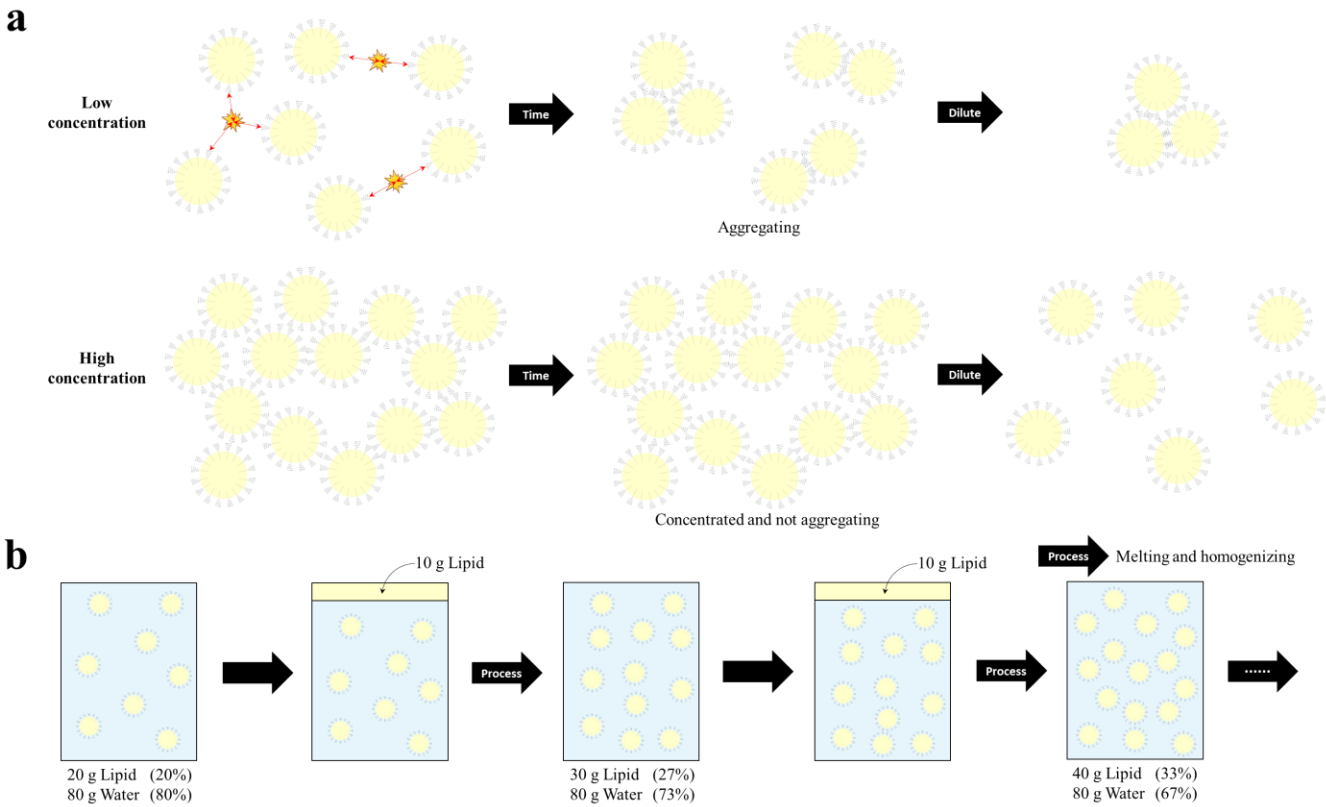

Figure I-3. (a) Stabilization effect in highly concentrated lipid nanoparticle (LNP) system and (b) scheme for the process of highly concentrated LNPs.

I-3-6. Economic Feasibility

In fact, foods are not high value product as compared with pharmaceutics and cosmetics. For this reason, ingredient and energy costs for LNP production should be cut down as much as possible. Fortunately, LNPs can be prepared using various excipients including all of food-grade bioactives, lipids, and emulsifiers, e.g. curcumin as a food additive, various hydrogenated oils, and proteins such as β-lactoglobulin and casein. Because LNP system is little modified from emulsion system (replacement of oils with solid lipids), the LNP is economically feasible to be adapted in food industry like as the emulsion is traditionally utilized. In addition, HPH and microfluidization used as the industrial scale techniques for producing LNPs have been widely applied in food industry. Thereby, so far as mentioned earlier, it appears that the LNP system can be utilized as a substitute of emulsion system in food industrial fields.

I-4. Summary and Perspectives

LNPs, including SLN and NLC, as a carrier system use the solid state lipids as a lipid phase, which are simply modified from the emulsion using the oils as a lipid phase. Since the development, LNPs have been utilized as a substitute of conventional carrier systems (emulsion and liposome) in pharmaceutics and cosmetics, due to their superior protectability and controllability for incorporated bioactive materials. In addition, LNPs could be nontoxic in the body due to their use of physiological ingredients. Despite many problems relating the colloidal stability and the bioactive loading of LNPs, these have been improved by the efforts of many researchers. LNPs for oral administration exploit the strategy to enhance the bioavailability of the encapsulated bioactives by using the enterocyte absorption of the mixed micelles containing the bioactive in small intestinal environment, which are now generally used for new improved delivery of oral dosage form. Many food scientists have striven the various food-grade bioactive materials-loaded LNPs to apply into food system, as far as known, but there is no product for foods up to now. Fortunately, in the food industrial field, there are a lot of food-grade excipients (solid lipids, oils, and emulsifiers) with a GRAS status and the validated production lines to prepare the LNP system including sterilization and storage as well. Therefore, producers wanting to use the LNPs in the food industrial field have only to choose and design the type, ratio, and concentration of solid lipids, oils, and emulsifiers under considering the purpose

of LNP usage with regard to target foods, target systems (e.g. mouth, stomach, intestine, and circulatory system), organoleptic properties, and economic feasibility. If the choice and design for LNP production are reasonable, we can see the products using LNP system in food markets soon.

I-5. References

(1) Kris-Etherton, P. M.; Hecker, K. D.; Bonanome, A.; Coval, S. M.; Binkoski, A. E.; Hilpert, K. F.; Griel, A. E.; Etherton, T. D. Bioactive compounds in foods: their role in the prevention of cardiovascular disease and cancer. *Am. J. Med.* **2002,** *113*, 71-88.

(2) Manach, C.; Scalbert, A.; Morand, C.; Rémésy, C.; Jiménez, L. Polyphenols: food sources and bioavailability. *Am. J. Clin. Nutr.* **2004,** *79*, 727-747.

(3) Tamjidi, F.; Shahedi, M.; Varshosaz, J.; Nasirpour, A. Nanostructured lipid carriers (NLC): A potential delivery system for bioactive food molecules. *Innov. Food Sci. Emerg. Technol.* **2013,** *19*, 29-43.

(4) Mishra, B.; Patel, B. B.; Tiwari, S. Colloidal nanocarriers: a review on formulation technology, types and applications toward targeted drug delivery. *Nanomed.-Nanotechnol. Biol. Med.* **2010,** *6*, 9-24.

(5) Soussan, E.; Cassel, S.; Blanzat, M.; Rico-Lattes, I. Drug delivery by soft matter: matrix and vesicular carriers. *Angew. Chem.-Int. Edit.* **2009,** *48*, 274-288.

(6) Taylor, P. Ostwald ripening in emulsions. *Adv. Colloid Interface Sci.* **1998,** *75*, 107-163.

(7) Cercaci, L.; Rodriguez-Estrada, M. T.; Lercker, G.; Decker, E. A. Phytosterol oxidation in oil-in-water emulsions and bulk oil. *Food Chem.* **2007,** *102*, 161-167.

(8) Decker, E. A. Phenolics: prooxidants or antioxidants? *Nutr. Rev.* **1997,** *55*, 396-398.

(9) Aditya, N. P.; Ko, S. Solid lipid nanoparticles (SLNs): delivery vehicles for food bioactives. *RSC Adv.* **2015,** *5*, 30902-30911.

(10) Lucks, J. S.; Müller, R. H.; Konig, B. Solid lipid nanoparticles (SLN)-an alternative parenteral drug carrier system. *Eur. J. Pharm. Biopharm.* **1992,** *38*, 33S.

(11) Schwarz, C.; Mehnert, W.; Lucks, J. S.; Müller, R. H. Solid lipid nanoparticles (SLN) for controlled drug delivery. I. Production, characterization and sterilization. *J. Control. Release* **1994,** *30*, 83-96.

(12) Mehnert, W.; Mäder, K. Solid lipid nanoparticles: production, characterization and applications. *Adv. Drug Deliv. Rev.* **2001,** *47*, 165-196.

(13) Müller, R. H.; Radtke, M.; Wissing, S. A. Nanostructured lipid matrices for improved microencapsulation of drugs. *Int. J. Pharm.* **2002,** *242*, 121-128.

(14) Müller, R. H.; Mäder, K.; Gohla, S. Solid lipid nanoparticles (SLN) for controlled drug delivery–a review of the state of the art. *Eur. J. Pharm. Biopharm.* **2000,** *50*, 161-177.

(15) zur Mühlen, A.; Schwarz, C.; Mehnert, W. Solid lipid nanoparticles (SLN) for controlled drug delivery–drug release and release mechanism. *Eur. J. Pharm. Biopharm.* **1998,** *45*, 149-155.

(16) Schwarz, C.; Mehnert, W. Freeze-drying of drug-free and drug-loaded solid lipid nanoparticles (SLN). *Int. J. Pharm.* **1997,** *157*, 171-179.

(17) Su, Z.; Niu, J.; Xiao, Y.; Ping, Q.; Sun, M.; Huang, A.; You, W.; Sang, X.; Yuan, D. Effect of octreotide–polyethylene glycol (100) monostearate modification on the pharmacokinetics and cellular uptake of nanostructured lipid carrier loaded with hydroxycamptothecine. *Mol. Pharm.* **2011,** *8*, 1641-1651.

(18) Venkateswarlu, V.; Manjunath, K. Preparation, characterization and *in vitro* release kinetics of clozapine solid lipid nanoparticles. *J. Control. Release* **2004,** *95*, 627-638.

(19) Bhaskar, K.; Anbu, J.; Ravichandiran, V.; Venkateswarlu, V.; Rao, Y. M. Lipid nanoparticles for transdermal delivery of flurbiprofen: formulation, *in vitro*, *ex vivo* and *in vivo* studies. *Lipids Health Dis.* **2009,** *8*, 1-15.

(20) Das, S.; Ng, W. K.; Tan, R. B. H. Are nanostructured lipid carriers (NLCs) better than solid lipid nanoparticles (SLNs): development, characterizations and comparative evaluations of clotrimazole-loaded SLNs and NLCs? *Eur. J. Pharm. Sci.* **2012,** *47*, 139-151.

(21) Westesen, K.; Bunjes, H.; Koch, M. H. J. Physicochemical characterization of lipid nanoparticles and evaluation of their drug loading capacity and sustained release potential. *J. Control. Release* **1997,** *48*, 223-236.

(22) Pardeike, J.; Weber, S.; Haber, T.; Wagner, J.; Zarfl, H. P.; Plank, H.; Zimmer, A. Development of an itraconazole-loaded nanostructured lipid carrier (NLC) formulation for pulmonary application. *Int. J. Pharm.* **2011,** *419*, 329-338.

(23) Schöler, N.; Olbrich, C.; Tabatt, K.; Müller, R. H.; Hahn, H.; Liesenfeld, O. Surfactant, but not the size of solid lipid nanoparticles (SLN) influences viability and cytokine production of macrophages. *Int. J. Pharm.* **2001,** *221*, 57-67.

(24) Souto, E. B.; Wissing, S. A.; Barbosa, C. M.; Müller, R. H. Development of a controlled release formulation based on SLN and NLC for topical clotrimazole delivery. *Int. J. Pharm.* **2004,** *278*, 71-77.

(25) González-Mira, E.; Egea, M. A.; Garcia, M. L.; Souto, E. B. Design and ocular tolerance of flurbiprofen loaded ultrasound-engineered NLC. *Colloid Surf. B-Biointerfaces* **2010,** *81*, 412-421.

(26) Tsai, M.; Wu, P.; Huang, Y.; Chang, J.; Lin, C.; Tsai, Y.; Fang, J. Baicalein loaded in tocol nanostructured lipid carriers (tocol NLCs) for enhanced stability and brain targeting. *Int. J. Pharm.* **2012,** *423*, 461-470.

(27) Müller, R. H.; Runge, S.; Ravelli, V.; Mehnert, W.; Thünemann, A. F.; Souto, E. B. Oral bioavailability of cyclosporine: solid lipid nanoparticles (SLN®) versus drug nanocrystals. *Int. J. Pharm.* **2006,** *317*, 82-89.

(28) Abdelbary, G.; Fahmy, R. H. Diazepam-loaded solid lipid nanoparticles: design and characterization. *AAPS PharmSciTech* **2009,** *10*, 211-219.

(29) Liu, J.; Hu, W.; Chen, H.; Ni, Q.; Xu, H.; Yang, X. Isotretinoin-loaded solid lipid nanoparticles with skin targeting for topical delivery. *Int. J. Pharm.* **2007,** *328*, 191-195.

(30) Liu, C.; Wu, C. Optimization of nanostructured lipid carriers for lutein delivery. *Colloid Surf. A-Physicochem. Eng. Asp.* **2010,** *353*, 149-156.

(31) Fang, J.; Fang, C.; Liu, C.; Su, Y. Lipid nanoparticles as vehicles for topical psoralen delivery: solid lipid nanoparticles (SLN) versus nanostructured lipid carriers (NLC). *Eur. J. Pharm. Biopharm.* **2008,** *70*, 633-640.

(32) Chen, C.; Tsai, T.; Huang, Z.; Fang, J. Effects of lipophilic emulsifiers on the oral administration of lovastatin from nanostructured lipid carriers: physicochemical characterization and pharmacokinetics. *Eur. J. Pharm. Biopharm.* **2010,** *74*, 474-482.

(33) González-Mira, E.; Nikolić, S.; Garcia, M. L.; Egea, M. A.; Souto, E. B.; Calpena, A. C. Potential use of nanostructured lipid carriers for topical delivery of flurbiprofen. *J. Pharm. Sci.* **2011,** *100*, 242-251.

(34) Schubert, M. A.; Müller-Goymann, C. C. Solvent injection as a new approach for manufacturing lipid nanoparticles–evaluation of the method and process parameters. *Eur. J. Pharm. Biopharm.* **2003,** *55*, 125-131.

(35) Piao, H.; Ouyang, M.; Xia, D.; Quan, P.; Xiao, W.; Song, Y.; Cui, F. *In vitro–in vivo* study of CoQ10-loaded lipid nanoparticles in comparison with nanocrystals. *Int. J. Pharm.* **2011,** *419*, 255-259.

(36) Üner, M.; Wissing, S. A.; Yener, G.; Müller, R. H. Skin moisturizing effect and skin penetration of ascorbyl palmitate entrapped in solid lipid nanoparticles (SLN) and nanostructured lipid carriers (NLC) incorporated into hydrogel. *Pharmazie* **2005,** *60*, 751-755.

(37) Liu, J.; Gong, T.; Wang, C.; Zhong, Z.; Zhang, Z. Solid lipid nanoparticles loaded with insulin by sodium cholate-phosphatidylcholine-based mixed micelles: preparation and characterization. *Int. J. Pharm.* **2007,** *340*, 153-162.

(38) Hejri, A.; Khosravi, A.; Gharanjig, K.; Hejazi, M. Optimisation of the formulation of β-carotene loaded nanostructured lipid carriers prepared by solvent diffusion method. *Food Chem.* **2013,** *141*, 117-123.

(39) Cavalli, R.; Caputo, O.; Carlotti, M. E.; Trotta, M.; Scarnecchia, C.; Gasco, M. R. Sterilization and freeze-drying of drug-free and drug-loaded solid lipid nanoparticles. *Int. J. Pharm.* **1997,** *148*, 47-54.

(40) Hu, F.; Jiang, S.; Du, Y.; Yuan, H.; Ye, Y.; Zeng, S. Preparation and characterization of stearic acid nanostructured lipid carriers by solvent diffusion method in an aqueous system. *Colloid Surf. B-Biointerfaces* **2005,** *45*, 167-173.

(41) Wang, Y.; Wu, W. In situ evading of phagocytic uptake of stealth solid lipid nanoparticles by mouse peritoneal macrophages. *Drug Deliv.* **2006,** *13*, 189-192.

(42) Kheradmandnia, S.; Vasheghani-Farahani, E.; Nosrati, M.; Atyabi, F. Preparation and characterization of ketoprofen-loaded solid lipid nanoparticles

made from beeswax and carnauba wax. *Nanomed.-Nanotechnol. Biol. Med.* **2010,** *6*, 753-759.

(43) Tan, S. W.; Billa, N.; Roberts, C. R.; Burley, J. C. Surfactant effects on the physical characteristics of Amphotericin B-containing nanostructured lipid carriers. *Colloid Surf. A-Physicochem. Eng. Asp.* **2010,** *372*, 73-79.

(44) Teeranachaideekul, V.; Souto, E. B.; Junyaprasert, V. B.; Müller, R. H. Cetyl palmitate-based NLC for topical delivery of Coenzyme Q 10–Development, physicochemical characterization and *in vitro* release studies. *Eur. J. Pharm. Biopharm.* **2007,** *67*, 141-148.

(45) Shahgaldian, P.; Da Silva, E.; Coleman, A. W.; Rather, B.; Zaworotko, M. J. Para-acyl-calix-arene based solid lipid nanoparticles (SLNs): a detailed study of preparation and stability parameters. *Int. J. Pharm.* **2003,** *253*, 23-38.

(46) Jebors, S.; Leydier, A.; Wu, Q.; Bertino Ghera, B.; Malbouyre, M.; Coleman, A. W. Solid lipid nanoparticles (SLNs) derived from para-acyl-calix [9]-arene: preparation and stability. *J. Microencapsul.* **2010,** *27*, 561-571.

(47) Yang, X.; Li, Y.; Li, M.; Zhang, L.; Feng, L.; Zhang, N. Hyaluronic acid-coated nanostructured lipid carriers for targeting paclitaxel to cancer. *Cancer Lett.* **2013,** *334*, 338-345.

(48) Huang, Z. Development and evaluation of lipid nanoparticles for camptothecin delivery: a comparison of solid lipid nanoparticles, nanostructured lipid carriers, and lipid emulsion. *Acta Pharmacol. Sin.* **2008,** *29*, 1094-1102.

(49) Hung, L. C.; Basri, M.; Tejo, B. A.; Ismail, R.; Nang, H. L. L.; Hassan, H. A.; May, C. Y. An improved method for the preparations of nanostructured lipid carriers containing heat-sensitive bioactives. *Colloid Surf. B-Biointerfaces* **2011,** *87*, 180-186.

(50) Gokce, E. H.; Korkmaz, E.; Tuncay-Tanriverdi, S.; Dellera, E.; Sandri, G.; Bonferoni, M. C.; Ozer, O. A comparative evaluation of coenzyme Q10-loaded liposomes and solid lipid nanoparticles as dermal antioxidant carriers. *Int. J. Nanomed.* **2012,** *7*, 5109-5117.

(51) Li, X.; Nie, S.; Kong, J.; Li, N.; Ju, C. A controlled-release ocular delivery system for ibuprofen based on nanostructured lipid carriers. *Int. J. Pharm.* **2008,** *363*, 177-182.

(52) Ahmed El-Harati, A.; Charcosset, C.; Fessi, H. Influence of the formulation for solid lipid nanoparticles prepared with a membrane contactor. *Pharm. Dev. Technol.* **2006,** *11*, 153-157.

(53) Patravale, V. B.; Ambarkhane, A. V. Study of solid lipid nanoparticles with respect to particle size distribution and drug loading. *Pharmazie* **2003,** *58*, 392-395.

(54) Lippacher, A.; Müller, R. H.; Mäder, K. Investigation on the viscoelastic properties of lipid based colloidal drug carriers. *Int. J. Pharm.* **2000,** *196*, 227-230.

(55) Gasco, M. R. Method for producing solid lipid microspheres having a narrow size distribution. U.S. Patent Appl. 5/250,236, 1993.

(56) Yu, D.; Williams, G. R.; Yang, J.; Wang, X.; Yang, J.; Li, X. Solid lipid nanoparticles self-assembled from electrosprayed polymer-based microparticles. *J. Mater. Chem.* **2011,** *21*, 15957-15961.

(57) Heurtault, B.; Saulnier, P.; Pech, B.; Proust, J.; Benoit, J. A novel phase inversion-based process for the preparation of lipid nanocarriers. *Pharm. Res.* **2002,** *19*, 875-880.

(58) Freitas, C.; Müller, R. H. Correlation between long-term stability of solid lipid nanoparticles (SLN™) and crystallinity of the lipid phase. *Eur. J. Pharm. Biopharm.* **1999,** *47*, 125-132.

(59) Zhuang, C.; Li, N.; Wang, M.; Zhang, X.; Pan, W.; Peng, J.; Pan, Y.; Tang, X. Preparation and characterization of vinpocetine loaded nanostructured lipid carriers (NLC) for improved oral bioavailability. *Int. J. Pharm.* **2010,** *394*, 179-185.

(60) Mei, Z.; Chen, H.; Weng, T.; Yang, Y.; Yang, X. Solid lipid nanoparticle and microemulsion for topical delivery of triptolide. *Eur. J. Pharm. Biopharm.* **2003,** *56*, 189-196.

(61) Charcosset, C.; El-Harati, A.; Fessi, H. Preparation of solid lipid nanoparticles using a membrane contactor. *J. Control. Release* **2005,** *108*, 112-120.

(62) D'oria, C.; Charcosset, C.; Barresi, A. A.; Fessi, H. Preparation of solid lipid particles by membrane emulsification—Influence of process parameters. *Colloid Surf. A-Physicochem. Eng. Asp.* **2009,** *338*, 114-118.

(63) Cavalli, R.; Gasco, M. R.; Chetoni, P.; Burgalassi, S.; Saettone, M. F. Solid lipid nanoparticles (SLN) as ocular delivery system for tobramycin. *Int. J. Pharm.* **2002,** *238*, 241-245.

(64) Tiyaboonchai, W.; Tungpradit, W.; Plianbangchang, P. Formulation and characterization of curcuminoids loaded solid lipid nanoparticles. *Int. J. Pharm.* **2007,** *337*, 299-306.

(65) Trotta, M.; Cavalli, R.; Trotta, C.; Bussano, R.; Costa, L. Electrospray technique for solid lipid-based particle production. *Drug Dev. Ind. Pharm.* **2010,** *36*, 431-438.

(66) Luo, Y.; Chen, D.; Ren, L.; Zhao, X.; Qin, J. Solid lipid nanoparticles for enhancing vinpocetine's oral bioavailability. *J. Control. Release* **2006,** *114*, 53-59.

(67) Zhang, X.; Liu, J.; Qiao, H.; Liu, H.; Ni, J.; Zhang, W.; Shi, Y. Formulation optimization of dihydroartemisinin nanostructured lipid carrier using response surface methodology. *Powder Technol.* **2010,** *197*, 120-128.

(68) Montenegro, L.; Sarpietro, M. G.; Ottimo, S.; Puglisi, G.; Castelli, F. Differential scanning calorimetry studies on sunscreen loaded solid lipid

nanoparticles prepared by the phase inversion temperature method. *Int. J. Pharm.* **2011,** *415*, 301-306.

(69) Sun, M.; Nie, S.; Pan, X.; Zhang, R.; Fan, Z.; Wang, S. Quercetin-nanostructured lipid carriers: characteristics and anti-breast cancer activities *in vitro*. *Colloid Surf. B-Biointerfaces* **2014,** *113*, 15-24.

(70) Heiati, H.; Tawashi, R.; Phillips, N. C. Drug retention and stability of solid lipid nanoparticles containing azidothymidine palmitate after autoclaving, storage and lyophilization. *J. Microencapsul.* **1998,** *15*, 173-184.

(71) Pikal, M. J.; Shah, S.; Roy, M. L.; Putman, R. The secondary drying stage of freeze drying: drying kinetics as a function of temperature and chamber pressure. *Int. J. Pharm.* **1990,** *60*, 203-207.

(72) Ausborn, M.; Nuhn, P.; Schreier, H. Stabilization of liposomes by freeze-thaw- and lyophilization techniques: problems and opportunities. *Eur. J. Pharm. Biopharm.* **1992,** *38*, 133-139.

(73) Mobley, W. C.; Schreier, H. Phase transition temperature reduction and glass formation in dehydroprotected lyophilized liposomes. *J. Control. Release* **1994,** *31*, 73-87.

(74) Vemuri, S.; Yu, C.; Degroot, J. S.; Wangsatornthnakun, V.; Venkataram, S. Effect of sugars on freeze-thaw and lyophilization of liposomes. *Drug Dev. Ind. Pharm.* **1991,** *17*, 327-348.

(75) Crowe, L. M.; Crowe, J. H.; Rudolph, A.; Womersley, C.; Appel, L. Preservation of freeze-dried liposomes by trehalose. *Arch. Biochem. Biophys.* **1985,** *242*, 240-247.

(76) Zimmermann, E.; Müller, R. H.; Mäder, K. Influence of different parameters on reconstitution of lyophilized SLN. *Int. J. Pharm.* **2000,** *196*, 211-213.

(77) Freitas, C.; Müller, R. H. Spray-drying of solid lipid nanoparticles (SLN^{TM}). *Eur. J. Pharm. Biopharm.* **1998,** *46*, 145-151.

(78) Bunjes, H.; Steiniger, F.; Richter, W. Visualizing the structure of triglyceride nanoparticles in different crystal modifications. *Langmuir* **2007,** *23*, 4005-4011.

(79) Ban, C.; Lim, S.; Chang, P.; Choi, Y. J. Enhancing the stability of lipid nanoparticle systems by sonication during the cooling step and controlling the liquid oil content. *J. Agric. Food Chem.* **2014,** *62*, 11557-11567.

(80) Müller, R. H.; Petersen, R. D.; Hommoss, A.; Pardeike, J. Nanostructured lipid carriers (NLC) in cosmetic dermal products. *Adv. Drug Deliv. Rev.* **2007,** *59*, 522-530.

(81) Müller, R. H.; Radtke, M.; Wissing, S. A. Solid lipid nanoparticles (SLN) and nanostructured lipid carriers (NLC) in cosmetic and dermatological preparations. *Adv. Drug Deliv. Rev.* **2002,** *54*, S131-S155.

(82) Jenning, V.; Thünemann, A. F.; Gohla, S. H. Characterisation of a novel solid lipid nanoparticle carrier system based on binary mixtures of liquid and solid lipids. *Int. J. Pharm.* **2000,** *199*, 167-177.

(83) Jenning, V.; Mäder, K.; Gohla, S. H. Solid lipid nanoparticles (SLN™) based on binary mixtures of liquid and solid lipids: a ^{1}H-NMR study. *Int. J. Pharm.* **2000,** *205*, 15-21.

(84) Müller, R. H.; Maassen, S.; Schwarz, C. Solid lipid nanoparticles (SLN) as potential carrier for human use: interaction with human granulocytes. *J. Control. Release* **1997,** *47*, 261-269.

(85) Müller, R. H.; Maaβen, S.; Weyhers, H.; Specht, F.; Lucks, J. S. Cytotoxicity of magnetite-loaded polylactide, polylactide/glycolide particles and solid lipid nanoparticles. *Int. J. Pharm.* **1996,** *138*, 85-94.

(86) Wissing, S. A.; Kayser, O.; Müller, R. H. Solid lipid nanoparticles for parenteral drug delivery. *Adv. Drug Deliv. Rev.* **2004,** *56*, 1257-1272.

(87) Muchow, M.; Maincent, P.; Müller, R. H. Lipid nanoparticles with a solid matrix (SLN®, NLC®, LDC®) for oral drug delivery. *Drug Dev. Ind. Pharm.* **2008,** *34*, 1394-1405.

(88) Üner, M.; Yener, G. Importance of solid lipid nanoparticles (SLN) in various administration routes and future perspectives. *Int. J. Nanomed.* **2007,** *2*, 289.

(89) Ban, C.; Park, S. J.; Lim, S.; Choi, S. J.; Choi, Y. J. Improving flavonoid bioaccessibility using an edible oil-based lipid nanoparticle for oral delivery. *J. Agric. Food Chem.* **2015,** *63*, 5266-5272.

(90) Shi, Y.; Burn, P. Lipid metabolic enzymes: emerging drug targets for the treatment of obesity. *Nat. Rev. Drug Discov.* **2004,** *3*, 695-710.

(91) Müller, R. H.; Rühl, D.; Runge, S. A. Biodegradation of solid lipid nanoparticles as a function of lipase incubation time. *Int. J. Pharm.* **1996,** *144*, 115-121.

(92) Bargoni, A.; Cavalli, R.; Caputo, O.; Fundarò, A.; Gasco, M. R.; Zara, G. P. Solid lipid nanoparticles in lymph and plasma after duodenal administration to rats. *Pharm. Res.* **1998,** *15*, 745-750.

(93) Neves, A. R.; Lúcio, M.; Martins, S.; Lima, J. L.; Reis, S. Novel resveratrol nanodelivery systems based on lipid nanoparticles to enhance its oral bioavailability. *Int. J. Nanomed.* **2013,** *8*, 177-187.

(94) Jeong, J. H.; Park, T. G.; Kim, S. H. Self-assembled and nanostructured siRNA delivery systems. *Pharm. Res.* **2011,** *28*, 2072-2085.

(95) Manjappa, A. S.; Chaudhari, K. R.; Venkataraju, M. P.; Dantuluri, P.; Nanda, B.; Sidda, C.; Sawant, K. K.; Murthy, R. S. R. Antibody derivatization and conjugation strategies: application in preparation of stealth immunoliposome to target chemotherapeutics to tumor. *J. Control. Release* **2011,** *150*, 2-22.

(96) Gupta, Y.; Jain, A.; Jain, S. K. Transferrin-conjugated solid lipid nanoparticles for enhanced delivery of quinine dihydrochloride to the brain. *J. Pharm. Pharmacol.* **2007,** *59*, 935-940.

(97) Xiang, Q.; Wang, M.; Chen, F.; Gong, T.; Jian, Y.; Zhang, Z.; Huang, Y. Lung-targeting delivery of dexamethasone acetate loaded solid lipid nanoparticles. *Arch. Pharm. Res.* **2007,** *30*, 519-525.

(98) Tamjidi, F.; Shahedi, M.; Varshosaz, J.; Nasirpour, A. Design and characterization of astaxanthin-loaded nanostructured lipid carriers. *Innov. Food Sci. Emerg. Technol.* **2014,** *26*, 366-374.

(99) Li, M.; Zahi, M. R.; Yuan, Q.; Tian, F.; Liang, H. Preparation and stability of astaxanthin solid lipid nanoparticles based on stearic acid. *Eur. J. Lipid Sci. Technol.* **2015**.

(100) Zhang, L.; Hayes, D. G.; Chen, G.; Zhong, Q. Transparent dispersions of milk-fat-based nanostructured lipid carriers for delivery of β-carotene. *J. Agric. Food Chem.* **2013,** *61*, 9435-9443.

(101) Lacatusu, I.; Mitrea, E.; Badea, N.; Stan, R.; Oprea, O.; Meghea, A. Lipid nanoparticles based on omega-3 fatty acids as effective carriers for lutein delivery. Preparation and *in vitro* characterization studies. *J. Funct. Food.* **2013,** *5*, 1260-1269.

(102) dos Santos, P. P.; Paese, K.; Guterres, S. S.; Pohlmann, A. R.; Costa, T. H.; Jablonski, A.; Flôres, S. H.; de Oliveira Rios, A. Development of lycopene-loaded lipid-core nanocapsules: physicochemical characterization and stability study. *J. Nanopart. Res.* **2015,** *17*, 1-11.

(103) Lim, S.; Lee, M.; Kim, C. Altered chemical and biological activities of all-trans retinoic acid incorporated in solid lipid nanoparticle powders. *J. Control. Release* **2004,** *100*, 53-61.

(104) Carneiro, G.; Silva, E. L.; Pacheco, L. A.; de Souza-Fagundes, E. M.; Corrêa, N. C. R.; de Goes, A. M.; de Oliveira, M. C.; Ferreira, L. A. M. Formation of ion pairing as an alternative to improve encapsulation and anticancer activity of all-trans retinoic acid loaded in solid lipid nanoparticles. *Int. J. Nanomed.* **2012,** *7*, 6011.

(105) Teeranachaideekul, V.; Müller, R. H.; Junyaprasert, V. B. Encapsulation of ascorbyl palmitate in nanostructured lipid carriers (NLC)—effects of formulation parameters on physicochemical stability. *Int. J. Pharm.* **2007,** *340*, 198-206.

(106) Üner, M.; Wissing, S. A.; Yener, G.; Müller, R. H. Solid lipid nanoparticles (SLN) and nanostructured lipid carriers (NLC) for application of ascorbyl palmitate. *Pharmazie* **2005,** *60*, 577-582.

(107) Trombino, S.; Cassano, R.; Muzzalupo, R.; Pingitore, A.; Cione, E.; Picci, N. Stearyl ferulate-based solid lipid nanoparticles for the encapsulation and stabilization of β-carotene and α-tocopherol. *Colloid Surf. B-Biointerfaces* **2009,** *72*, 181-187.

(108) Liu, C.; Wu, C.; Fang, J. Characterization and formulation optimization of solid lipid nanoparticles in vitamin K1 delivery. *Drug Dev. Ind. Pharm.* **2010,** *36*, 751-761.

(109) Zhang, Z.; Huang, Y.; Gao, F.; Bu, H.; Gu, W.; Li, Y. Daidzein–phospholipid complex loaded lipid nanocarriers improved oral absorption: *in vitro* characteristics and *in vivo* behavior in rats. *Nanoscale* **2011,** *3*, 1780-1787.

(110) Zhang, Z.; Huang, Y.; Gao, F.; Gao, Z.; Bu, H.; Gu, W.; Li, Y. A self-assembled nanodelivery system enhances the oral bioavailability of daidzein: *in vitro* characteristics and *in vivo* performance. *Nanomedicine* **2011,** *6*, 1365-1379.

(111) Aditya, N. P.; Shim, M.; Lee, I.; Lee, Y. S.; Im, M.; Ko, S. Curcumin and genistein coloaded nanostructured lipid carriers: *in vitro* digestion and antiprostate cancer activity. *J. Agric. Food Chem.* **2013,** *61*, 1878-1883.

(112) Zhang, W.; Li, X.; Ye, T.; Chen, F.; Sun, X.; Kong, J.; Yang, X.; Pan, W.; Li, S. Design, characterization, and *in vitro* cellular inhibition and uptake of optimized genistein-loaded NLC for the prevention of posterior capsular opacification using response surface methodology. *Int. J. Pharm.* **2013,** *454*, 354-366.

(113) Fathi, M.; Varshosaz, J.; Mohebbi, M.; Shahidi, F. Hesperetin-loaded solid lipid nanoparticles and nanostructure lipid carriers for food fortification: preparation, characterization, and modeling. *Food Bioprocess Technol.* **2013,** *6*, 1464-1475.

(114) Liu, Y.; Wang, L.; Zhao, Y.; He, M.; Zhang, X.; Niu, M.; Feng, N. Nanostructured lipid carriers versus microemulsions for delivery of the poorly water-soluble drug luteolin. *Int. J. Pharm.* **2014,** *476*, 169-177.

(115) Lv, F.; Hasan, M.; Dang, H.; Hassan, S. G.; Meng, W.; Deng, Y.; Dai, R. Optimized Luteolin Loaded Solid Lipid Nanoparticle Under Stress Condition for Enhanced Bioavailability in Rat Plasma. *J. Nanosci. Nanotechnol.* **2015,** *15*, 1-7.

(116) Bazylińska, U.; Pucek, A.; Sowa, M.; Matczak-Jon, E.; Wilk, K. A. Engineering of phosphatidylcholine-based solid lipid nanocarriers for flavonoids delivery. *Colloid Surf. A-Physicochem. Eng. Asp.* **2014,** *460*, 483-493.

(117) Li, H.; Zhao, X.; Ma, Y.; Zhai, G.; Li, L.; Lou, H. Enhancement of gastrointestinal absorption of quercetin by solid lipid nanoparticles. *J. Control. Release* **2009,** *133*, 238-244.

(118) Liu, L.; Tang, Y.; Gao, C.; Li, Y.; Chen, S.; Xiong, T.; Li, J.; Du, M.; Gong, Z.; Chen, H. Characterization and biodistribution *in vivo* of quercetin-loaded cationic nanostructured lipid carriers. *Colloid Surf. B-Biointerfaces* **2014,** *115*, 125-131.

(119) Priano, L.; Esposti, D.; Esposti, R.; Castagna, G.; De Medici, C.; Fraschini, F.; Gasco, M. R.; Mauro, A. Solid lipid nanoparticles incorporating melatonin as new model for sustained oral and transdermal delivery systems. *J. Nanosci. Nanotechnol.* **2007,** *7*, 3596-3601.

(120) Yuan, H.; Wang, L.; Du, Y.; You, J.; Hu, F.; Zeng, S. Preparation and characteristics of nanostructured lipid carriers for control-releasing

progesterone by melt-emulsification. *Colloid Surf. B-Biointerfaces* **2007,** *60*, 174-179.

(121) Cavalli, R.; Peira, E.; Caputo, O.; Gasco, M. R. Solid lipid nanoparticles as carriers of hydrocortisone and progesterone complexes with β-cyclodextrins. *Int. J. Pharm.* **1999,** *182*, 59-69.

(122) Pandita, D.; Kumar, S.; Poonia, N.; Lather, V. Solid lipid nanoparticles enhance oral bioavailability of resveratrol, a natural polyphenol. *Food Res. Int.* **2014,** *62*, 1165-1174.

(123) Khan, S.; Baboota, S.; Ali, J.; Narang, R. S.; Narang, J. K. Chlorogenic acid stabilized nanostructured lipid carriers (NLC) of atorvastatin: formulation, design and *in vivo* evaluation. *Drug Dev. Ind. Pharm.* **2016,** *42*, 209-220.

(124) Nepal, P. R.; Han, H.; Choi, H. Preparation and *in vitro–in vivo* evaluation of Witepsol® H35 based self-nanoemulsifying drug delivery systems (SNEDDS) of coenzyme Q 10. *Eur. J. Pharm. Sci.* **2010,** *39*, 224-232.

(125) Ramalingam, P.; Ko, Y. T. Enhanced oral delivery of curcumin from N-trimethyl chitosan surface-modified solid lipid nanoparticles: pharmacokinetic and brain distribution evaluations. *Pharm. Res.* **2015,** *32*, 389-402.

(126) Muchow, M.; Schmitz, E. I.; Despatova, N.; Maincent, P.; Müller, R. H. Omega-3 fatty acids-loaded lipid nanoparticles for patient-convenient oral bioavailability enhancement. *Pharmazie* **2009,** *64*, 499-504.

(127) Picone, P.; Bondi, M. L.; Picone, P.; Bondi, M. L.; Montana, G.; Bruno, A.; Pitarresi, G.; Giammona, G.; Di Carlo, M. Ferulic acid inhibits oxidative stress and cell death induced by Ab oligomers: improved delivery by solid lipid nanoparticles. *Free Radic. Res.* **2009,** *43*, 1133-1145.

(128) Madureira, A. R.; Campos, D. A.; Oliveira, A.; Sarmento, B.; Pintado, M. M.; Gomes, A. M. Insights into the protective role of solid lipid nanoparticles on rosmarinic acid bioactivity during exposure to simulated gastrointestinal conditions. *Colloid Surf. B-Biointerfaces* **2016,** *139*, 277-284.

(129) Ozturk, B.; Argin, S.; Ozilgen, M.; McClements, D. J. Formation and stabilization of nanoemulsion-based vitamin E delivery systems using natural biopolymers: whey protein isolate and gum arabic. *Food Chem.* **2015,** *188*, 256-263.

(130) Ye, R.; Harte, F. Casein maps: effect of ethanol, pH, temperature, and $CaCl_2$ on the particle size of reconstituted casein micelles. *J. Dairy Sci.* **2013,** *96*, 799-805.

Chapter II. Enhancing the Stability of Lipid Nanoparticle Systems by Sonication during the Cooling Step and Controlling the Liquid Oil Content

Published in Journal of Agricultural and Food Chemistry

(C. Ban, S. Lim, P.-S. Chang, and Y. J. Choi, *J. Agric. Food Chem.* 2014, 62, 11557-11567)

II-1. Introduction

Colloidal systems are a commonly used carrier platform for the delivery of bioactive components.1 However, further applications of some traditional systems including liposomes and emulsions are limited due to the nonavailability of a cheap liposome and the low physical instability of emulsions caused by the incorporated material, respectively (1). Recently, lipid nanoparticles (LNPs), including solid lipid nanoparticles (SLNs) and nanostructured lipid carriers (NLCs), have drawn attention for their enhanced protectability and tailorability (2). In the early 1990s, a SLN prepared using biocompatible lipid was introduced as an advanced drug delivery system (3). Besides its economic merit, SLNs provide several advantages such as the strong protective capability of materials carried by immobilization in the solid matrix (4). However, the disadvantages of SLNs, such as the insufficient loading capacity and the expulsion of loaded materials during storage, led to the development of NLCs, which were composed of a solid/liquid two-phase hybridized lipid matrix (5−8).

The LNP as a colloidal carrier system has been manipulated to obtain unique features based on advanced technologies and analytical studies, including morphological characterization by transmission electron microscopy (9) and determination of crystalline structures by X-ray diffraction (10−12) and of the thermal properties by differential scanning calorimetry (13, 14). For example, investigations of SLN crystallization revealed that morphological changes in individual particles

cause SLN aggregation (15). Changes in the polymorphic structure of the lipid matrix from α to β drive transformation of the crystalline structure from a spherical to a needle-shape, which increases the surfactant-depleted areas (hydrophobic patches) of SLNs (16−19). In this case, individual particles (well-dispersed initially) become unstable and aggregate due to interactions between hydrophobic patches to minimize the uncovered surface area facing the solvent. Subsequently, unstable SLNs may aggregate followed by gelation when the amount of available surfactants is not sufficient or the rate of diffusion of available surfactants suspending in aqueous phase onto the interface is not high enough to stabilize the hydrophobic patches. For the same reason, the shear force is known to cause gelation and aggregation of LNP suspensions (20). Moreover, the partial coalescence of oil droplets containing crystals during cooling procedure could be also taken into account as the reason for the aggregation (21, 22).

Emulsifiers unexpectedly form micelles at high temperatures during LNP preparation (23, 24). This effect reduces the amount of available surfactants to cover the surface of LNPs and ultimately exacerbates the LNP aggregation problem (25, 26). Thus, the addition of sufficient emulsifier during the cooling process could prevent aggregation and gelation of SLN (25). On the basis of this hypothesis, hydrophobic patches of the SLN that form a nonspherical shape are stabilized using an emulsifier. In addition, methods to improve the stability of SLN suspensions have been proposed, including (i) using a lipid source that prevents or retards the α to β polymorphic

transition, (ii) adding sufficient emulsifier to completely cover the LNP surfaces in both the liquid and solid states, and (iii) using an emulsifier that prevents particle aggregation by increasing the repulsion.

Despite the general use in foods, the permissible amount of emulsifier is often limited by regulations in many countries. Thus, it is not appropriate to use much emulsifier in the preparation of the LNP system for food applications. Meanwhile, sonication is commonly used to prepare emulsion systems, and the cavitation caused by sonication has various physical effects including dispersing molecules in liquids. In this paper, to prevent severe aggregation of LNPs, the effect of sonication during the cooling process was exploited rather than the addition of more emulsifier. For the LNP system, fully hydrogenated canola oil (FHCO) and liquid canola oil (LCO) were used as the solid and liquid lipids, respectively. I explored how the lipid oil (LCO) contents in the FHCO LNPs and the sonication time during the cooling process affected the stability of the dispersion system.

II-2. Materials and Methods

II-2-1. Chemicals

Lotte Samkang Co. Ltd. (Seoul, Korea) provided us with FHCO, which was composed of 79.5 wt % stearic acid, 8.8 wt % palmitic acid, 4.2 wt % oleic acid, 1.8 wt % lauric acid, 1.6 wt % arachidic acid, 1.4 wt % linoleic acid, 0.9 wt % myrisitc acid, and 1.8 wt % other ingredients. LCO was obtained from CJ Cheiljedang Co. (Seoul, Korea) and consisted of 58.3 wt % oleic acid, 20.0 wt % linoleic acid, 8.3 wt % linolenic acid, 4.4 wt % palmitic acid, 1.8 wt % stearic acid, 1.3 wt % erucic acid, 0.6 wt % arachidic acid, and 5.3 wt % other ingredients. Tween 20 (polyoxyethylene sorbitan monolaurate) was purchased from Sigma-Aldrich Co. (St. Louis, MO, USA). All other chemicals were of analytical reagent grade.

II-2-2. Lipid Nanoparticle Preparation

Oil-in-water emulsions were prepared by mixing 5 wt % lipid phase with 95 wt % aqueous phase (10 mM phosphate buffer, 1.67 wt % Tween 20, i.e., a third of the lipid phase weight, pH 7) at 85 °C. The lipid phase was prepared using blended bulk lipid consisting of FHCO and LCO. FHCO was liquefied by heating to 85 °C, and LCO was heated to 85 °C. A range of LCO-to-FHCO weight ratios was used to prepare the lipid phases (0, 10, 20, and 30 wt % of LCO). Coarse oil-in-water emulsions were prepared by homogenizing the oil and aqueous phases together using a high-speed blender (Ultra-Turrax T25D, Ika Werke GmbH & Co., Staufen, Germany) at 8000 rpm for 1 min and then at 11000 rpm for 1 min. The droplet size was further reduced by sonication (VCX 750, Sonics & Materials Inc., Newtown, CT, USA) for 4 min at an amplitude of 60% and a duty cycle of 1 s. To prevent lipid crystallization during emulsion preparation, all experiments were conducted at 95 °C, which was above the melting temperature of FHCO. After droplet size reduction, postsonication (4, 5, or 6 min) was applied to the emulsions as they cooled to 25 °C in a jacketed beaker, after which samples were maintained at room temperature (25 °C). The temperature changes in the emulsion samples during the process were monitored using a data logger (Agilent 34970A, Agilent Technologies Inc., Santa Clara, CA, USA).

II-2-3. Microscopic Observation

A drop of LNP sample was placed on a microscope slide and covered using a coverslip. The microstructure of the aggregated particles was observed using a conventional optical microscope (DCM130, Hangzhou HauXin IC Technology Inc., Hangzhou, China) equipped with a digital camera (DCM130E, BW Optics Co., Nanjing, China) and digital image processing software (ScopePhoto version 3.0, Hangzhou Scopetek Opto-Electric Co., Hangzhou, China).

The nanostructure of LNPs prepared using the postsonication process was observed using a transmission electron microscope (JEM1010, JEOL, Tokyo, Japan). First, LNP samples diluted with double-distilled water were placed on a film-coated copper grid and negatively stained with a 1 % (w/v) aqueous solution of phosphotungstic acid for 30 s; ultimately, the overflow phosphotunstic acid on the sample was wiped off by filter paper before drying for 1 day at room temperature before observation (27).

II-2-4. Determination of Rheological Properties

Storage modulus (G') and phase angles (δ) of the LNPs undergoing a sol-to-gel transition were measured using a Rheostress RS 100 (Haake Instruments, Karlsruhe, Germany) equipped with a cone and plate measurement system (diameter = 35 mm, cone angle = 1°) and a designated gap of 50 μm to avoid the effects of single particles. Initially, the shear stress that could cause the gelation of all fresh samples but not destroy the networks among gelled LNPs was determined by the rotational flow test. The stress level of 3 Pa was suitable to observe a time effect of shearing to gelation. Consequently, all time sweep tests were conducted under the controlled stress mode at a stress of 3 Pa and a frequency of 1 Hz.

II-2-5. Differential Scanning Calorimetry (DSC) Measurement

The polymorphism of the blended bulk lipids and lipid phases in the prepared suspensions was determined using a differential scanning calorimeter (Diamond DSC, PerkinElmer, Waltham, MA, USA). Each sample (20 ± 5 mg) was placed in a hermetic aluminum pan, which was sealed and equilibrated at room temperature overnight prior to the measurements. An empty pan was used as a reference. The DSC scan started at 25 °C, increased by 5 °C min^{-1} to 95 °C, and then decreased by 5 °C min^{-1} to 10 °C. The crystallinity index (CI) was calculated on the basis of heating thermograms to determine the degree of crystallinity of lipid nanoparticles using the equation (28)

$$\mathrm{CI}\ (\%) = \frac{\Delta H_{\mathrm{m\ LNP}}\ (\mathrm{J\ g^{-1}}) \times 100}{\Delta H_{\mathrm{m\ FHCO}}\ (\mathrm{J\ g^{-1}}) \times c_{\mathrm{L}}\ (\%)} \times 100$$

where $\Delta H_{\mathrm{m\ LNP}}$ is the melting enthalpy of LNPs, $\Delta H_{\mathrm{m\ FHCO}}$ is the melting enthalpy of bulk FHCO, and c_{L} is the concentration of the lipid phase (i.e., 5 wt %).

II-2-6. Powder X-ray Diffraction (XRD) Analysis

The XRD patterns for FHCO stored overnight at room temperature were collected using the X-ray diffractometer (Bruker model D8 advance, Karlsruhe, Germany) with Cu Kα radiation at λ = 1.54 Å (30 kV, 30 mA). Both results of small-angle X-ray scattering (2θ = 0−9.1°, 0.005°/s) and wide-angle X-ray scattering (2θ = 0−40°, 0.2°/s) were obtained with a general area detector diffraction system.

II-2-7. Measurement of Lipid Nanoparticle Size

The microstructural size of the LNP microstructure was measured using a laser diffraction analyzer (S3500, Microtrac Inc., Montgomeryville, PA, USA) to figure out the size distribution of aggregated LNPs in the fresh LNP system before (fresh sample) and after the gelation (gelled sample). Samples were stirred continuously throughout the measurements to ensure that they were homogeneous with the water flow option. The particle size was reported as the mean diameter in micrometers of the volume distribution, $\mathrm{MV} = \sum V_i d_i / \sum V_i$ (where V_i is the volume percent of particles of diameter d_i in the population).

The gelled LNPs (4.5 mL) were diluted with 40.5 mL of double-distilled water (DDW) in a vial. For the separation of the layer containing the creamed (creaming layer) and noncreamed LNPs (aqueous layer), the vial containing diluted LNPs was tightly sealed with a screw cap and kept overnight at room temperature. The LNPs in the aqueous layer were collected by filtering with a glass microfiber filter with a 1 μm pore size (GF/B, Whatman Ltd., Fisons, Loughborough, UK) to figure out the size of noncreamed LNP, and their mean nanostructural diameter (z average) was measured using a Zetasizer (Nano ZS, Malvern Instruments Ltd., Worcestershire, UK) using a helium−neon laser (λ = 633 nm).

II-2-8. Quantification of Stable Lipid Nanoparticles

The diluted LNPs in the vials were passed through a glass microfiber filter with a 1 μm pore size (GF/B, Whatman Ltd.). The micrometer-sized and aggregated LNPs remaining on the filter were weighed after drying in an oven at 50 °C. The difference in filter weight before and after the procedure, which is the weight of the gelled or aggregated LNPs, was recorded.

II-2-9. Determination of Tween 20 Surface Load

From the TEM observations, the shape of LNPs was close to a sphere. Therefore, Tween 20 surface load (Γ_s) was calculated as $\Gamma_s = C_a D/6\Phi$, where C_a is the concentration of the emulsifier adsorbed to the surface of lipid nanoparticles, D is the mean diameter (z average), and Φ is the lipid phase volume fraction (i.e., 0.05 lipid phase) (29). C_a was determined by subtracting the concentration of Tween 20 suspended as single molecules or micelles from the initial concentration of total emulsifier in the water phase. A total of 2.5 mL of the previously diluted and filtered LNP dispersion was injected into the Sephadex G-25 column (GE Healthcare, Chalfont St Giles, UK) filled with DDW. Next, 1 mL of DDW was serially added, and then each fraction eluted from the column was collected in a microtube. Next, aliquots (1 mL) of the fractions in the fifth and sixth microtubes were selected as samples in which the Tween 20 molecules did not participate in emulsifying activity. Colorimetry for Tween 20 quantification has been reported previously (30). Briefly, each sample (1 mL) was dried at 80 °C in an oven. The sample was then cooled, and 0.4 mL of ammonium cobaltothiocyanate (ACTC) solution and 0.8 mL of dichloromethane were added. The ACTC solution was fabricated using 3 g of cobalt nitrate hexahydrate and 18 g of ammonium thiocyanate in 100 mL of DDW. Samples were vortexed for 5 s and centrifuged at 10400 RCF for 10 min (Centrifuge Smart 15, Hanil Science Industrial Co., Ltd., Incheon, Korea). After centrifuging, the dichloromethane layer was transferred to a micro quartz cell, and the absorbance at

623.5 nm was determined using a spectrophotometer (Pharmaspec UV-1700, Shimadzu Corp., Kyoto, Japan). The amount of Tween 20 molecules in the LNP dispersion was calculated using standard curves ranging from 0.0167 to 0.0833 wt % for Tween 20 (r^2 = 0.9976).

II-2-10. Statistical Analysis

All results were analyzed using Tukey's significant difference test with IBM SPSS Statistics version 21.0 (IBM Co., Armonk, NY, USA). Data represent the averages of at least three independent experiments or measurements.

II-3. Results and Discussion

II-3-1. Lipid Nanoparticle Preparation

To differentiate the LNP preparation method from the general methods (1, 6, 31), a new step, postsonication (PS), was added. After size reduction, sonication was performed for <6 min in a jacketed beaker maintained at 25 °C. Regardless of the PS time and the liquid oil content in the oil phase, all LNP solutions reached the melting temperature (T_m) and the crystallization temperature (T_c) of their lipids in approximately 4 and 6 min in the jacketed beaker at 25 °C, respectively (Figure II-1). When the temperature of the LNP solution was lower than the T_c of the blended oil, the sonication could partially coalesce the crystallized particles and the oil droplets as the source of turbulent flow rather than preventing the aggregation of LNPs (21, 22). Therefore, all PS should be performed at temperatures above the Tc of the lipid phase, that is, 4−6 min.

All LNP samples prepared using the lipid containing the LCO concentration at 0−30 wt % would be solidified after the preparation. In other words, the LNP samples were not separately prepared as each of the solidified particles and the liquid droplets in a system, but fabricated as the solid state particles. However, in the LNP system prepared using the lipid containing 40 wt % LCO, both the solid state particles and the liquid state droplets were indirectly verified with DSC thermograms cooling from 95 to −65 °C and then heating from −65 to 95 °C (Figure II-2). In both the

cooling and heating graphs, LNP samples prepared using the lipid at 0−30 wt % LCO did not have the characteristic peaks, whereas distinguishing subzero peaks were observed in both LNP and an emulsion system prepared with 40 wt % LCO and 100 wt % LCO. Thus, the maximum LCO concentration for preparing the LNP system in the present study should be < 40 wt %.

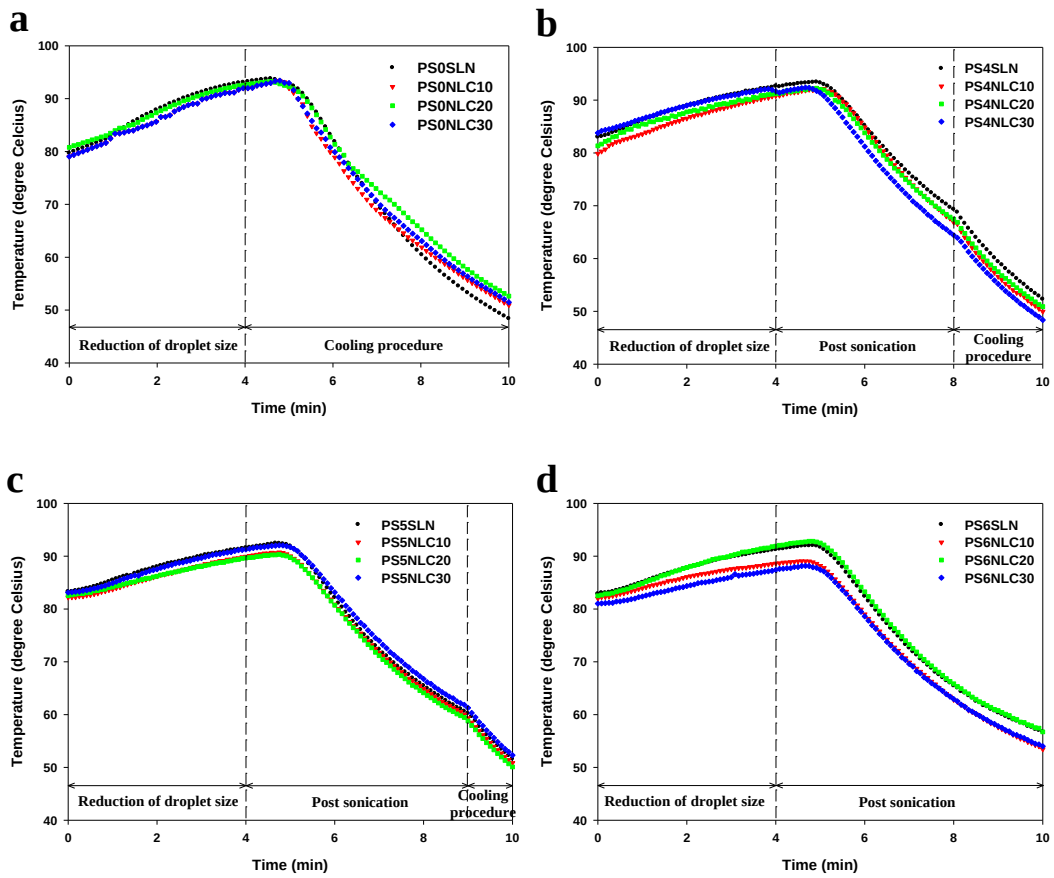

Figure II-1. Temperature profiles during preparation of lipid nanoparticle suspension by postsonication. (a) 0, (b) 4, (c) 5, and (d) 6 min. In the legend, the number following PS (0, 4, 5, and 6) represents the PS procedure time; SLN, NLC10, NLC20, and NLC30 indicate samples prepared using 0, 10, 20, and 30 wt %, respectively, liquid canola oil in the lipid phase.

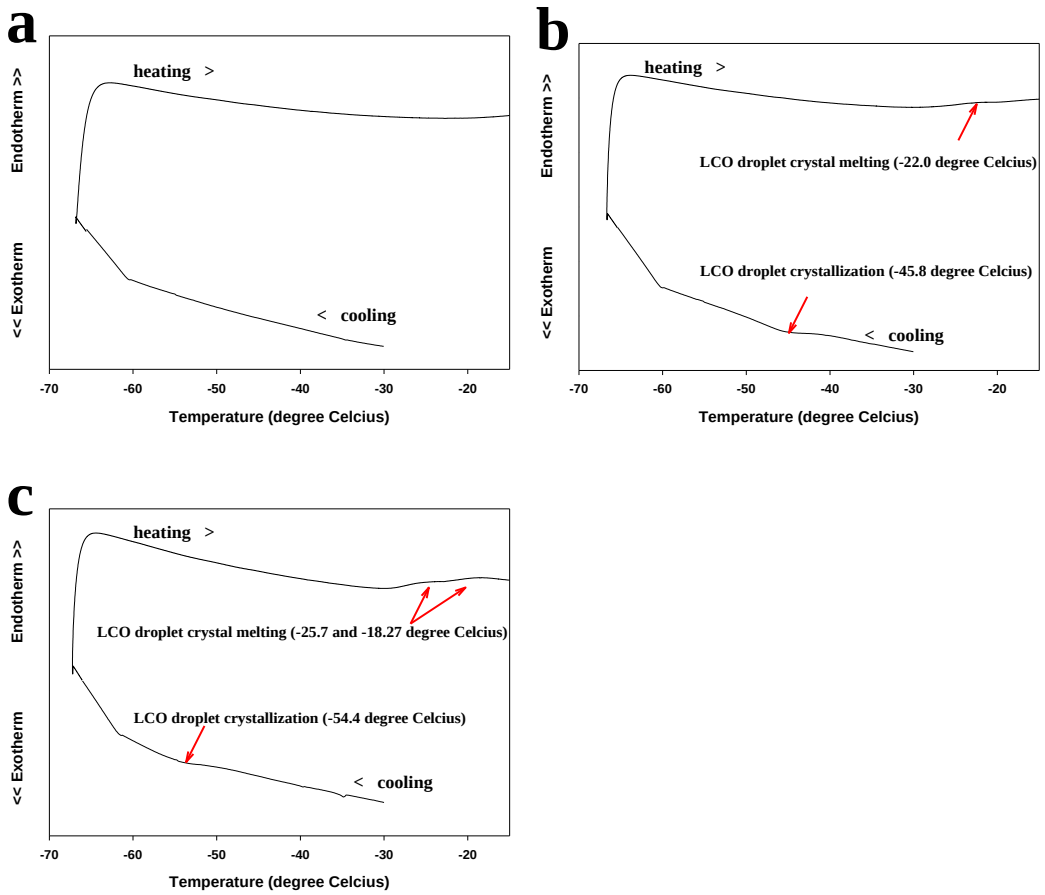

Figure II-2. Cooling and heating thermographs of the lipid nanoparticles or the emulsion in DSC measurement. Samples prepared using the post-sonication for 6 min fabricated and the LCO concentration at (a) 30, (b) 40, and (c) 100 in the lipid phase, respectively.

II-3-2. Visual Stability of Lipid Nanoparticles

Collisions between some crystallized particles and some noncrystallized droplets could bring partial coalescence during cooling procedure for the LNP preparation (21), which could force the solid particles together after the fabrication. Additionally, the hydrophobic patches exposed to aqueous solution interacted and aggregated to reduce the surface area exposed to aqueous solution (32). As a result, the partially coalesced LNPs and the LNPs with surfactant-depleted patches on the surfaces naturally formed aggregates of a micrometer-level size. The creaming phenomenon of highly aggregated LNPs by the partial coalescence and the aggregation when the gelled LNP dispersion was diluted by a 10th part is observed in Figure II-3. All samples were divided into two layers, that is, the creaming layer and the aqueous layer, and the length of the vertical line on the samples represents the thickness of the aqueous layer. These observations suggested that increases in the PS time and the LCO content of the oil phase enhance LNP stability.

Stokes' law for hindered settling could explain the creaming phenomenon of the dispersion system composed of LNPs (33). Under the same composition, the effect of the particle size on the creaming rate predominates over the density difference. Therefore, the aggregated and gelled particles in micrometer size creamed readily, whereas the stable nanosize LNPs were well-dispersed in aqueous solution. Particle size measurement of the aqueous layer was conducted to verify this conjecture. All LNPs in the aqueous layer had mean particle size values (z average) of 114.7−202.3

nm and a unimodal size distribution in the nanoscale range (Table II-1 and Figure II-4). This supports my hypothesis that LNPs in the aqueous layer are nonaggregated particles.

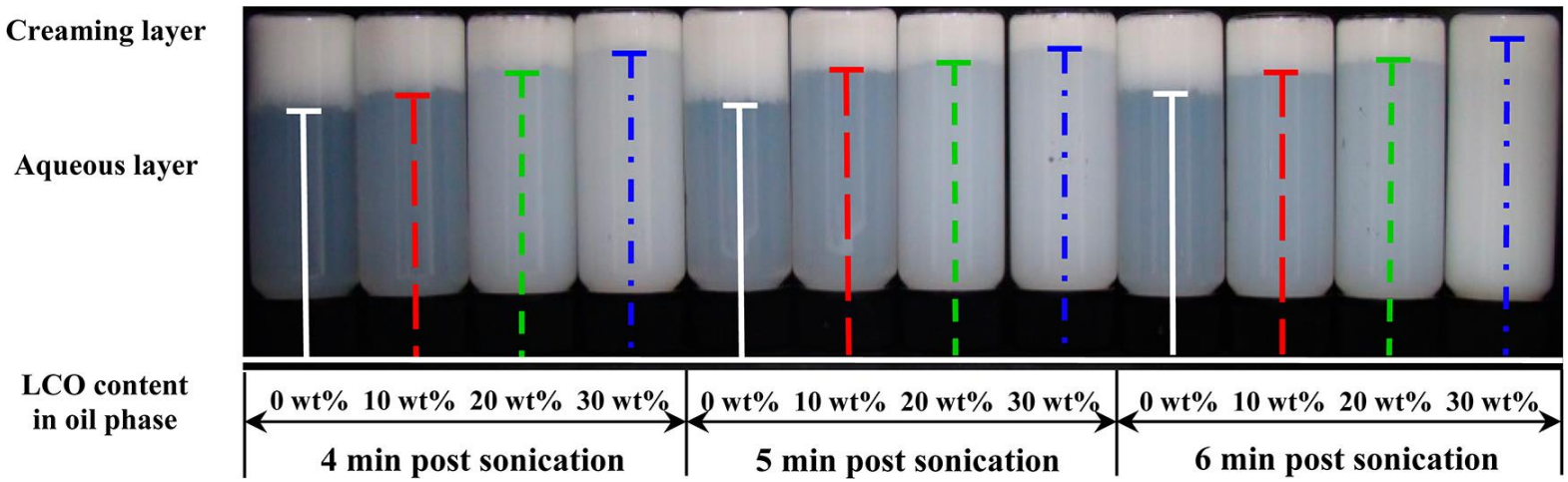

Figure II-3. Creaming pattern of the blank lipid nanoparticle dispersion diluted 10-fold.

Table II-1. Mean Diameters (z average) of Nonaggregated Lipid Nanoparticles in the Aqueous Layer[a]

sample		
post sonication (min)	LCO content (wt %)	z average (nm)
0	0	114.7 ± 1.1 j
	10	122.1 ± 3.0 i
	20	139.1 ± 0.7 g
	30	177.8 ± 1.3 c
4	0	124.3 ± 0.5 hi
	10	143.0 ± 1.5 g
	20	154.5 ± 1.0 f
	30	188.2 ± 0.5 b
5	0	128.5 ± 1.0 h
	10	152.8 ± 1.5 f
	20	162.3 ± 0.1 e
	30	191.6 ± 0.3 b
6	0	142.0 ± 4.0 g
	10	154.2 ± 1.7 f
	20	167.6 ± 0.5 d
	30	202.3 ± 1.6 a

[a]Different letters a−j in a column are significantly different at $p < 0.05$.

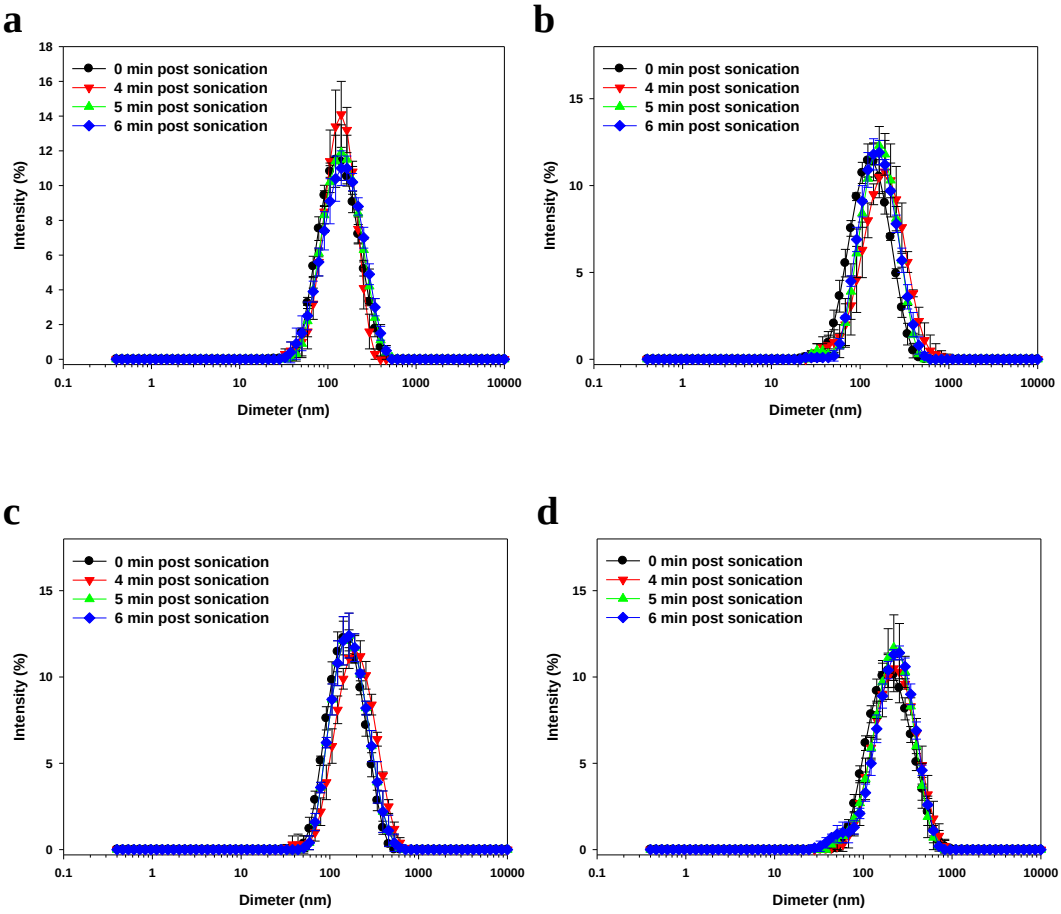

Figure II-4. Particle size distribution of nonaggregated lipid nanoparticles. (a) SLN; (b) 10% NLC; (c) 20% NLC, and (d) 30% NLC.

II-3-3. Morphological Characteristics of Lipid Nanoparticles and Gelation Phenomenon

The freshly fabricated LNPs showed fluid properties. However, gelation of all LNP samples had occurred after the application of shear stress >3 Pa, and the fluid characteristics were lost (data not shown). This phenomenon is in agreement with a previous study (19). Gelation of the LNPs can be accelerated by the interaction between hydrophobic patches on the LNPs, which were created by morphological changes, because the probability of particle collision is increased by shearing. Meanwhile, the partial coalescence among particles could not happen by shearing because the lipid matrix composing LNPs was solidified after the preparation (21). Therefore, hydrophobic interactions could be an important factor for network formation with LNPs, resulting in their gelation.

Panels a−d of Figure II-5 show microstructural morphologies of LNPs fabricated using LCO at diverse concentrations (0−30 wt %) using the PS step for 5 min after shearing and aggregating. LNP flocs at a micrometer-size were independently observed in all samples. The flocs consisted of LNPs, and comparatively small LNPs were suspended in the remaining space within the flocs. The LNPs comprising flocs might have hydrophobic patches or partially coalesced particles; that is, nonstable LNPs and the small LNPs suspended in the water phase might have been covered with Tween 20, that is, stable LNPs. Although it was assumed that LNPs composing flocs underwent morphological changes, shapes

extremely deviated from a sphere were not observed among the LNPs in flocs.

After gelation by shearing, the aggregated LNP size changed significantly (Table II-2). Before shearing, the LNPs generally showed a large decrease in mean particle diameter with increasing LCO content in the lipid phase. At the same LCO content in the lipid phase, intensive aggregation of the LNPs was observed as the PS time increased, with the exception of the 0 and 30 wt % LCO LNP. However, there was no trend in the change in LNP size following gelation. In addition, multiple peaks in the particle size distribution became unimodal after shearing, independent of the PS time and the LCO-to-FHCO weight ratio. For example, on aggregation in samples fabricated using PS for 5 min, whereas a single peak in a sample prepared using 0 wt % LCO contents simply shifted from 20.17 to 16.96 μm, multiple peaks in samples fabricated using 10, 20, and 30 wt % LCO contents (10% LCO, 1.50 and 14.27 μm; 20% LCO, 1.26 and 11.00 μm; 30% LCO, 1.16, 11.00, and 44.00 μm) formed unimodal peaks at 16.96, 16.96, 15.56, and 18.50 μm, respectively (Figure II-6). Surfactants on the surface of solidified LNPs could not reemulsify the interface of LNP aggregates. Moreover, LNP aggregates could not be fully coalesced, which could be just rearranged in another size. Therefore, these results could indirectly support that the shearing in LNP systems could cause the aggregation and gelation of LNPs.

Panels a−d in Figure II-7 show the nanostructural morphologies of LNPs prepared using various LCO contents (0−30 wt %) in the oil phase. The majority of each LNPs observed in the TEM images were nanoscaled, whereas micrometer-sized

particles were rarely observed. In other words, either the LNPs making up the flocs or the LNPs suspended individually were composed of nanoscale LNPs. This observation suggested that although PS could not completely prevent floc formation, it facilitated maintenance of single particles at a nanoscale size. In addition, the shape of all LNPs in the microscopy was more similar to the sphere rather than the needle-shape referred to by several researchers (16, 19). This morphological shape similar to the sphere might come from the effects of the PS and the LCO content in the lipid matrix, which could cause the increase of surfactant coverage and improve the colloidal stability of the LNP system. Briefly, FHCO droplets melted during the size reduction for the LNP preparation are cooled and crystallized as FHCO LNPs during the cooling procedure. Among the crystallized LNPs, stable LNPs, which are sufficiently stabilized by Tween 20 and have no hydrophobic patch, would maintain their nanoscale without the aggregation, but nonstable LNPs, which have the hydrophobic patches on the particle, would be aggregated and micrometer-sized after forming the flocs. Moreover, after shearing, the aggregation of the nonstable LNPs would be worse and LNP system would be gelated.

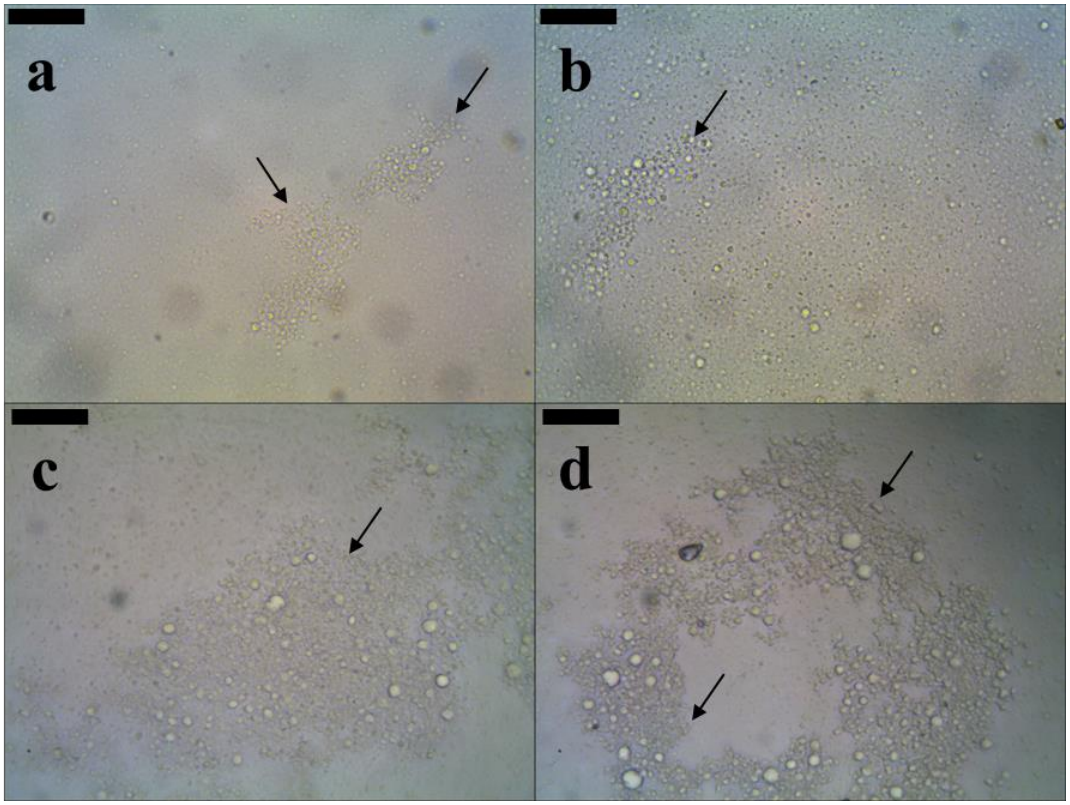

Figure II-5. Microstructural images of lipid nanoparticles prepared by postsonication for 5 min after shearing and aggregating (optical microscopy). (a) SLN; (b) 10% NLC; (c) 20% NLC, and (d) 30% NLC (arrows indicate flocs of aggregated lipid nanoparticles, and scale bars represent 20 μm).

Table II-2. Mean Diameters (MV) of Aggregated Lipid Nanoparticles before and after Gelling[a]

sample		MV (μm)	
postsonication (min)	LCO content (wt %)	before shearing	after shearing
0	0	6.27 ± 0.54 fg	18.43 ± 1.26 def
	10	5.86 ± 0.59 g	15.39 ± 0.65 g
	20	3.42 ± 0.41 i	17.35 ± 0.57 efg
	30	5.46 ± 0.08 gh	26.00 ± 1.42 b
4	0	20.10 ± 0.29 ab	16.15 ± 0.17 fg
	10	10.39 ± 0.71 d	17.28 ± 0.59 efg
	20	5.60 ± 0.39 g	17.97 ± 0.33 cde
	30	3.54 ± 0.34 hi	20.74 ± 0.15 cd
5	0	21.95 ± 0.21 a	18.63 ± 0.87 def
	10	15.13 ± 0.20 c	19.14 ± 1.11 de
	20	8.20 ± 1.27 ef	17.62 ± 0.09 efg
	30	4.80 ± 0.31 ghi	23.59 ± 0.24 bc
6	0	19.98 ± 0.59 ab	18.20 ± 0.53 defg
	10	18.25 ± 0.49 b	16.46 ± 0.66 efg
	20	8.75 ± 0.58 de	22.42 ± 0.64 c
	30	5.94 ± 1.59 g	34.44 ± 2.80 a

[a]Different letters a−i in a column are significantly different at $p < 0.05$.

a-x

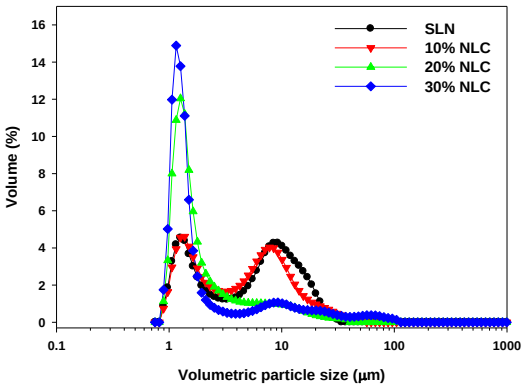

a-y

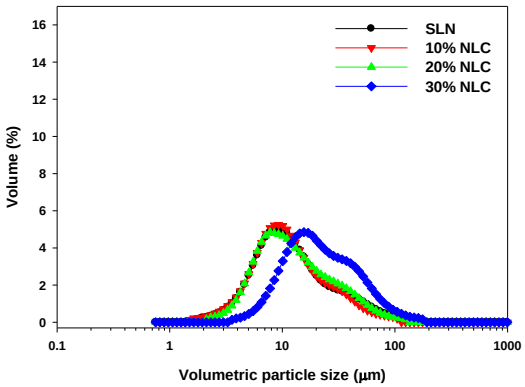

b-x

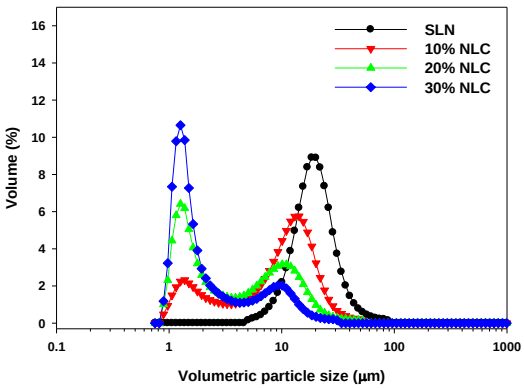

b-y

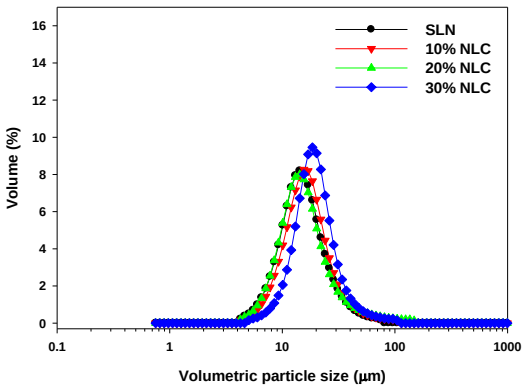

c-x

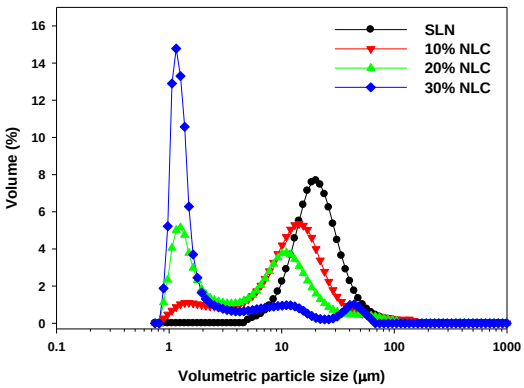

c-y

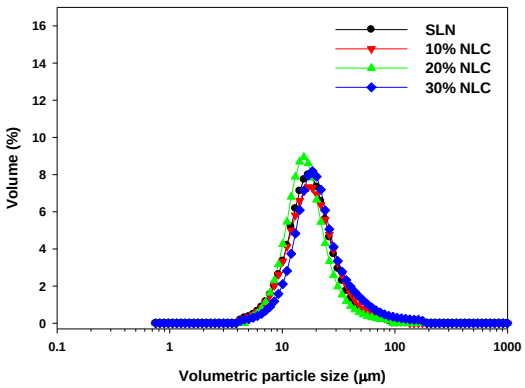

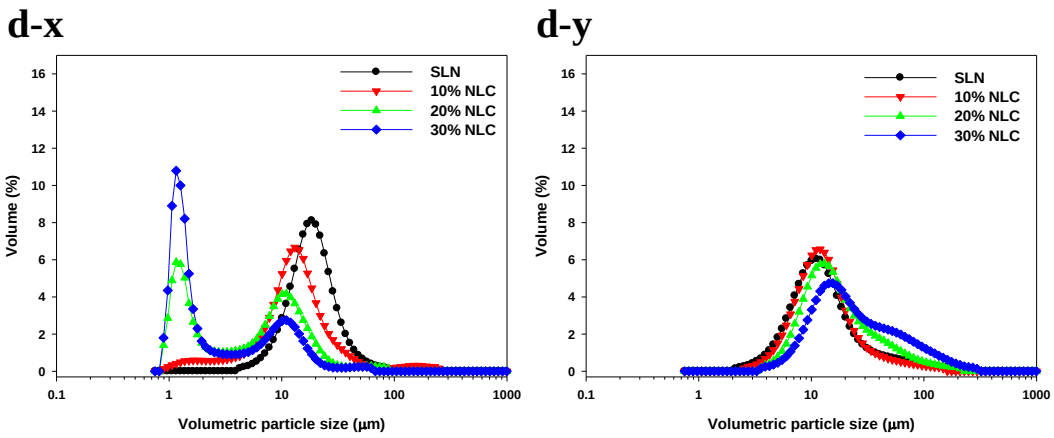

Figure II-6. Particle size distribution of aggregated lipid nanoparticles. Samples fabricated with (a) 0, (b) 4, (c) 5, and (d) 6 min post sonication; (x) before and (y) after applying shear.

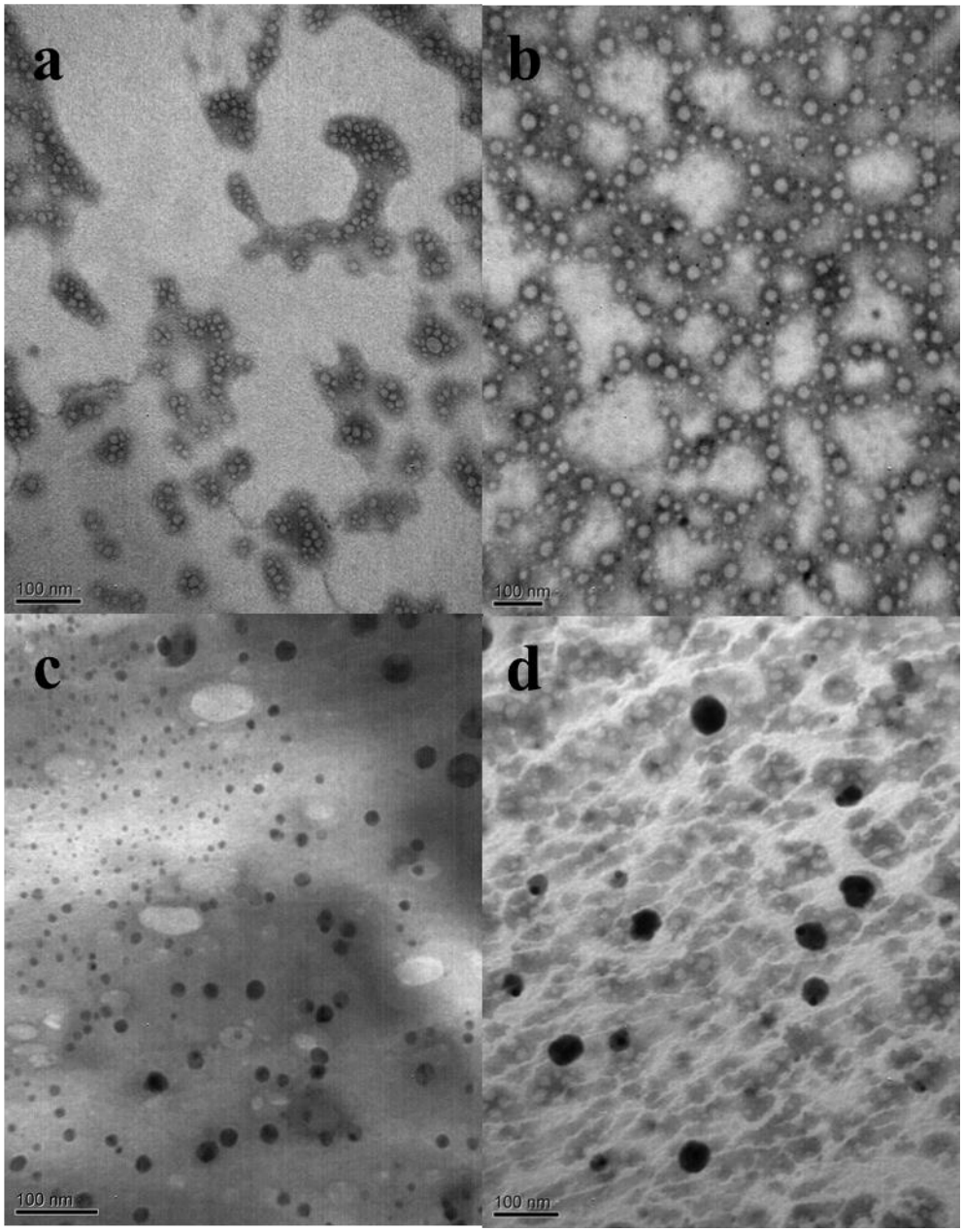

Figure II-7. Nanostructural images of lipid nanoparticles prepared by postsonication for 5 min (TEM). (a) SLN; (b) 10% NLC; (c) 20% NLC, and (d) 30% NLC.

II-3-4. Rheological Properties of Lipid Nanoparticles

Changes in G' and δ were monitored to determine the gelation time during the oscillatory dynamic measurement (Figure II-8). Before a certain time, G' remained close to zero and δ was maintained at a relatively high level (close to 90°), which indicated that the LNP suspension remained fluid. However, over time, the G' of all LNP suspensions increased and their δ decreased, indicating that gelation occurred. With a higher LCO content in the oil phase and a longer PS time, gelation time was extended. Because the gelling phenomena of LNPs were derived from the building of networks with the LNPs and their flocs, a greater gelation time meant that the collision of LNPs and their flocs to create the gel network occurred less frequently at the same shear force. This may be indirect evidence that the LNPs prepared using a longer PS time and greater LCO contents in the oil phase contained more LNPs that did not play a role in gel network formation.

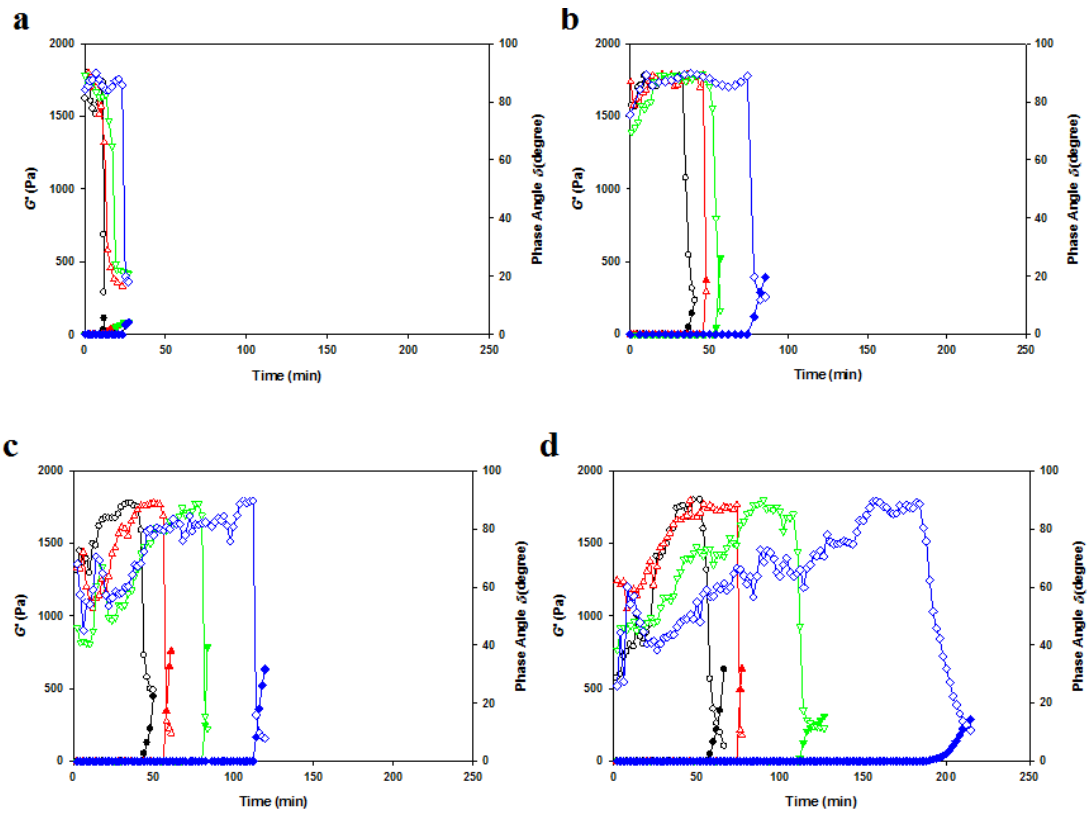

Figure II-8. Storage modulus (*G′*) and phase angle (*δ*) of lipid nanoparticle suspensions during the oscillation time sweep test. (a) SLN; (b) 10% NLC; (c) 20% NLC; (d) 30% NLC (solid circles, up triangles, down triangles, and diamonds are the *G′* values of suspensions prepared by postsonication for 0, 4, 5, and 6 min, respectively; and open circles, up triangles, down triangles, and diamonds are the *δ* values of suspensions prepared by postsonication for 0, 4, 5, and 6 min, respectively).

II-3-5. Thermal Properties of Bulk Lipids and Lipid Nanoparticles

The most abundant fatty acid in FHCO was stearic acid, which suggests that FHCO was composed of tristearin and other minor triacylglycerides. Therefore, the thermal properties of FHCO were expected to be similar to those of tristearin.

In the present study, the DSC thermogram taken after overnight storage at 25 °C showed a single peak corresponding to the melting of β-polymorphic form crystals (Figure II-9a). In other studies, multiple melting peaks of α, β′, and β forms were reported (34). The reason for this discrepancy is transformation of α-form into β-form crystals during overnight storage. The melting temperature (T_m) of the β-polymorphic forms of pure tristearin was 72.1 °C, and the T_c of the α-polymorphic form was 51 °C (35). The T_m (69.6 °C for β-polymorphic form) and T_c (44.8 °C for α-polymorphic form) of FHCO were similar to those of tristearin (Table II-3). The specific XRD lines (0.46, 0.39, and 0.37 nm with WAXS and 4.49 nm with SAXS) for the β form of FHCO in the current study were similar to the previous findings in the case of tristearin (Figure II-10) (35, 36).

The thermogram patterns of FHCO blended with LCO in various weight ratios would be similar to the pattern of FHCO, which comprised a melting peak of the β form and a crystallization peak of the α form (Figure II-9b−d). However, the T_m and T_c of the β- and α-polymorphic forms for each blended lipid differed from those for FHCO (Table II-3).

During heating from 25 to 95 °C, the β-form T_m (69.1 °C) of the lipid mixed

with 90 wt % FHCO and 10 wt % LCO was similar to the T_m (69.6 °C) of FHCO, whereas melting temperatures (both 67.3 °C) of the blended FHCOs with 20 and 30 wt % LCO were lower than the Tm of the FHCO. Melting enthalpies (ΔH_m) of bulk lipids decreased with increasing LCO contents, although enthalpies for the FHCO and the lipid mixed with 90 wt % FHCO and 10 wt % LCO were similar. In addition, all ΔH_m values for the lipids blended with LCO at each ratio (10−30 wt %) were greater than their own theoretical ΔH_m values. In other words, lipids mixed with FHCO and LCO formed more β-form crystals than all β crystals of FHCO comprising the blended lipid matrix. This result suggested that triacylglycerol molecules in FHCO could be cocrystallized with molecules in LCO as the β-form crystals, which is in agreement with other research (37, 38).

With regard to melting of the lipid phase in the LNP system, in the lipid and LNP suspension prepared using the same LCO contents, the T_m values of the lipid phase in the LNP suspension were generally ~2.5 °C lower than those of the bulk lipid. However, the trend of the LNP, in which greater LCO contents decreased the T_m, was similar to those of bulk lipids. Moreover, T_m values of the lipid phase were independent of PS times for preparation. The crystallinity indices (CI) decreased with increasing PS time and LCO contents. In other words, the additional sonication, PS, and the LCO in the lipid phase would inhibit lipid crystal formation.

The CI values of LNP suspensions were lower than those at the time for the crystallization of all FHCO molecules. For example, the lipid phase of the PS6NLC30

sample (Table II-3) consisted of 70 wt % FHCO; nevertheless, the CI of the sample was 57.5%. This may be because LCO in the LNP interferes with formation of the perfect arrangement among FHCO β crystals (39). As a result, the decrease in crystal formation, which originated from increasing both the LCO content and PS time, improved the stability of the LNP system, which is discussed in the following section.

During cooling from 95 to 10 °C, the α-form T_c (44.8 °C) of the FHCO was lower than the T_c (45.2 °C) of the lipid mixed with 90 wt % FHCO and 10 wt % LCO, and the T_c values of the remainder, which were bulk lipids blended with 80 and 70 wt % FHCO and 20 and 30 wt % LCO, decreased with increasing LCO contents. The absolute values of the crystallization enthalpy (ΔH_c) of bulk lipids from 0 to 20 wt % LCO contents decreased from 61.5 to 52.7 J g^{-1}, whereas the absolute values of the ΔH_c of bulk lipids containing 20 and 30 wt % LCO were similar. In addition, on the basis of a comparison of experimental data and the theoretical values corresponding to the amount of FHCO, this result was in agreement with the melting enthalpies (ΔH_m).

The T_c of the α-polymorphic form of emulsified tripalmitin at the nanoscale is lower than that of bulk tripalmitin (25). This phenomenon was also observed in this study (Table II-3). During the DSC scan, the LNPs melted during heating from 25 to 95 °C and then crystallized during cooling from 95 to 10 °C. The LNPs that did not participate in gelation formed individual liquid droplets at the nanoscale during heating, but either they partially coalesced during the LNP preparation or the highly

gelled LNPs, which were attached to each other by hydrophobic interactions, underwent full coalescence and eventually formed large micrometer-scale liquid oil droplets. The DSC thermograms during cooling showed that LNP crystallization occurred at lower temperatures (T_{c2}) for the lipid droplets that were not coalesced compared to the coalesced (T_{c1}) LNPs. The T_{c1} was similar to the T_c of the bulk lipid (FHCO or blended FHCO/LCO), which is in agreement with previous studies (15, 25, 40, 41).

The ratios of the enthalpy values ($\Delta H_{c2}/\Delta H_{c1}$, ΔH_{c2}, and ΔH_{c1} for T_{c2} and T_{c1}, respectively) could be used to determine the quantity of LNPs that did not take part in the partial coalescence and the gelation. As $\Delta H_{c2}/\Delta H_{c1}$ increased, the quantity of particles not participating in the destabilization (the partial coalescence and the gelation) of LNPs increased. The increase in the LCO content in the oil phase increased $\Delta H_{c2}/\Delta H_{c1}$ (Table II-3). Previous findings stated that a higher liquid oil content in the oil phase enhanced the stability of LNPs (41, 42). In this study, the increase in the LCO content of the oil phase improved the stability of the LNPs. In addition, the $\Delta H_{c2}/\Delta H_{c1}$ values increased with increasing PS time. This observation supported the hypothesis that additional sonication during the cooling step of LNP preparation improves the stability of LNPs.

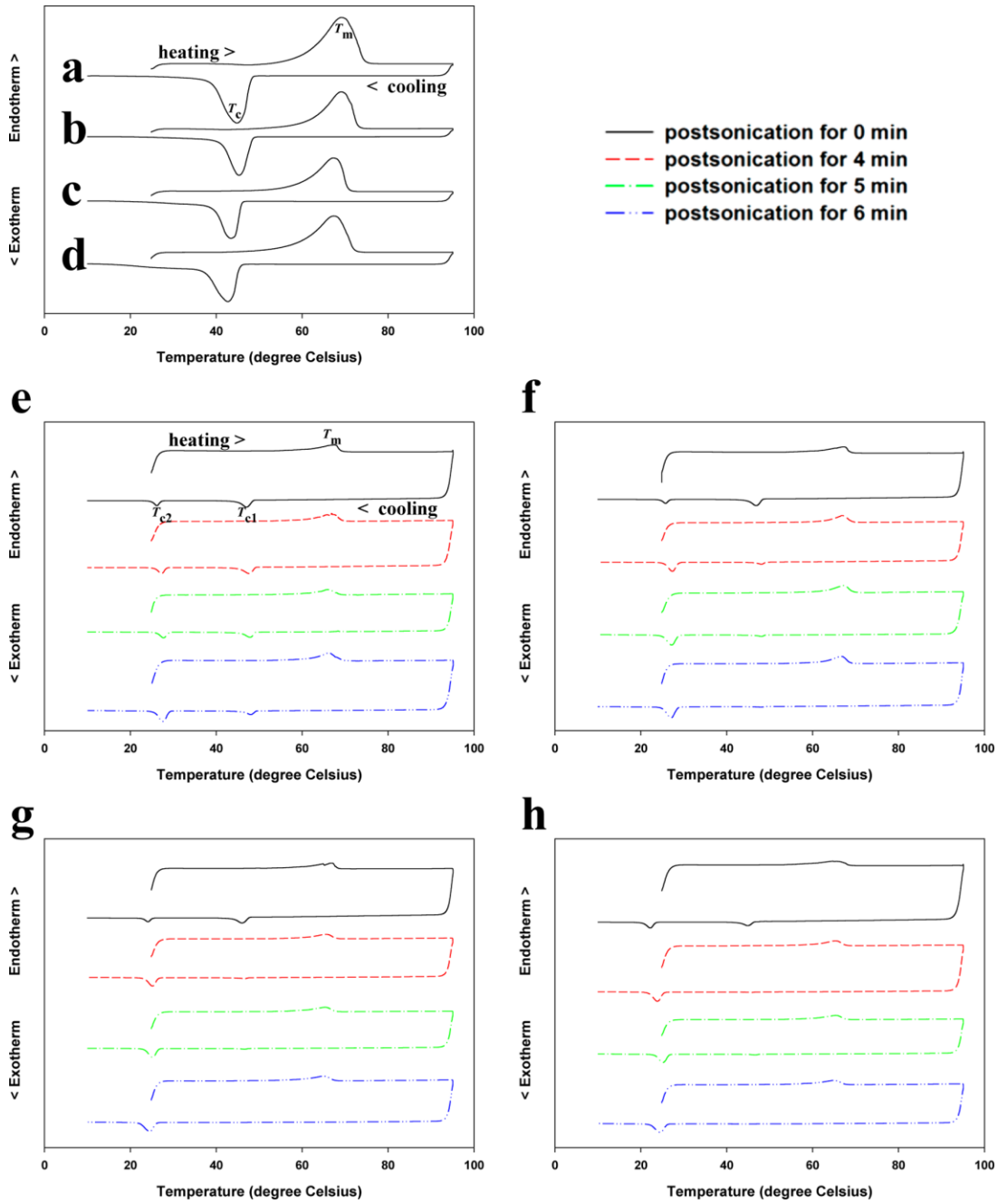

Figure II-9. DSC thermograms of bulk FHCO lipids and lipid nanoparticle suspensions. Bulk lipids containing (a) 0, (b) 10, (c) 20, and (d) 30 wt % LCO; (e) SLN; (f) 10% NLC; (g) 20% NLC; (h) 30% NLC.

Table II-3. Melting and Crystallization Temperatures and Enthalpy Values of Bulk Lipids and Lipid Nanoparticle Suspensions during Heating and Cooling on DSC[a]

	Heating			Cooling				
Sample	T_m (°C)	ΔH_m (J g^{-1})	CI (%)	T_c (°C)	T_{c1} (°C)	T_{c2} (°C)	ΔH_c (J g^{-1})	$\Delta H_{c2}/\Delta H_{c1}$
Bulk lipid								
0%LCO	69.6 ± 0.4 y	86.6 ± 1.8 x	-	44.8 ± 0.1 x	-	-	-61.5 ± 0.2 x	-
10%LCO	69.1 ± 0.2 y	86.5 ± 0.9 x	-	45.2 ± 0.1 w	-	-	-60.3 ± 0.3 y	-
20%LCO	67.3 ± 0.3 z	70.8 ± 2.0 y	-	43.4 ± 0.1 y	-	-	-52.7 ± 0.1 z	-
30%LCO	67.3 ± 0.1 z	66.0 ± 0.4 z	-	42.7 ± 0.1 z	-	-	-53.0 ± 0.1 z	-
Lipid phase								
PS0SLN	67.6 ± 0.2 ab	4.3 ± 0.0 a	98.2 ± 0.8 a	-	48.2 ± 0.2 a	27.2 ± 0.1 a	-	0.4 ± 0.0 i
PS0NLC10	67.3 ± 0.0 ab	4.0 ± 0.1 cd	91.3 ± 1.7 cd	-	47.9 ± 0.1 a	27.3 ± 0.1 a	-	0.4 ± 0.0 i
PS0NLC20	66.4 ± 0.4 bcd	3.4 ± 0.1 f	79.1 ± 2.6 f	-	46.3 ± 0.4 bc	24.6 ± 0.2 b	-	0.4 ± 0.0 i
PS0NLC30	65.5 ± 0.3 de	2.8 ± 0.0 hi	64.9 ± 0.6 hi	-	45.3 ± 0.2 e	23.3 ± 0.1 c	-	1.1 ± 0.1 i
PS4SLN	67.7 ± 0.8 a	4.2 ± 0.1 ab	98.1 ± 1.2 ab	-	47.7 ± 0.4 a	27.3 ± 0.1 a	-	0.8 ± 0.0 i
PS4NLC10	66.8 ± 0.1 ab	3.8 ± 0.0 de	87.9 ± 1.0 de	-	47.8 ± 0.2 a	27.3 ± 0.3 a	-	4.5 ± 0.5 gh
PS4NLC20	65.0 ± 0.2 e	3.1 ± 0.1 g	72.0 ± 1.1 g	-	46.3 ± 0.4 bc	24.5 ± 0.0 b	-	15.2 ± 0.7 f
PS4NLC30	64.7 ± 0.5 e	2.7 ± 0.1 ij	65.7 ± 1.1 ij	-	45.5 ± 0.1 de	23.1 ± 0.0 c	-	32.9 ± 3.9 d
PS5SLN	67.0 ± 0.7 ab	4.2 ± 0.1 ab	95.9 ± 2.2 ab	-	48.2 ± 0.2 a	27.9 ± 0.3 a	-	1.0 ± 0.0 i
PS5NLC10	66.9 ± 0.2 ab	3.8 ± 0.1 de	87.0 ± 1.4 de	-	48.2 ± 0.5 a	27.3 ± 0.1 a	-	8.7 ± 1.2 g
PS5NLC20	65.4 ± 0.2 de	3.0 ± 0.0 gh	68.2 ± 0.8 gh	-	46.3 ± 0.3 bcd	24.7 ± 0.5 b	-	27.3 ± 2.4 e
PS5NLC30	65.2 ± 0.2 e	2.6 ± 0.0 jk	59.9 ± 0.8 jk	-	45.6 ± 0.3 cde	23.3 ± 0.6 c	-	41.5 ± 4.7 c
PS6SLN	67.3 ±0.8 ab	4.1 ± 0.1 bc	93.7 ± 1.5 bc	-	47.9 ± 0.1 a	27.8 ± 0.2 a	-	2.7 ± 0.1 i
PS6NLC10	66.7 ±0.5 abc	3.7 ± 0.1 e	85.6 ± 1.2 e	-	48.0 ± 0.1 a	27.3 ± 0.2 a	-	17.0 ± 1.1 f
PS6NLC20	65.4 ±0.1 cde	2.8 ± 0.0 hi	65.0 ± 0.8 hi	-	46.5 ± 0.2 b	25.0 ± 0.2 b	-	53.7 ± 0.7 b
PS6NLC30	65.1 ±0.2 e	2.5 ± 0.1 k	57.5 ± 2.1 k	-	45.6 ± 0.2 cde	23.5 ± 0.3 c	-	76.6 ± 0.7 a

[a]Different letters w−z and a−k in a column within bulk lipid and lipid phase are significantly different at $p < 0.05$, respectively.

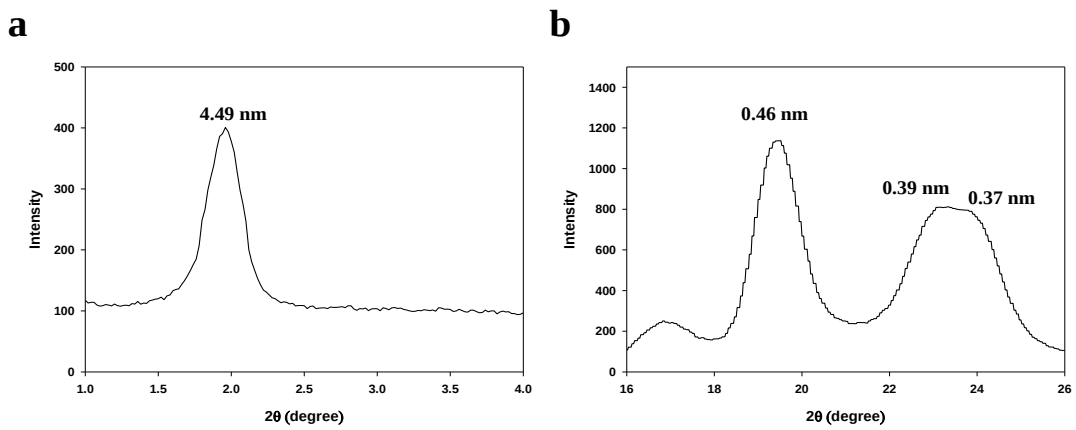

Figure II-10. X-ray diffractograms of bulk FHCO. (a) Small angle X-ray scattering, and (b) wide angle X-ray scattering.

II-3-6. Proposed Mechanisms of the Increased Stability of Lipid Nanoparticles Due to Additional Sonication and Liquid Canola Oil in the Oil Phase

Emulsifiers densely covering the surface of LNPs could prevent the FHCO from forming β-polymorphic crystals during cooling and storage (15). As discussed above, the formation of β crystals increases the likelihood of formation of hydrophobic patches on the surface of the particle. Thus, the increase in emulsifier density on the particle surface could prevent gelation and enhance the stability of LNPs. In the present study, the amount of Tween 20 per unit surface area of LNPs is shown in Table II-4, which was based on the assumption that the shape of all LNPs was similar to a sphere. The Tween 20 surface load increased in proportion with increasing PS processing time or the LCO content in the oil phase. In particular, the surface load of the sample prepared using 6 min of PS and a 30 wt % LCO content was 10.29 mg m^{-2}. Despite the lower ratio (1/3) of the amount of Tween 20 to the lipid phase volume, this value was greater than that (8.1 mg m^{-2}) for SLN prepared using 10 wt % lipid and 10 wt % Tween 20 (1/1) reported by Nik et al. (34). Therefore, both the additional sonication process during cooling and the presence of liquid oil in the lipid matrix might result in effective emulsification of LNP by Tween 20 in contrast to that found by other researchers.

There are three possible reasons for the existence of both the stable and nonstable particles: (i) particle size of all lipid droplets is not equal, (ii) cavitation effect of a sonication method can not act perfectly even on all droplets during the LNP

preparation, and (iii) perfect control of crystallization and partial coalescence as a deterioration mechanism is not possible during the LNP preparation. Thereby, both stable (nonaggregated) and nonstable (aggregated) particles were dispersed in an LNP sample system. Among the nonstable particles, partially coalesced particles cannot be transformed into the stable particles after the preparation because the particles are already solidified, and nonstable particles having hydrophobic patches could not be also converted to the stable particles unless more emulsifier is added in the LNP dispersion system, because the finished crystallization of the particles already determine the particle shape. Meanwhile, the stable particles cannot be partially coalesced due to their solid state but can be aggregated during long period storage due to the collision between particles having Browinian motion. For this reason, in this study, yield values of LNPs were measured within a day after the preparation. The nonaggregated stable LNPs were nanosized particles, but the aggregated nonstable particles were micrometer-sized. The stable particles could pass through the filter (pore size = 1 μm), whereas the aggregated particles remained on the filter. The contents of the nonaggregated LNPs are shown in Table II-4. The amount of stable nanoparticles increased with increasing PS time and LCO content in the oil phase, which was similar to the tendency in the Tween 20 surface load. This result confirmed that a longer PS time and a greater LCO content in the oil phase are suitable conditions for preparing stable LNP systems.

In the conventional method for LNP preparation (Figure II-11a), the formation

of Tween 20 micelles at high temperature could reduce the amount of Tween 20 molecules available to stabilize the interface between the oil and water phases (23, 24) and induce the formation of coalesced micrometer-sized oil droplets. During the cooling procedure, these coalesced micrometer droplets at T_{c1} could be crystallized and transformed to destabilized particles with hydrophobic patches, which may be partially coalesced with noncrystallized liquid droplets (21). What was worse, nanoparticles with low Tween 20 surface load levels could be crystallized at T_{c2} and transformed into unstable particles having hydrophobic patches (25, 26), which could be aggregates of nonstable particles. Consequently, flocs of these nonstable particles, which are the partially coalesced particles or the particles aggregated by hydrophobic patches, could float and be creamed.

In the present study, the positive effects on LNP stability of PS and liquid oil content could be explained by two mechanisms. First, the PS during the cooling procedure induces Tween 20 molecules to form micelles, which move and stabilize the LNP surface (Figure II-11b). That is, Tween 20 molecules at higher temperature would be more stable in the form of micelles and less likely to adsorb at the interface of the LNP (23, 24). The PS could break the micelles and enhance the coating of the LNP by Tween 20. Therefore, the nanosized oil droplets processed with the PS, which are not coalesced, could crystallize at the T_{c2} and disperse throughout the system. Because the surfactant covering the lipid would compete with the lipid crystallization at the interface (28, 34) the PS process could decrease the CI of LNPs, as discussed

in a previous section (Table II-3). In other words, the better adsorption of surfactants at the interface, caused by the longer PS, could more effectively inhibit the crystallization of lipid matrices. Second, the liquid oil could interfere with crystallization of the oil phase and decrease the likelihood of morphological transition from a sphere to a rod shape (Figure II-11c). Thus, the increase in liquid oil content in the oil phase could not only prevent the formation of hydrophobic patches but also reduce the surface area. This could contribute to the reduction of Tween 20 surface load (Table II-4). Consequently, these synergetic effects that originated from the additional sonication during cooling and the presence of liquid oil in the oil phase increased the stability of the lipid nanoparticle system.

According to the characteristics of the blended lipid, FHCO and LCO are appropriate for use as carrier matrix lipids and for the application of LNPs in food systems. The PS step prevents the intensive aggregation and gelation of LNPs, which have been problems in LNP systems. These results confirmed the hypothesis that PS and the LCO content of a lipid matrix could improve LNP stability. Compared with the traditional methods for LNP preparation, the process introduced in this study could allow food companies to fabricate more stable LNPs. In conclusion, stable FHCO LNP systems as carrier systems of bioactive materials could be used for functional foods.

Table II-4. Tween 20 Surface Load and the Quantity Values of Nonaggregated Lipid Nanoparticles[a]

sample			
postsonication (min)	LCO content (wt %)	Tween 20 surface load (mg m^{-2})	content of nonaggregated particle (%)
0	0	6.34 ± 0.03 h	34.9 ± 0.2 i
	10	6.39 ± 0.06 h	34.6 ± 0.7 i
	20	6.44 ± 0.01 h	35.7 ± 0.9 hi
	30	7.50 ± 0.04 ef	49.1 ± 1.8 fg
4	0	6.65 ± 0.14 gh	39.5 ± 1.5 ghi
	10	7.39 ± 0.08 f	54.7 ± 5.7 ef
	20	8.00 ± 0.03 d	63.9 ± 3.9 de
	30	9.57 ± 0.09 b	76.7 ± 3.8 bc
5	0	6.98 ± 0.10 g	42.2 ± 2.6 ghi
	10	7.77 ± 0.12 de	61.4 ± 4.2 de
	20	8.47 ± 0.10 c	70.6 ± 5.8 bcd
	30	9.77 ± 0.10 b	80.6 ± 2.7 ab
6	0	7.44 ± 0.05 ef	47.1 ± 5.6 fgh
	10	7.95 ± 0.14 d	66.6 ± 3.3 cd
	20	8.58 ± 0.09 c	78.6 ± 5.5 b
	30	10.29 ± 0.35 a	90.1 ± 4.7 a

[a]Different letters a−i in a column are significantly different at $p < 0.05$.

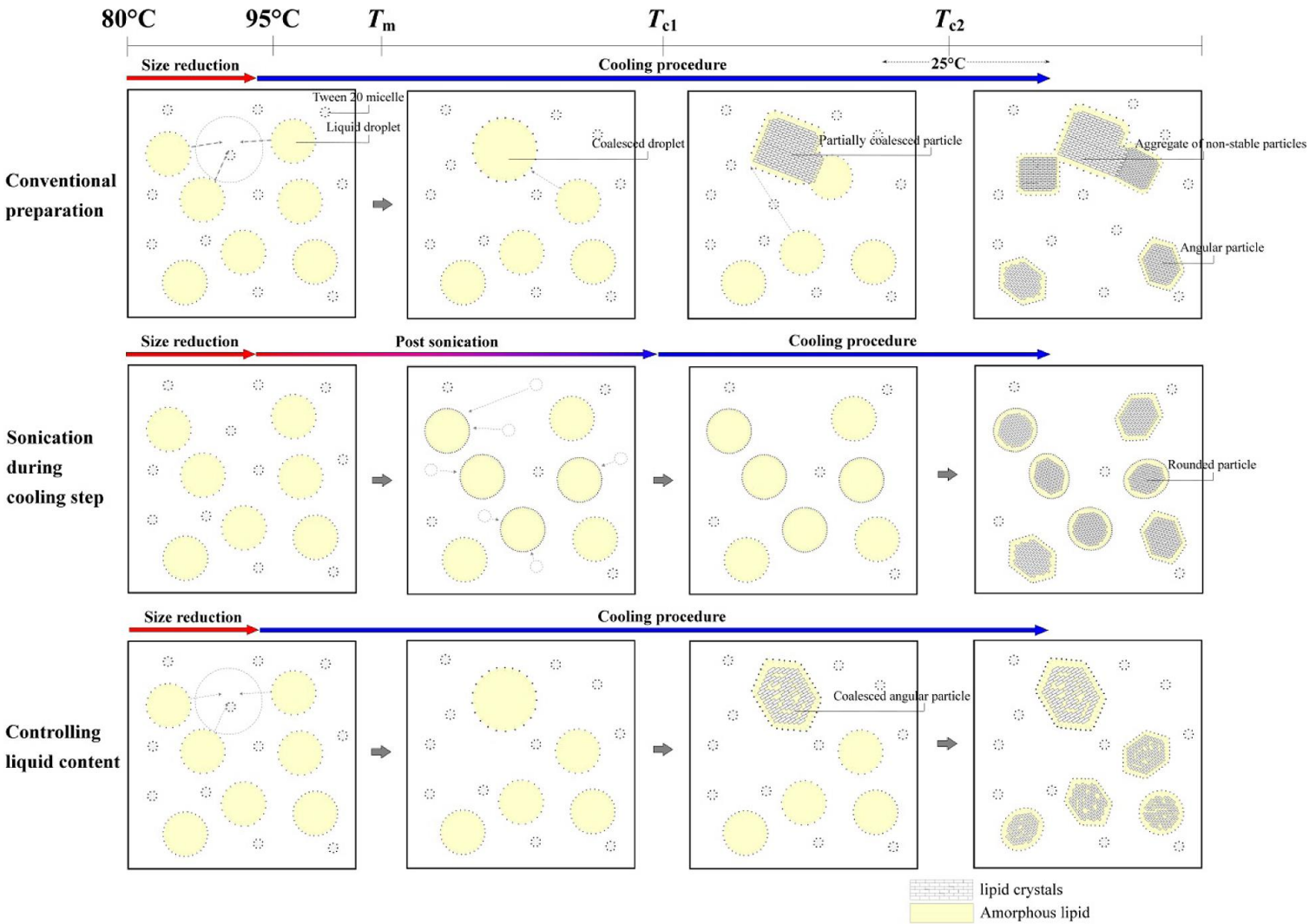
80°C
95°C
T_m
T_{c1}
T_{c2}
Size reduction
Cooling procedure
25°C
Tween 20 micelle
Liquid droplet
Coalesced droplet
Partially coalesced particle
Aggregate of non-stable particles
Angular particle
Conventional preparation
Size reduction
Post sonication
Cooling procedure
Rounded particle
Sonication during cooling step
Size reduction
Cooling procedure
Coalesced angular particle
Controlling liquid content
lipid crystals
Amorphous lipid

Figure II-11. Schematic representation of the dispersion stability of lipid nanoparticles. Fabrication using the (a, top) conventional preparation, (b, middle) additional sonication (postsonication) during cooling, and (c, bottom) a solid lipid phase containing liquid canola oil.

II-4. References

(1) Müller, R. H.; Mäder, K.; Gohla, S. H. Solid lipid nanoparticles (SLN) for controlled drug delivery − a review of the state of the art. *Eur. J. Pharm. Biopharm.* **2000**, *50*, 161−177.

(2) Müller, R. H.; Radtke, M.; Wissing, S. A. Nanostructured lipid matrices for improved microencapsulation of drugs. *Int. J. Pharm.* **2002**, *242*, 121−128.

(3) Müller, R. H. *Colloidal Carriers for Controlled Drug Delivery and Targeting: Modification, Characterization and in Vivo Distribution*; Taylor & Francis: Boca Raton, FL, USA, 1991.

(4) Wissing, S. A.; Kayser, O.; Müller, R. H. Solid lipid nanoparticles for parenteral drug delivery. *Adv. Drug Delivery Rev.* **2004**, *56*, 1257−1272.

(5) Hu, F. Q.; Jiang, S. P.; Du, Y. Z.; Yuan, H.; Ye, Y. Q.; Zeng, S. Preparation and characteristics of monostearin nanostructured lipid carriers. *Int. J. Pharm.* **2006**, *314*, 83−89.

(6) Mehnert, W.; Mäder, K. Solid lipid nanoparticles: production, characterization and applications. *Adv. Drug Delivery Rev.* **2001**, *47*, 165−196.

(7) Ricci, M.; Puglia, C.; Bonina, F.; Giovanni, C. D.; Giovagnoli, S.; Rossi, C. Evaluation of indomethacin percutaneous absorption from nanostructured lipid carriers (NLC): *in vitro* and *in vivo* studies. *J. Pharm. Sci.* **2005**, *94*, 1149−1159.

(8) Souto, E. B.; Müller, R. H. Investigation of the factors influencing the

incorporation of clotrimazole in SLN and NLC prepared by hot high-pressure homogenization. *J. Microencapsul.* **2006**, *23*, 377−388.

(9) Hu, F. Q.; Jiang, S. P.; Du, Y. Z.; Yuan, H.; Ye, Y. Q.; Zeng, S. Preparation and characterization of stearic acid nanostructured lipid carriers by solvent diffusion method in an aqueous system. *Colloids Surf., B* **2005**, *45*, 167−173.

(10) Jenning, V.; Gohla, S. H. Encapsulation of retinoids in solid lipid nanoparticles (SLN). *J. Microencapsul.* **2001**, *18*, 149−158.

(11) Souto, E. B.; Wissing, S. A.; Barbosa, C. M.; Müller, R. H. Development of a controlled release formulation based on SLN and NLC for topical clotrimazole delivery. *Int. J. Pharm.* **2004**, *278*, 71−77.

(12) Souto, E. B.; Wissing, S. A.; Barbosa, C. M.; Müller, R. H. Evaluation of the physical stability of SLN and NLC before and after incorporation into hydrogel formulations. *Eur. J. Pharm. Biopharm.* **2004**, *58*, 83−90.

(13) Jores, K.; Mehnert, W.; Drechsler, M.; Bunjes, H.; Johann, C.; Mäder, K. Investigations on the structure of solid lipid nanoparticles (SLN) and oil-loaded solid lipid nanoparticles by photon correlation spectroscopy, field-flow fractionation and transmission electron microscopy. *J. Controlled Release* **2004**, *95*, 217−227.

(14) Castelli, F.; Puglia, C.; Sarpietro, M. G.; Rizza, L.; Bonina, F. Characterization of indomethacin-loaded lipid nanoparticles by differential scanning calorimetry. *Int. J. Pharm.* **2005**, *304*, 231−238.

(15) Helgason, T.; Awad, T. S.; Kristbergsson, K.; McClements, D. J.; Weiss, J. Effect of surfactant surface coverage on formation of solid lipid nanoparticles (SLN). *J. Colloid Interface Sci.* **2009**, *334*, 75−81.

(16) Bunjes, H.; Steiniger, F.; Richter, W. Visualizing the structure of triglyceride nanoparticles in different crystal modifications. *Langmuir* **2007**, *23*, 4005−4011.

(17) Hatziantoniou, S.; Deli, G.; Nikas, Y.; Demetzos, C.; Papaioannou, G. T. Scanning electron microscopy study on nanoemulsions and solid lipid nanoparticles containing high amounts of ceramides. *Micron* **2007**, *38*, 819−823.

(18) Jenning, V.; Schäfer-Korting, M.; Gohla, S. H. Vitamin A-loaded solid lipid nanoparticles for topical use: drug release properties. *J. Controlled Release* **2000**, *66*, 115−126.

(19) Westesen, K.; Siekmann, B. Investigation of the gel formation of phospholipid-stabilized solid lipid nanoparticles. *Int. J. Pharm.* **1997**, *151*, 35−45.

(20) Freitas, C.; Müller, R. H. Correlation between long-term stability of solid lipid nanoparticles (SLN) and crystallinity of the lipid phase. *Eur. J. Pharm. Biopharm.* **1999**, *47*, 125−132.

(21) Boode, K.; Walstra, P. Partial coalescence in oil-in-water emulsions. 1. Nature of the aggregation. *Colloids Surf., A* **1993**, *81*, 121−137.

(22) Vanapalli, S. A.; Coupland, J. N. Emulsions under shear – the formation and properties of partially coalesced lipid structures. *Food Hydrocolloids* **2001**, *15*, 507−512.

(23) Alexandridis, P.; Alan Hatton, T. Poly (ethylene oxide)-poly (propylene oxide)-poly (ethylene oxide) block copolymer surfactants in aqueous solutions and at interfaces: thermodynamics, structure, dynamics, and modeling. *Colloids Surf., A* **1995**, *96*, 1−46.

(24) Ruiz, C. C.; Molina-Bolívar, J.; Aguiar, J.; MacIsaac, G.; Moroze, S.; Palepu, R. Effect of ethylene glycol on the thermodynamic and micellar properties of Tween 20. *Colloid Polym. Sci.* **2003**, *281*, 531−541.

(25) Helgason, T.; Awad, T. S.; Kristbergsson, K.; McClements, D. J.; Weiss, J. Influence of polymorphic transformations on gelation of tripalmitin solid lipid nanoparticle suspensions. *J. Am. Oil Chem. Soc.* **2008**, *85*, 501−511.

(26) Trujillo, C. C.; Wright, A. J. Properties and stability of solid lipid particle dispersions based on canola stearin and Poloxamer 188. *J. Am. Oil Chem. Soc.* **2010**, *87*, 715−730.

(27) Jia, L.; Zhang, D.; Li, Z.; Duan, C.; Wang, Y.; Feng, F.; Wang, F.; Liu, Y.; Zhang, Q. Nanostructured lipid carriers for parenteral delivery of silybin: biodistribution and pharmacokinetic studies. *Colloids Surf., B* **2010**, *80*, 213−218.

(28) Schubert, M. A.; Müller-Goymann, C. C. Characterisation of surface-modified solid lipid nanoparticles (SLN): influence of lecithin and nonionic emulsifier. *Eur. J. Pharm. Biopharm.* **2005**, *61*, 77−86.

(29) McClements, D. J. Critical review of techniques and methodologies for characterization of emulsion stability. *Crit. Rev. Food Sci.* **2007**, *47*, 611−649.

(30) Khossravi, M.; Kao, Y. H.; Mrsny, R. J.; Sweeney, T. D. Analysis methods of polysorbate 20: a new method to assess the stability of polysorbate 20 and established methods that may overlook degraded polysorbate 20. *Pharm. Res.* **2002**, *19*, 634−639.

(31) Manjunath, K.; Venkateswarlu, V. Pharmacokinetics, tissue distribution and bioavailability of clozapine solid lipid nanoparticles after intravenous and intraduodenal administration. *J. Controlled Release* **2005**, *107*, 215−228.

(32) Silverstein, T. P. The real reason why oil and water don't mix. *J. Chem. Educ.* **1998**, *75*, 116.

(33) Reiffers-Magnani, C. K.; Cuq, J. L.; Watzke, H. J. Depletion flocculation and thermodynamic incompatibility in whey protein stabilised O/W emulsions. *Food Hydrocolloids* **2000**, *14*, 521−530.

(34) Nik, A. M.; Langmaid, S.; Wright, A. J. Nonionic surfactant and interfacial structure impact crystallinity and stability of β-carotene loaded lipid nanodispersions. *J. Agric. Food Chem.* **2012**, *60*, 4126−4135.

(35) Elisabettini, P.; Desmedt, A.; Durant, F. Polymorphism of stabilized and nonstabilized tristearin, pure and in the presence of food emulsifiers. *J. Am. Oil Chem. Soc.* **1996**, *73*, 187−192.

(36) Bunjes, H.; Westesen, K.; Koch, M. H. J. Crystallization tendency and polymorphic transitions in triglyceride nanoparticles. *Int. J. Pharm.* **1996**, *129*, 159−173.

(37) Danthine, S. Blending of hydrogenated low-erucic acid rapeseed oil, low-erucic acid rapeseed oil, and hydrogenated palm oil or palm oil in the preparation of shortenings. *J. Am. Oil Chem. Soc.* **2003**, *80*, 1069−1075.

(38) Himawan, C.; Starov, V. M.; Stapley, A. G. F. Thermodynamic and kinetic aspects of fat crystallization. *Adv. Colloid Interface Sci.* **2006**, *122*, 3−33.

(39) Teeranachaideekul, V.; Boonme, P.; Souto, E. B.; Müller, R. H.; Junyaprasert, V. B. Influence of oil content on physicochemical properties and skin distribution of Nile red-loaded NLC. *J. Controlled Release* **2008**, *128*, 134−141.

(40) Awad, T. S.; Helgason, T.; Kristbergsson, K.; Decker, E. A.; Weiss, J.; McClements, D. J. Effect of cooling and heating rates on polymorphic transformations and gelation of tripalmitin solid lipid nanoparticle (SLN) suspensions. *Food Biophys.* **2008**, *3*, 155−162.

(41) Qian, C.; Decker, E. A.; Xiao, H.; McClements, D. J. Solid lipid nanoparticles: effect of carrier oil and emulsifier type on phase behavior and physical stability. *J. Am. Oil Chem. Soc.* **2012**, *89*, 17−28.

(42) Yucel, U.; Elias, R. J.; Coupland, J. N. Effect of liquid oil on the distribution and reactivity of a hydrophobic solute in solid lipid nanoparticles. *J. Am. Oil Chem. Soc.* **2013**, *90*, 819−824.

Chapter III. Improving Flavonoid Bioaccessibility using an Edible Oil-Based Lipid Nanoparticle for Oral Delivery

Published in Journal of Agricultural and Food Chemistry

(C. Ban, S. J. Park, S. Lim, S. J. Choi, and Y. J. Choi, *J. Agric. Food Chem.* 2015, 63, 5266-5272)

III-1. Introduction

Quercetin is the representative flavonol in various vegetables and fruits such as onion and apple (1) and has antioxidative (2) anticarcinogenic (3), anti-inflammatory (4), antiaggregatory (5), and vasodilatory (6) effects. Naringenin and hesperetin are the representative flavanones in various fruits, such as orange, lemon, and grape (7); they have antioxidant (8) and anti-inflammatory (9) activities and influence lipid (10) and sex hormone metabolism (11). This could imply that quercetin, narigenin, and hesperetin, as the major flavonoids, are easy to take in from foods in the common diet and have crucial roles in human health. Despite their health benefits, the parent forms have low bioavailability because of their low water solubility. Although these compounds can be ingested as their glycosides, such as rutin, naringin, and hesperidin, directly from vegetables and orange/grape juices to increase bioavailability, plasma flavonoid levels are low in comparison to the amount ingested (12, 13). Moreover, as flavonoid glycosides are cleaved by enzymes and microflora before absorption in the small and large intestines, respectively, bioavailability could vary among individuals (1). Therefore, the bioavailability of the flavonoid parent forms must be improved.

Lipid nanoparticle (LNP) systems have drawn attention for using physiological lipids, protection of core materials, and improvement of the oral bioaccessibility of lipophilic materials; due to their submicron size, they have an

increased residence time by adhering to the gastrointestinal wall or entering the intervillar spaces (14). Some researchers have recently reported that the bioaccessibility of polyphenols such as resveratrol (15), curcumin, and genistein (16) was enhanced by LNP encapsulation. Despite the benefits of oral administration of bioactive lipophilic molecules such as flavonoids, colloidal stability problems such as aggregation impede food applications. The LNP matrix crystallizes into a β polymorphic form during cooling and can cause morphological changes in individual particles and increase surfactant-depleted areas (hydrophobic patches) of the LNP, resulting in aggregation due to interactions between hydrophobic patches that minimize the uncovered surface area facing the water phase (17). Additionally, partial coalescence of oil droplets containing crystals during cooling can cause aggregation (18, 19). Thus, methods to enhance stability have been reported, including using a lipid source that prevents or retards β-form crystallization (20) and using an emulsifier that prevents particle aggregation by increasing steric hindrance and electrostatic repulsive forces (21).

The behavior of flavonoid-loaded LNPs in the oral and gastrointestinal tracts has been described to demonstrate their benefits when the system is adopted to enhance bioaccessibility and protect against physical and biochemical stressors, such as salts, pH, and digestive enzymes (22). For the same reason, the digestion of LNPs encapsulating bioactive lipophilic components (nutraceuticals) has been evaluated extensively. LNPs mix with saliva in the mouth (neutral pH) after ingestion and then

travel to the stomach (pH 1−3), which provides complex flow and changes the pH, ionic strength, and digestive enzyme levels (23, 24) that could promote oxidation of nutraceuticals and particle aggregation due to flocculation and/or coalescence. After it enters the small intestine, the mixture of LNPs, saliva, and gastric juice is blended with duodenal and bile juices containing pancreatic lipase, colipase, bile salts, phospholipids, and bicarbonate, and digestive enzymes convert LNP triacylglycerides into monoglycerides and free fatty acids. The products of lipid digestion are taken up into bile salt/phospholipid micelles, and the mixed micelles incorporate the nutraceuticals, resulting in transportation of the micelles to the surfaces of enterocytes, where they are absorbed (21).

Therefore, LNPs encapsulating flavonoids must be resistant to the harsh conditions in the mouth and stomach to improve their bioaccessibility and protect them until they are absorbed into enterocytes. Unfortunately, many studies have investigated the individual digestion process of LNPs under *in vivo* and *in vitro* conditions of the mouth, stomach, or small intestine, making it difficult to describe the serial events occurring in an actual digestive system. In this study, the composition of LNPs prepared using food-grade materials−including fully hydrogenated canola oil as the solid lipid, liquid oils (liquid soybean oil, squalene, or canola oil) to prevent or retard crystallization, Tween 20 as a nonionic emulsifier to produce a steric effect, and soybean lecithin as an ionic emulsifier providing electrostatic repulsive force−was optimized in terms of colloidal stability. Furthermore, the fates of quercetin-,

naringenin-, and hesperetin-loaded LNPs during the serial events of digestion in the mouth, stomach, and small intestine were mimicked in simulated digestive media.

III-2. Materials and Methods

III-2-1. Chemicals

Lotte Samkang Co. Ltd. (Seoul, Korea) provided fully hydrogenated canola oil (FHCO), which was composed of 79.5 wt % stearic acid, 8.8 wt % palmitic acid, 4.2 wt % oleic acid, 1.8 wt % lauric acid, 1.6 wt % arachidic acid, 1.4 wt % linoleic acid, 0.9 wt % myristic acid, and 1.8 wt % other ingredients. Liquid soybean oil (LSO; 49.3 wt % linoleic acid, 23.2 wt % oleic acid, 10.2 wt % palmitic acid, 4.9 wt % linolenic acid, 3.8 wt % stearic acid, 0.3 wt % arachidic acid, 0.2 wt % lauric acid, 0.2 wt % erucic acid, 0.1 wt % myristic acid, and 7.7 wt % other ingredients) and liquid canola oil (LCO; 58.3 wt % oleic acid, 20.0 wt % linoleic acid, 8.3 wt % linolenic acid, 4.4 wt % palmitic acid, 1.8 wt % stearic acid, 1.3 erucic acid, 0.6 wt % arachidic acid, and 5.3 wt % other ingredients) were obtained from CJ Cheiljedang Co. (Seoul, Korea). Squalene (>98%; SQ) was obtained from Alfa Aesar (Heysham, England). Tween 20 (T20; polyoxyethylene sorbitan monolaurate) and soybean lecithin (SL) were purchased from Sigma-Aldrich Co. (St. Louis, MO, USA) and Fisher Scientific (Pittsburgh, PA, USA), respectively. Quercetin and naringenin were obtained from MP Biomedicals LLC (Solon, OH, USA), and hesperetin was obtained from Sigma-Aldrich Co. All other chemicals were of analytical reagent grade.

III-2-2. Lipid Nanoparticle Production

The LNPs were prepared using an oil-in-water emulsion technique with a high-speed blender and sonication probe as reported previously by us (17), with a slight modification. First, the lipid (5 wt %) and aqueous (95 wt %) phases were heated to 85 °C, mixed using a high-speed blender (Ultra-Turrax T25D, Ika Werke GmbH & Co., Staufen, Germany) at 8000 rpm for 1 min and then at 11000 rpm for 1 min, and maintained at 85 °C; the lipid phase of the blank LNPs was a mixture of 5−3.5 wt % FHCO (100−70 wt % of the lipid phase) and 0−1.5 wt % of each liquid oil (0−30 wt % of the lipid phase) among LSO, LCO, and SQ; and the aqueous phase was prepared by adding an emulsifier mixture (one-third of the lipid phase weight) composed of T20 (100−0 wt % of the emulsifier mixture) and SL (0−100 wt % of the mixture) in doubly distilled water (DDW) containing 0.02 wt % sodium azide. After the coarse oil-in-water emulsion was produced, the droplet size was further reduced by sonication (VCX 750, Sonics & Materials Inc., Newtown, CT, USA) for 4 min at 60% amplitude, a duty cycle of 1 s, and 95 °C. After the droplet size was reduced, postsonication for 6 min was applied to the emulsions during cooling to 25 °C in a jacketed beaker, and the samples were maintained at room temperature (25 °C).

The lipid phase was composed of FHCO blended with 30 wt % SQ of the phase to prepare the LNP-loaded flavonoid molecules (quecetin, naringenin, and hesperetin) and the additional flavonoids of 0.1−0.5 wt % concentration in the lipid; a mixture of T20 (32.28 wt % of the mixture) and SL (67.72 wt % of the mixture) was

used as an emulsifier in the aqueous phase to optimize system stability. The lipid phase incorporating the flavonoids was stirred gently at 85 °C for 30 min, and the remaining production process was conducted as for the blank LNP.

III-2-3. Quantification of Nonaggregated Lipid Nanoparticles (Yield)

LNPs diluted 10-fold with DDW were passed through a 1 μm pore size glass microfiber filter (GF/B, Whatman Ltd., Loughborough, U.K.). The aggregated LNPs remaining on the filter (micrometer scale) were weighed after drying in an oven at 50 °C. The difference in filter weights before and after the procedure, which was the weight of the creamed or aggregated LNPs, was recorded.

III-2-4. Measurements of Lipid Nanoparticle Size and ζ Potential

The prepared LNPs (4.5 mL) were diluted with 40.5 mL of DDW in a vial to separate the layers containing the creamed (creaming layer) and noncreamed LNPs (aqueous layer). The vial containing the diluted samples was sealed tightly with a screw cap and incubated overnight at room temperature. The LNPs in the aqueous layer were collected by filtering with a 1 μm pore size glass microfiber filter (GF/B, Whatman Ltd.) to determine the size of the noncreamed LNP, and their mean particle size (z average) and polydispersity index (PDI) were measured using a Zetasizer instrument (Nano ZS, Malvern Instruments Ltd., Worcestershire, U.K.) operated at a 173° angle with a helium−neon laser (λ 633 nm). In addition, the ζ potential (ZP) was measured using the Zetasizer. The ZP measurement was based on the Smoluchowski equation at 25 °C with an electric field strength of 20 V cm^{-1}.

III-2-5. Entrapment Efficiency of the Flavonoid-Loaded Lipid Nanoparticles

A 1 mL portion of n-butanol was added to 1 mL of each LNP sample encapsulating the flavonoids (quercetin, naringenin, and hesperetin). The sample was vortexed for 10 s and then centrifuged at 10000 RCF for 10 min (Centrifuge Smart 15, Hanil Science Industrial Co., Ltd., Incheon, Korea). After centrifugation, the n-butanol layer was transferred to a microquartz cell, and the absorbance at 377.5 nm (quercetin), 291.5 nm (naringenin), and 289.5 nm (hesperetin) was determined using a spectrophotometer (Pharmaspec UV-170, Shimadzu Corp., Kyoto, Japan). The concentrations of quercetin, naringenin, and hesperetin in the n-butanol layer were calculated using standard curves ranging from 3.125 to 100 μg mL^{-1} for quercetin (R^2 = 0.9975), naringenin (R^2 = 0.9990), and hesperetin (R^2 = 0.9974). Flavonoid entrapment efficiencies (EE) of the LNP samples were determined using the equation

$$\text{EE}\ (\%) = \frac{W_\text{t} - W_\text{n}}{W_\text{t}} \times 100$$

where W_t is the total flavonoid molecule weight in the entire LNP sample system and W_n is the flavonoid molecule weight in the *n*-butanol layer after centrifugation.

III-2-6. Determining the *in Vitro* Digestion Patterns of the Lipid Nanoparticles

The simulated *in vitro* digestion test model was modified from the version described by Hur et al (25):

(I) preingestion: LNPs were filtered with a 1 μm pore sized filter

(II) mouth (pH 7; 5 min): 5 mL of filtered LNPs was blended with 6 mL simulated salivary medium

(III) stomach (pH 3; 2 h): 12 mL of simulated gastric juice was added

(IV) small intestine (pH 6.5−7; 2 h): simulated duodenal juice (12 mL), bile juice (6 mL), and NaHCO3 solution (2 mL) were added

The formulations of the simulated saliva medium and gastric, duodenal, and bile juices are shown in Table III-1. All samples were stirred (60 rpm) in a shaking water bath (BS-31, JEIO Tech., Seoul, Korea) during the *in vitro* digestion test and maintained at 37 °C to mimic gastrointestinal tract motility. After each digestion step (I−IV), the size distribution of samples was measured using the Zetasizer.

After 4 h 5 min of digestion, the relative bioaccessibility of the flavonoid (quecetin, naringenin, and hesperetin) was determined as described earlier (16), with modifications. Briefly, 2 mL of digesta was centrifuged at 1500 RCF for 30 min, and 1 mL of the supernatant was recentrifuged at 16000 RCF for 20 min. A 0.2 mL aliquot of the supernatant was collected and diluted 10-fold with 1.8 mL of methanol, and the solution was centrifuged at 16000 RCF for 20 min. The concentration of flavonoids in the supernatant was quantified using a spectrophotometer and calculated using

standard curves ranging from 0.625 to 10 μg mL^{-1} for quercetin (λ 384 nm, R^2 = 0.9971), naringenin (λ 325 nm, R^2 = 0.9990), and hesperetin (λ 324.5 nm, R^2 = 0.9999). The relative bioaccessibility of the flavonoids in the digested micellar fraction was determined using the equation

$$\text{bioaccessibility (\%)} = \frac{W_t - W_s}{W_t} \times 100$$

where W_s is the weight of the flavonoid molecules in the supernatant after digestion and centrifugation. In addition to the flavonoid-encapsulated LNPs, equivalent quantities (150 μg mL^{-1}) of quercetin, naringenin, and hesperetin in their native forms were also investigated.

The protectibility (%) of LNPs for flavonoids against harsh conditions (pH and salt) was determined after each digestion step (II−IV) without enzymes. After each step, 0.2 mL of digesta was collected and diluted 10-fold with 1.8 mL of methanol and centrifuged at 16000 RCF for 20 min. The concentration of flavonoids in the supernatant was quantified using a spectrophotometer and calculated using standard curves ranging from 0.625 to 10 μg mL^{-1}: step II, quercetin (λ 389 nm, R^2 = 0.9999), naringenin (λ 325.5 nm, R^2 = 1.0000), and hesperetin (λ 325.5 nm, R^2 = 0.9999); step III, quercetin (λ 379 nm, R^2 = 1.0000), naringenin (λ 290 nm, R^2 = 0.9998), and hesperetin (λ 287.5 nm, R^2 = 0.9998); step IV, quercetin (λ 389 nm, R^2 = 0.9999), naringenin (λ 325 nm, R^2 = 1.0000), and hesperetin (λ 325 nm, R^2 = 1.0000). The protectibility of the LNPs incorporating the flavonoids against the enzyme-free digestion medium was determined by the equation

$$\text{protectibility (\%)} = \frac{W_t - W_s}{W_e} \times 100$$

where W_e is the weight of the flavonoids encapsulated in the LNPs immediately after preparation.

The release patterns of the flavonoids from the LNPs were studied using dialysis bags with a 12 kDa molecular weight cutoff. The bags were immersed in DDW for 12 h before use. They were filled with 1 mL of the flavonoid-loaded LNP sample, tightly sealed, and suspended in 49 mL of 50 % (v/v) ethanol to produce a sink condition. The enzyme-free simulated *in vitro* digestion medium mixture was added, and the bags were rotated at 100 rpm in a 37 °C water bath. At predetermined time intervals, a 1 mL aliquot was withdrawn from the medium mixture, and 1 mL of fresh medium was replaced immediately. Next, the absorbance of the aliquot at the wavelengths for quercetin (377.5 nm), naringenin (291.5 nm), and hesperetin (289.5 nm) was measured with a spectrophotometer. The concentrations of quercetin, naringenin, and hesperetin in the aliquots were calculated using standard curves ranging from 3.125 to 250 μg mL^{-1} for quercetin (R^2 = 0.9996), naringenin (R^2 = 0.9999), and hesperetin (R^2 = 0.9999).

Table III-1. Formulations and Concentrations of the Various Media and Juices for the Simulated *in Vitro* Digestion Test of Blank Lipid Nanoparticles

	saliva medium	gastric juice	duodenal juice	bile juice
inorganic solution	20 mL $NaHCO_3$ 84.7 g L^{-1}	15.7 mL NaCl 175.3 g L^{-1}	40 mL NaCl 175.3 g L^{-1}	30 mL NaCl 175.3 g L^{-1}
	10 mL KCl 89.6 g L^{-1}	9.2 mL KCl 89.6 g L^{-1}	40 mL $NaHCO_3$ 84.7 g L^{-1}	60.3 mL $NaHCO_3$ 84.7 g L^{-1}
	10 mL NaH_2PO_4 88.8 g L^{-1}	18 mL $CaCl_2{\cdot}2H_2O$ 22.2 g L^{-1}	6.3 mL KCl 89.6 g L^{-1}	4.2 mL KCl 89.6 g L^{-1}
	1.7 mL NaCl 175.3 g L^{-1}	3.0 mL NaH_2PO_4 88.8 g L^{-1}	9 mL $CaCl_2{\cdot}2H_2O$ 22.2 g L^{-1}	10 mL $CaCl_2{\cdot}2H_2O$ 22.2 g L^{-1}
	10 mL Na_2SO_4 57 g L^{-1}	10 mL NH_4Cl 30.6 g L^{-1}	10 mL KH_2PO_4 8 g L^{-1}	150 µL HCl 35% g g^{-1}
	10 mL KSCN 20 g L^{-1}	6.5 mL HCl 35% g g^{-1}	10 mL $MgCl_2$ 5 g L^{-1}	
			180 µL HCl 35% g g^{-1}	
organic solution	8 mL urea 25 g L^{-1}	34 mL urea 25 g L^{-1}	4 mL urea 25 g L^{-1}	10 mL urea 25 g L^{-1}
		10 mL glucose 65 g L^{-1}		
		10 mL glucosamine hydrochloride 33 g L^{-1}		
		10 mL glucuronic acid 2 g L^{-1}		
add to mixture	15 mg uric acid	1 g BSA	1 g BSA	1.8 g BSA
inorganic + organic	25 mg mucin	3 g mucin	9 g pancreatin	30 g bile
solution	290 mg α-amylase	2.5 g pepsin	1.5 g lipase	
pH	6.8	1.3	8.1	8.2

III-2-7. Statistical Analysis

All results were analyzed using Tukey's significant difference test using the IBM SPSS Statistics version 21.0 software (IBM Co., Armonk, NY, USA). Data represent means of at least three independent experiments or measurements. A p value <0.05 was considered to indicate a significant difference.

III-3. Results and Discussion

III-3-1. Stability of the Blank Lipid Nanoparticles

The partially coalesced LNPs and the LNPs with surfactant-depleted patches on the surfaces formed micrometer-sized aggregates (17). According to Stokes' law, the particle size effect on the creaming rate predominates over the density difference at the same composition. Therefore, the aggregated micrometer-sized particles creamed readily, whereas the stable nanosized LNPs were well-dispersed in aqueous solution (17).

The creaming phenomenon of the LNP aggregates was observed when blank LNPs prepared with 100 wt % FHCO as the lipid phase were diluted 10-fold with DDW (Figure III-1a). The micrometer-sized LNP aggregates and the nanosized LNPs formed creaming and aqueous layers, respectively. The particle size of all blank LNPs prepared with 100 wt % FHCO was 123.2−165.1 nm, indicating that submicron-sized particles comprised the aqueous layer. Thus, the thickness of the aqueous layer reflected the number of LNPs stably produced on a nanosize scale, which was related to the colloidal stability of the LNP system.

The aqueous layers of samples stabilized with a single emulsifier (SL contents: 0 and 100 wt %) were thinner than those emulsified with T20 and SL (SL contents: 25, 50, and 75 wt %). Additionally, the yields of the 25, 50, and 75 wt % SL content samples were larger than those of the 0 and 100 wt % SL content samples (Table III-

A1 in the Appendix), suggesting that combined use of T20 and SL enhanced the colloidal stability of the LNP system, which agrees with other studies (26). This tendency was also applied to the LNP samples fabricated using a lipid mixture with FHCO and liquid oil (LSO, SQ, or LCO) as the lipid phase (Figure III-1b−d).

It was observed in my previous study that increasing the liquid oil content in the LNP lipid phase improves the colloidal stability of the system (17), which was confirmed here (Figure III-1b−d). Furthermore, the thickness of the aqueous layer differed when the liquid oil type was changed. Therefore, LNP samples with SQ as the liquid oil in the lipid matrix had the thickest aqueous layer at the same liquid oil and SL contents. This result is in agreement with the yield data (Table III-A1 in the Appendix). These results suggest that using SQ as the liquid oil could produce optimum colloidal stability among LSO, SQ, and LCO. The reason for the best stability of the LNP system using SQ could be due to the fatty acid composition in the oils (LSO and LCO) and SL. Long-chained saturated fatty acids in triacylglycerides of LSO (10.2 wt % palmitic acid, 3.8 wt % stearic acid, and 0.3 wt % arachidic acid) and LCO (4.4 wt% palmitic acid, 1.8 wt% stearic acid, and 0.6 wt% arachidic acid) may help the LNP matirix more crystallizing as compared to the sample with squalene, due to the co-crystallization with long-chained saturated fatty acids in triacylglycerides of FHCO (79.5 wt % stearic acid, 8.8 wt % palmitic acid, and 1.6 wt % arachidic acid). Moreover, the long-chained saturated fatty acids in LSO and LCO may increase the potential that triacylglycerides in LSO and LCO are

crystallized with the long-chained fatty acids in SL at the interface, unlike the situation for squalene. Consequently, the preparation formula of blank LNP was optimized by using SQ as the liquid oil.

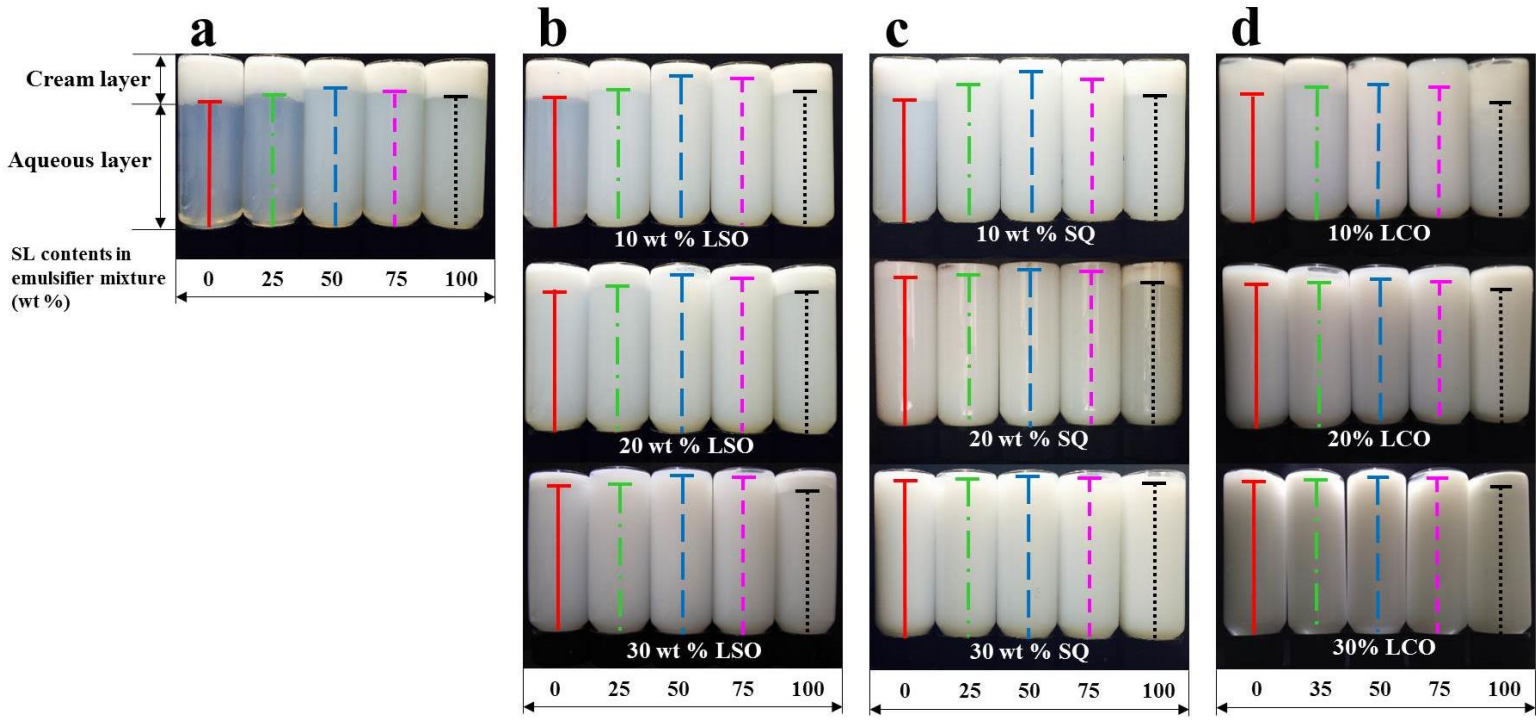

Figure III-1. Creaming pattern of the blank lipid nanoparticle dispersion diluted 10-fold. (a) blank lipid nanoparticle dispersions prepared using 100 wt % fully hydrogenated canola oil (FHCO) as the lipid phase; blank lipid nanoparticle dispersions prepared using a mixture of 90−70 wt % FHCO and 10−30 wt % liquid oil, including (b) liquid soybean oil (LSO), (c) squalene (SQ), or (d) liquid canola oil (LCO) as the lipid phase.

III-3-2. Characteristics of Lipid Nanoparticles

As shown in the previous section, SQ in the lipid phase produced the most stable LNPs, and utilizing the combination of T20 and SL increased the stability. Thus, SQ and SL contents in blank LNPs may be the main factors determining colloidal stability. Consequently, the optimum SQ and SL contents (SQ content, 30 wt %; SL content, 67.72 wt %) for preparing blank LNPs were determined in terms of the stability using RSM (Appendix), and the formula was applied also to preparation of the flavonoid-loaded LNPs. Their physicochemical characteristics are shown in Table III-2.

All LNP systems had similar yields and PDI values. Moreover, no changes in the particle size (144.9−156.2 nm) or the ZP (−45.1 to −40.5 mV) values were observed, regardless of the concentration and type of flavonoid. In other words, the flavonoid molecules in the LNP did not affect the physicochemical characteristics (yield, particle size, PDI, and ZP). Therefore, an LNP system encapsulating flavonoids at 0.1−0.5 wt % of the lipid phase would have colloidal stability similar to that of the blank system optimized. According to the ZP result, flavonoid molecules were not positioned at the LNP interface but at the interior space of the particle. In an assumption of this previous result, the particle size and PDI of LNPs could be only influenced by the viscosity of lipid matrix during the manufacturing process, more specifically, the size reduction procedure, because the viscosity is one of the major factors to determine the particle size and PDI. However, according to the particle size

and PDI results, the flavonoid content at 0.1−0.5 wt % did not affect the particle size and PDI. These results suggest that flavonoid encapsulation in LNPs at such a low level can not affect the LNPs' physicochemical properties including the yield value at all.

Flavonoids are generally water insoluble, and the octanol/water distribution coefficients of quercetin, naringenin, and hesperetin at pH 7.0 (log *P*) were 2.74, 2.30, and 2.59, respectively (27). Therefore, quercetin, naringenin, and hesperetin in a hydrophobic solvent including oil are more soluble than the flavonoids in water. Even though low oil content (5 wt %) could induce partitioning flavonoids from the oil to the water phase during LNP preparation, flavonoid molecules may have a low concentration in the water phase due to a low concentration of flavonoids in the oil phase (0.1−0.5 wt %) (28). Furthermore, after the preparation, the solid lipid matrix in LNPs could block the migration of flavonoids to the water (29). Thus, a high flavonoid EE was expected for all LNPs, but it was not detected (Table III-2). The EE value was the highest at the 0.3 wt % flavonoid concentration, regardless of the flavonoid type. Hence, the LNPs with a 0.3 wt % flavonoid concentration were chosen for the *in vitro* digestion assay in terms of their high EE values.

Table III-2. Nonaggregated Particle Content (Yield), Particle Size, Polydispersity Index (PDI), ζ Potential (ZP), and Entrapment Efficiency (EE) Values of Blank (BLK) and Flavonoid-Loaded Lipid Nanoparticles (LNPs)[a]

code name	flavonoid concn (wt %) Q	N	H	yield (%)	particle size (nm)	PDI	ZP (mV)	EE (%)
BLK LNP	-	-	-	94.4 ± 0.4 a	155.7 ± 0.4 ab	0.15 ± 0.01 a	-41.8 ± 0.5 abcd	-
0.1Q LNP	0.1	-	-	94.7 ± 0.4 a	152.7 ± 1.7 abcd	0.16 ± 0.02 a	-45.1 ± 0.8 g	69.7 ± 1.9 ef
0.2Q LNP	0.2	-	-	94.7 ± 0.1 a	153.7 ± 0.8 abc	0.19 ± 0.01 a	-44.2 ± 0.5 fg	74.6 ± 1.3 de
0.3Q LNP	0.3	-	-	94.5 ± 0.1 a	154.7 ± 2.2 ab	0.16 ± 0.02 a	-43.6 ± 0.4 defg	81.0 ± 0.9 bc
0.4Q LNP	0.4	-	-	94.8 ± 0.2 a	148.9 ± 0.9 e	0.17 ± 0.03 a	-42.8 ± 0.6 cdef	71.3 ± 2.9 ef
0.5Q LNP	0.5	-	-	95.4 ± 0.1 a	144.9 ± 0.8 f	0.16 ± 0.00 a	-43.9 ± 0.6 efg	67.9 ± 0.4 f
0.1N LNP	-	0.1	-	94.1 ± 0.8 a	156.2 ± 0.2 a	0.14 ± 0.02 a	-42.4 ± 0.3 bcde	80.0 ± 0.4 cd
0.2N LNP	-	0.2	-	94.1 ± 0.3 a	152.1 ± 0.6 bcde	0.16 ± 0.01 a	-40.6 ± 0.7 ab	89.0 ± 2.0 a
0.3N LNP	-	0.3	-	94.2 ± 1.1 a	149.9 ± 0.4 de	0.14 ± 0.03 a	-42.1 ± 0.6 abcde	90.0 ± 0.5 a
0.4N LNP	-	0.4	-	94.2 ± 0.9 a	148.8 ± 1.8 e	0.16 ± 0.02 a	-42.3 ± 0.5 abcde	85.8 ± 1.4 ab
0.5N LNP	-	0.5	-	94.1 ± 0.2 a	149.1 ± 0.2 de	0.17 ± 0.01 a	-42.9 ± 0.3 cdef	88.0 ± 0.4 a
0.1H LNP	-	-	0.1	94.9 ± 0.3 a	155.2 ± 2.7 ab	0.18 ± 0.01 a	-40.5 ± 1.0 a	72.5 ± 4.0 ef
0.2H LNP	-	-	0.2	94.8 ± 0.3 a	154.7 ± 0.2 ab	0.17 ± 0.01 a	-42.2 ± 0.5 abcde	82.1 ± 1.5 bc
0.3H LNP	-	-	0.3	94.2 ± 0.4 a	154.8 ± 0.2 ab	0.17 ± 0.01 a	-40.8 ± 0.7 ab	90.0 ± 2.5 a
0.4H LNP	-	-	0.4	94.3 ± 0.9 a	150.9 ± 0.8 cde	0.16 ± 0.02 a	-41.7 ± 0.6 abc	88.7 ± 1.2 a
0.5H LNP	-	-	0.5	94.9 ± 0.8 a	149.9 ± 1.2 de	0.16 ± 0.02 a	-42.1 ± 0.7 abcd	89.7 ± 1.1 a

[a]Different letters a−g in a column are significantly different at $p < 0.05$. Abbreviations: quercetin, Q; naringenin, N; hesperetin, H.

III-3-3. *In Vitro* Digestion of Lipid Nanoparticles

The purpose of encapsulating flavonoids in nanosized LNPs is to increase their bioaccessibility (21). Thus, the LNPs incorporating flavonoids must not degrade or aggregate until arrival in the small intestine. The loss of emulsifiers on the particle surface could induce aggregation (30), or the colloidal particles could aggregate due to the high salt or low pH conditions due to the electrostatic attraction (22). Fortunately, the initial particle size values of the optimized blank LNPs and all flavonoid-loaded LNPs were maintained under the high-salt conditions of the *in vitro* mouth (Figure III-2), indicating nonaggregation of the LNPs due to salts and nondegradation due to α-amylase. Phospholipids consisting of the SL covering the LNPs have a positive charge under basic conditions, whereas the molecules have a negative charge under acidic conditions (31). Thus, the SL molecules on the LNP surface aggregated the LNPs due to interactions between the phospholipids and the divalent cations in gastric juice. However, despite the low-pH conditions of *in vitro* gastric juice; i.e., pH 3, the particle size of all LNPs after the 2 h incubation was similar to the initial size (Figure III-2). This result may have been due to the action of T20 as a costabilizer. This nonionic surfactant can sterically stabilize the particles under low-pH conditions (32), and the emulsion system stabilized with T20 showed good stability under simulated gastric conditions (16). After 2 h of digestion in the small intestine juice, all particle size values increased ~5-fold over those preingestion due to degradation and aggregation of the particles (Figure III-2). The emulsifiers

(T20 and SL) coating the surface were hydrolyzed by lipase, resulting in aggregation of the particles or displacement of the emulsifiers by bile salts, which exposed the LNPs to lipolysis by digestive enzymes (16). Polyethylene glycol and lauric acid in a T20 molecule are linked through an ester bond. The ester bond in T20 is not cut off under acid conditions like the gastric condition, but is hydrolyzed and saponified by hydroxide under basic conditions. Thereby, steric effect of T20 at the interface of LNPs can sufficiently protect the LNP aggregation under the gastric digestion. However, in the small intestinal digestion, T20 molecules at the interface could be hydrolyzed by pancreatic lipase and replaced by bile salts, then T20 cannot prevent the lipid matrix hydrolysis by the lipase no more. After enzymatic hydrolysis, lipid degradation products such as monoglycerides and fatty acids form mixed micelles with the bile salts, phospholipids in SL, and the degraded T20 fragments. As a result, the particle size of the mixed micelles increased ~5-fold over that preingestion. Thus, these optimum LNP-loaded flavonoids were not degraded in the mouth or stomach and were digested in the small intestine.

Flavonoids have many health benefits but have limited bioavailability due to low permeability across the apical surface of intestinal epithelial cells (33). A lipid-based delivery system (LNPs) was adopted to overcome this problem. As mentioned previously, the LNP system is degraded in the intestine by bile salts and digestive enzymes, which results in formation of mixed micelles. Flavonoids incorporated into LNPs would solubilize well in these micelles, whereas a native flavonoid would not

be easily taken up by intestinal epithelial cells. The micelles amassed at the epithelial surface are absorbed by enterocytes (16), which would increase the quantity of bioaccessible and bioavailable flavonoids. In this regard, the experimental data could endorse the previous discussion (Figure III-3). The flavonoid bioaccessibilities (%) of the fabricated LNP samples were greater than that of the native flavonoid (quercetin, ~12-fold; naringenin, ~5-fold; hesperetin, ~5-fold). The high bioaccessibility of the quercetin-loaded LNPs may be due to the considerable hydrophobicity (log P = 2.74) (27). All LNP systems prepared successfully increased flavonoid bioaccessibility. These results were in agreement with previously reported research in cases of curcumin and genistein (16).

The antioxidant activity of flavonoids is sensitive to pH (34) and salt (35), which could decrease the therapeutic benefit due to the dramatic changes in pH and ion concentrations encountered during oral digestion. The LNPs were incubated with *in vitro* media without enzymes during digestion tests (mouth, stomach, and small intestine) to evaluate the protectibility of flavonoid-loaded LNPs. During the serial digestion test, the protectibility values of quercetin-, naringenin-, and hesperetin-loaded LNPs decreased to 97, 96, and 95%, respectively (Figure III-4), which meant successful protection of the flavonoids by the LNP system against harsh conditions such as low pH and high concentration of salts. *In vitro* degradation of other bioactive materials (curcumin and genistein) has also been reported at similar levels (16). Therefore, the LNP system protected the flavonoids from pH and salt changes during

digestion, and the protected flavonoids could maintain their antioxidant activity.

The *in vitro* flavonoid release test from LNPs was conducted in a medium comprising saliva and gastric, duodenal, and bile juices to mimic the small intestine. The reason for using a medium without digestive enzymes was to separate LNP degradation from the flavonoid release effect. Because of the low water solubility of flavonoids, 50 % (v/v) ethanol was added to provide a sink condition in the enzyme-free mixture medium. Almost 100% of the flavonoids within the LNPs were released from the matrix into the medium during the 8 h release test (Figure III-5). The quercetin-, naringenin-, and hesperetin-loaded LNPs released ~74% of the quercetin, 81% of the naringenin, and 86% of the hesperetin into the medium, respectively, 2 h (small intestine residence time) after beginning the test. Although the condition was accelerated by 50% ethanol, these values were larger in comparison with those reported in other studies (16, 36). Lipid crystallization was initiated from the LNP core during cooling while the LNPs were prepared, and the core lipid crystals may have pushed flavonoids to the outer shell of the LNP, resulting in a flavonoid-enriched shell and rapid release of the flavonoids (37). Nevertheless, this burst release did not affect flavonoid solubility in the mixed micelle, bioaccessibility (%), that formed after degradation by digestive enzymes (Figure III-3). Consequently, the LNP system optimized for colloidal stability successfully enhanced the bioaccessibility of quercetin, naringenin, and hesperetin.

The flavonoid-loaded LNP system, which was optimized by controlling the

SQ and SL contents, protected the encapsulated flavonoid molecules against the harsh conditions of the *in vitro* digestion test until arrival in the small intestine. Moreover, flavonoids incorporated in LNPs were solubilized well into micelles mixed with the LNP digesta (fatty acids, monoglycerides, etc.), bile salts, and phospholipids at the end of the simulated digestion. Consequently, the LNP system using edible materials successfully protected flavonoids and improved bioaccessibility of flavonoids. In conclusion, this work may serve as a basis for further studies to develop an oral delivery system for nonbioaccessible molecules, such as flavonoids, for functional foods.

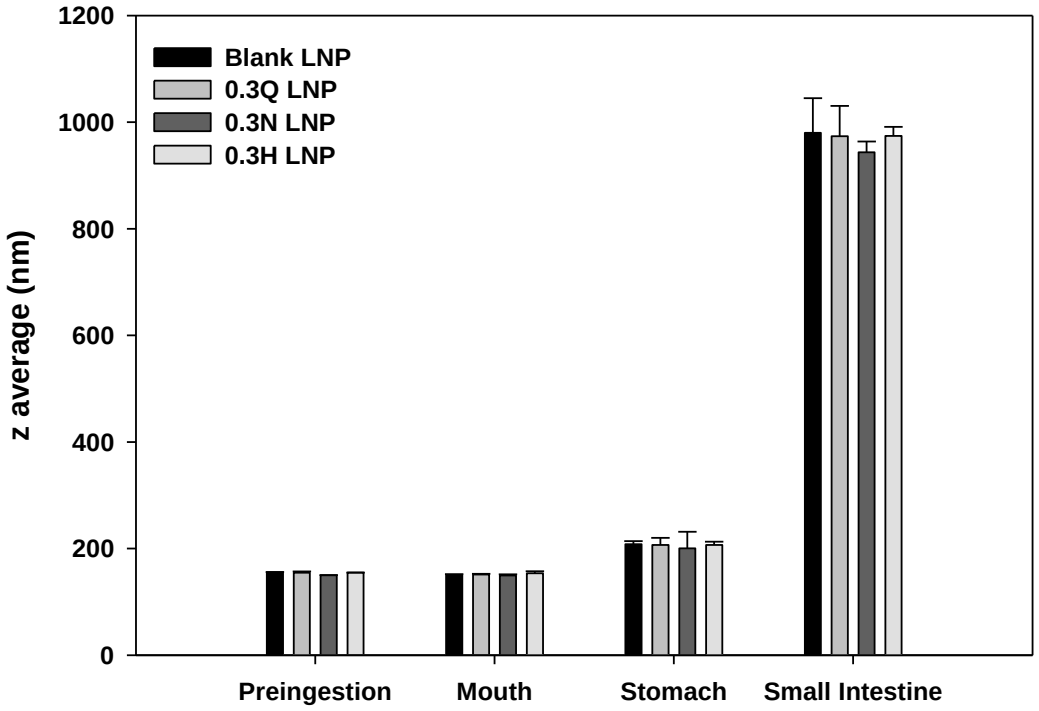

Figure III-2. Particle size (z average) changes in blank and lipid nanoparticles (LNPs). 0.3 wt % quercetin (0.3Q), 0.3 wt % naringenin (0.3N), and 0.3 wt % hesperetin (0.3H) after simulated *in vitro* digestion tests (preingestion, mouth, stomach, and small intestine).

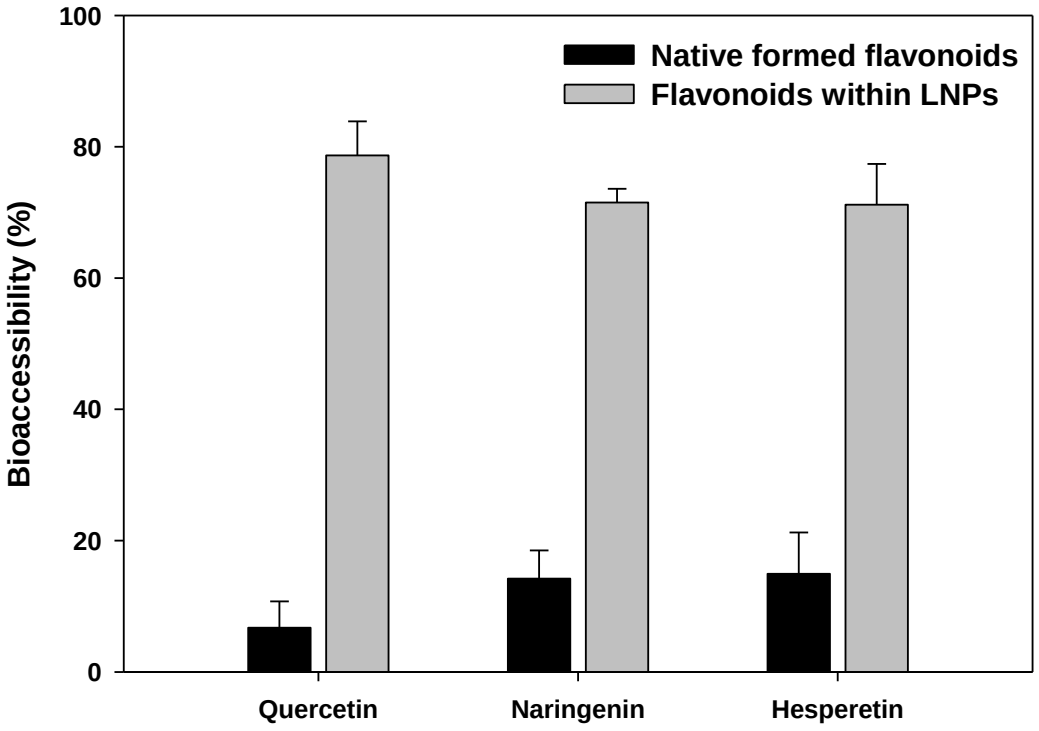

Figure III-3. Bioaccessibility (%) of quercetin, naringenin, and hesperetin contents in the digested micellar fraction after simulated digestion.

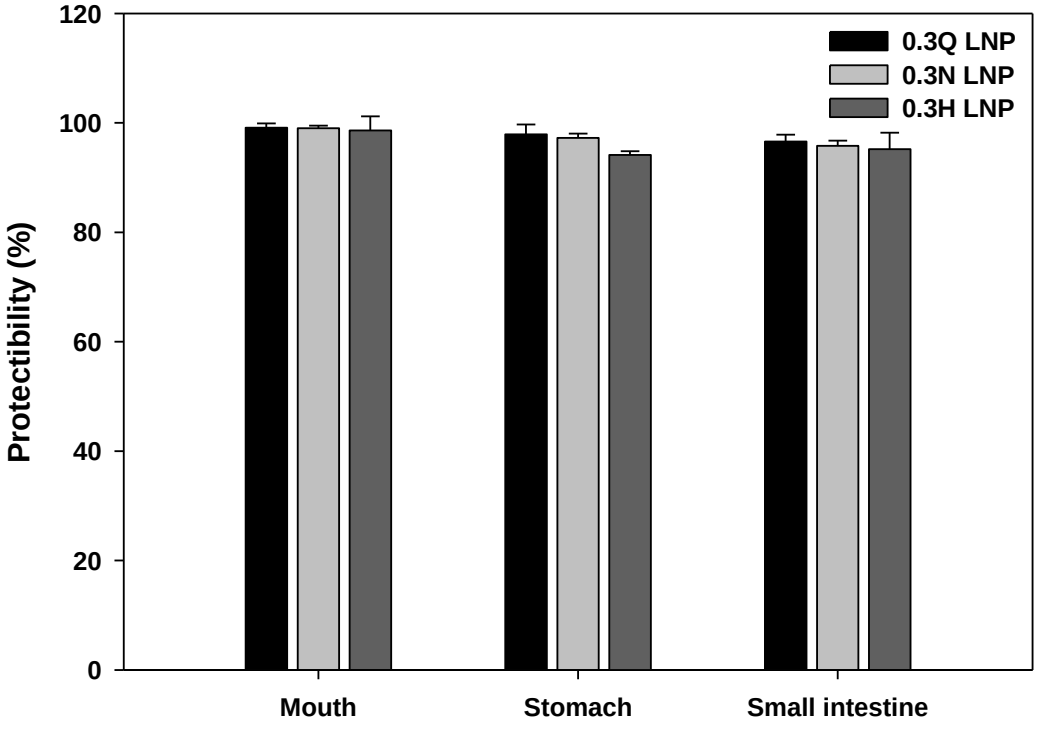

Figure III-4. Protectibility (%) of flavonoid-loaded LNPs for flavonoids after incubation in an enzyme-free simulated digestion medium.

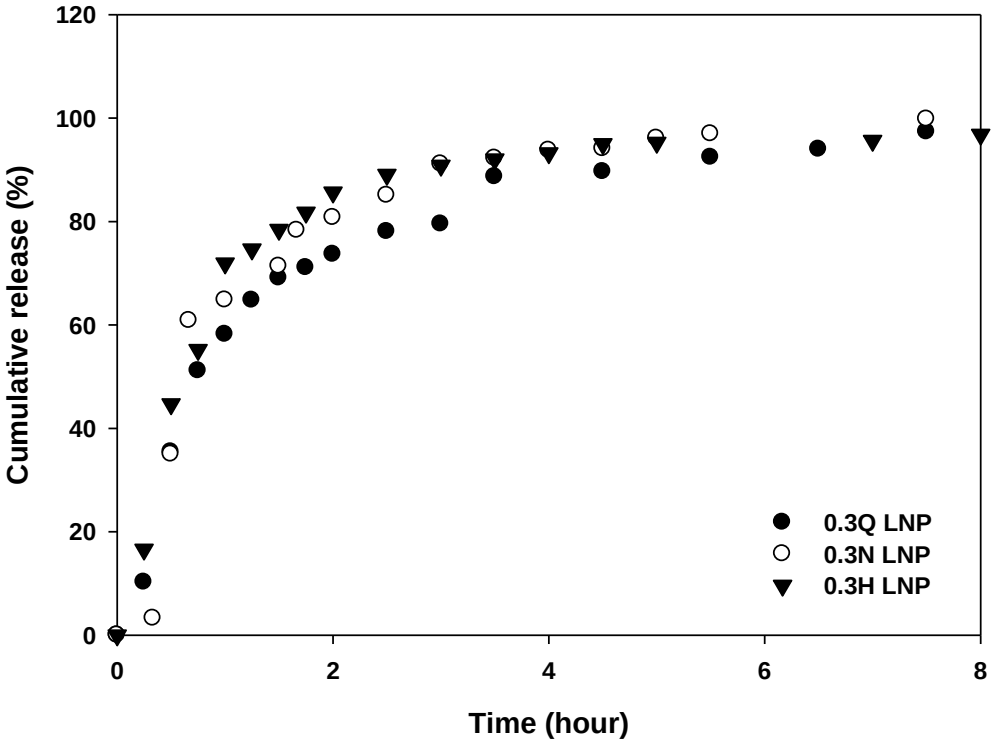

Figure III-5. ***In vitro*** **cumulative release profiles of flavonoid molecules from the lipid matrix in the enzyme-free simulated digestion medium.** Using a dialysis membrane under sink conditions (50 % v/v ethanol).

III-4. References

(1) Erlund, I. Review of the flavonoids quercetin, hesperetin, and naringenin. Dietary sources, bioactivities, bioavailability, and epidemiology. *Nutr. Res. (N. Y., NY, U. S.)* **2004**, *24*, 851−874.

(2) Hayek, T.; Fuhrman, B.; Vaya, J.; Rosenblat, M.; Belinky, P.; Coleman, R.; Elis, A.; Aviram, M. Reduced progression of atherosclerosis in apolipoprotein E−deficient mice following consumption of red wine, or its polyphenols quercetin or catechin, is associated with reduced susceptibility of LDL to oxidation and aggregation. *Arterioscler., Thromb., Vasc. Biol.* **1997**, *17*, 2744−2752.

(3) Deschner, E. E.; Ruperto, J.; Wong, G.; Newmark, H. L. Quercetin and rutin as inhibitors of azoxymethanol-induced colonic neoplasia. *Carcinogenesis* **1991**, *12*, 1193−1196.

(4) Ferry, D. R.; Smith, A.; Malkhandi, J.; Fyfe, D. W.; Anderson, D.; Baker, J.; Kerr, D. J. Phase I clinical trial of the flavonoid quercetin: pharmacokinetics and evidence for *in vivo* tyrosine kinase inhibition. *Clin. Cancer Res.* **1996**, *2*, 659−668.

(5) Pignatelli, P.; Pulcinelli, F. M.; Celestini, A.; Lenti, L.; Ghiselli, A.; Gazzaniga, P. P.; Violi, F. The flavonoids quercetin and catechin synergistically inhibit platelet function by antagonizing the intracellular production of hydrogen

peroxide. *Am. J. Clin. Nutr.* **2000**, *72*, 1150−1155.

(6) Pérez-Vizcaíno, F.; Ibarra, M.; Cogolludo, A. L.; Duarte, J.; Zaragozá-Arnáez, F.; Moreno, L.; López-López, G.; Tamargo, J. Endothelium-independent vasodilator effects of the flavonoid quercetin and its methylated metabolites in rat conductance and resistance arteries. *J. Pharmacol. Exp. Ther.* **2002**, *302*, 66−72.

(7) Justesen, U.; Knuthsen, P.; Leth, T. Quantitative analysis of flavonols, flavones, and flavanones in fruits, vegetables and beverages by high-performance liquid chromatography with photo-diode array and mass spectrometric detection. *J. Chromatogr. A* **1998**, *799*, 101−110.

(8) Miyake, Y.; Yamamoto, K.; Tsujihara, N.; Osawa, T. Protective effects of lemon flavonoids on oxidative stress in diabetic rats. *Lipids* **1998**, *33*, 689−695.

(9) Manthey, J. A.; Guthrie, N.; Grohmann, K. Biological properties of citrus flavonoids pertaining to cancer and inflammation. *Curr. Med. Chem.* **2001**, *8*, 135−153.

(10) Kurowska, E. M.; Spence, J. D.; Jordan, J.; Wetmore, S.; Freeman, D. J.; Piché, L. A.; Serratore, P. HDL-cholesterol-raising effect of orange juice in subjects with hypercholesterolemia. *Am. J. Clin. Nutr.* **2000**, *72*, 1095−1100.

(11) Kuiper, G. G. J. M.; Lemmen, J. G.; Carlsson, B. O.; Corton, J. C.; Safe, S. H.; van der Saag, P. T.; van der Burg, B.; Gustafsson, J. Interaction of estrogenic chemicals and phytoestrogens with estrogen receptor β. *Endocrinology* **1998**,

139, 4252−4263.

(12) Erlund, I.; Silaste, M. L.; Alfthan, G.; Rantala, M.; Kesäniemi, Y. A.; Aro, A. Plasma concentrations of the flavonoids hesperetin, naringenin and quercetin in human subjects following their habitual diets, and diets high or low in fruit and vegetables. *Eur. J. Clin. Nutr.* **2002**, *56*, 891−898.

(13) Erlund, I.; Meririnne, E.; Alfthan, G.; Aro, A. Plasma kinetics and urinary excretion of the flavanones naringenin and hesperetin in humans after ingestion of orange juice and grapefruit juice. *J. Nutr.* **2001**, *131*, 235−241.

(14) Luo, Y.; Chen, D.; Ren, L.; Zhao, X.; Qin, J. Solid lipid nanoparticles for enhancing vinpocetine's oral bioavailability. *J. Controlled Release* **2006**, *114*, 53−59.

(15) Pandita, D.; Kumar, S.; Poonia, N.; Lather, V. Solid lipid nanoparticles enhance oral bioavailability of resveratrol, a natural polyphenol. *Food Res. Int.* **2014**, *62*, 1165−1174.

(16) Aditya, N. P.; Shim, M.; Lee, I.; Lee, Y.; Im, M.; Ko, S. Curcumin and genistein coloaded nanostructured lipid carriers: *in vitro* digestion and antiprostate cancer activity. *J. Agric. Food Chem.* **2013**, *61*, 1878−1883.

(17) Ban, C.; Lim, S.; Chang, P.; Choi, Y. J. Enhancing the stability of lipid nanoparticle systems by sonication during the cooling step and controlling the liquid oil content. *J. Agric. Food Chem.* **2014**, *62*, 11557−11567.

(18) Boode, K.; Walstra, P. Partial coalescence in oil-in-water emulsions 1. Nature of

the aggregation. *Colloids Surf., A* **1993**, *81*, 121−137.

(19) Vanapalli, S. A.; Coupland, J. N. Emulsions under shear−the formation and properties of partially coalesced lipid structures. *Food Hydrocolloids* **2001**, *15*, 507−512.

(20) Helgason, T.; Awad, T. S.; Kristbergsson, K.; McClements, D. J.; Weiss, J. Influence of polymorphic transformations on gelation of tripalmitin solid lipid nanoparticle suspensions. *J. Am. Oil Chem. Soc.* **2008**, *85*, 501−511.

(21) McClements, D. J.; Xiao, H. Potential biological fate of ingested nanoemulsions: influence of particle characteristics. *Food Funct.* **2012**, *3*, 202−220.

(22) Li, Z.; Jiang, H.; Xu, C.; Gu, L. A review: Using nanoparticles to enhance absorption and bioavailability of phenolic phytochemicals. *Food Hydrocolloids* **2015**, *43*, 153−164.

(23) van Aken, G. A. Modelling texture perception by soft epithelial surfaces. *Soft Matter* **2010**, *6*, 826−834.

(24) Kong, F.; Singh, R. Disintegration of solid foods in human stomach. *J. Food Sci.* **2008**, *73*, R67−R80.

(25) Hur, S. J.; Joo, S. T.; Lim, B. O.; Decker, E. A.; McClements, J. D. Impact of salt and lipid type on *in vitro* digestion of emulsified lipids. *Food Chem.* **2011**, *126*, 1559−1564.

(26) Han, F.; Li, S.; Yin, R.; Liu, H.; Xu, L. Effect of surfactants on the formation and characterization of a new type of colloidal drug delivery system: nanostructured

lipid carriers. *Colloids Surf., A* **2008**, *315*, 210−216.

(27) *Flavonoids in Health and Disease*; Rice-Evans, C. A., Packer, L., Eds.; Marcel Dekker: New York, 2010.

(28) McClements, D. J. Crystals and crystallization in oil-in-water emulsions: Implications for emulsion-based delivery systems. *Adv. Colloid Interface Sci.* **2012**, *174*, 1−30.

(29) Müller, R. H.; Petersen, R. D.; Hommoss, A.; Pardeike, J. Nanostructured lipid carriers (NLC) in cosmetic dermal products. *Adv. Drug Delivery Rev.* **2007**, *59*, 522−530.

(30) Müller, R. H.; Rühl, D.; Runge, S. A. Biodegradation of solid lipid nanoparticles as a function of lipase incubation time. Int. *J. Pharm.* **1996**, *144*, 115−121.

(31) Mosqueira, V. C. F.; Legrand, P.; Pinto-Alphandary, H.; Puisieux, F.; Barratt, G. Poly (D, L-lactide) nanocapsules prepared by a solvent displacement process: Influence of the composition on physicochemical and structural properties. *J. Pharm. Sci.* **2000**, *89*, 614−626.

(32) Van Aken, G. A.; Bomhof, E.; Zoet, F. D.; Verbeek, M.; Oosterveld, A. Differences in *in vitro* gastric behaviour between homogenized milk and emulsions stabilised by Tween 80, whey protein, or whey protein and caseinate. *Food Hydrocolloids* **2011**, *25*, 781−788.

(33) Tian, X.; Yang, X.; Yang, X.; Wang, K. Studies of intestinal permeability of 36 flavonoids using Caco-2 cell monolayer model. *Int. J. Pharm.* **2009**, *367*, 58−64.

(34) Jovanovic, S. V.; Steenken, S.; Tosic, M.; Marjanovic, B.; Simic, M. G. Flavonoids as antioxidants. *J. Am. Chem. Soc.* **1994**, *116*, 4846−4851.

(35) Arora, A.; Nair, M. G.; Strasburg, G. M. Structure−activity relationships for antioxidant activities of a series of flavonoids in a liposomal system. *Free Radical Biol. Med.* **1998**, *24*, 1355−1363.

(36) Li, H.; Zhao, X.; Ma, Y.; Zhai, G.; Li, L.; Lou, H. Enhancement of gastrointestinal absorption of quercetin by solid lipid nanoparticles. *J. Controlled Release* **2009**, *133*, 238−244.

(37) Müller, R. H.; Radtke, M.; Wissing, S. A. Nanostructured lipid matrices for improved microencapsulation of drugs. *Int. J. Pharm.* **2002**, *242*, 121−128.

III-5. Appendix: Optimization Blank Lipid Nanoparticle Formula using Response Surface Methodology

III-5-1. Determining Crystallinity of the Lipid Nanoparticles

The melting enthalpies of the lipid phases in the prepared LNPs were determined using differential scanning calorimetery (DSC) (Diamond DSC, Perkin-Elmer, Waltham, MA, USA). Each sample (20 ± 5 mg) was placed in a hermetic aluminum pan, which was sealed and equilibrated at room temperature overnight prior to the measurements. An empty pan was used as a reference. The DSC scan started at 25 °C and was increased by 5 °C min^{-1} to 95 °C. The crystallinity index (CI) was calculated based on the thermographs to determine the degree of crystallinity of the lipid phase in LNPs using the equation (1):

$$\text{CI}\ (\%) = \frac{\Delta H_{\text{m LNP}}\ (\text{J g}^{-1}) \times 100}{\Delta H_{\text{m FHCO}}\ (\text{J g}^{-1}) \times c_{\text{L}}\ (\%)} \times 100$$

where $\Delta H_{\text{m LNP}}$ is the melting enthalpy of the LNPs, $\Delta H_{\text{m FHCO}}$ is the melting enthalpy of the bulk fully hydrogenated canola oil (i.e., 86.6 ± 1.8 J g^{-1}), and c_{L} is the lipid phase concentration (i.e., 5 wt %).

III-5-2. Determining the Optimum Formula for Blank Lipid Nanoparticles

Response surface methodology (RSM) with a central composite design was used to optimize colloidal stability of the LNP system, and the factor levels were coded suitably. Two factors were squalene (SQ) content (wt %) in the lipid phase (X_1) and soybean lecithin (SL) content (wt %) in the emulsifier mixture (X_2) at three different levels coded as −1 (low), 0 (middle), and +1 (high), and the range (X_1: 10–30 wt %; and X_2: 50–100 wt %) of two factors was selected in accordance with the yield values in preliminary experiments (Table III-A1). Experimental factorial design factors with coded levels/actual values and their yield, particle size, ζ potential (ZP), and CI were presented in Table III-A2. The data for analysis was obtained from the various response trials, which were subjected to multiple regression analysis. The equation fitted was:

$$Y = \beta_0 + \beta_1 X_1 + \beta_2 X_2 + \beta_{11} {X_1}^2 + \beta_{22} {X_2}^2 + \beta_{12} X_1 X_2$$

where Y is the predicted response, X is the coded levels, and β is the coefficient computed from the responses of the formulations.

Table III-A1. Nonaggregated Particle Content (Yield) of Blank Lipid Nanoparticles Prepared Using Liquid Soybean Oil (LSO), Squalene (SQ), or Liquid Canola Oil (LCO) as a Liquid Oil in Lipid Phase[a]

sample		yield (%)		
SL[b] (wt %)	Oil[c] (wt %)	LSO	SQ	LCO
0	0	38.5 ± 3.0 ghi	38.5 ± 3.0 gh	38.5 ± 3.0 gh
	10	43.5 ± 1.7 fg	50.9 ± 2.3 de	42.6 ± 3.0 fg
	20	48.4 ± 2.2 ef	52.8 ± 1.1 de	45.4 ± 4.4 fg
	30	49.8 ± 0.9 ef	54.0 ± 3.2 de	48.3 ± 2.7 ef
25	0	41.7 ± 3.4 fgh	41.7 ± 3.4 fg	41.7 ± 3.4 fg
	10	44.2 ± 3.8 fg	52.0 ± 4.4 de	43.4 ± 1.6 fg
	20	56.2 ± 3.6 de	58.5 ± 4.8 cd	49.3 ± 2.1 ef
	30	69.8 ± 6.2 bc	80.3 ± 1.2 b	65.0 ± 2.3 c
50	0	55.5 ± 1.3 de	55.5 ± 1.3 cde	55.5 ± 1.3 de
	10	56.0 ± 1.6 de	56.3 ± 1.8 cd	55.8 ± 0.8 de
	20	60.7 ± 4.1 d	63.2 ± 1.2 c	59.9 ± 2.1 cd
	30	86.2 ± 2.2 a	92.9 ± 0.5 a	79.6 ± 2.5 ab
75	0	47.6 ± 0.6 ef	47.6 ± 0.6 ef	47.6 ± 0.6 f
	10	62.1 ± 0.8 cd	62.9 ± 3.5 c	63.8 ± 3.4 cd
	20	75.6 ± 3.3 b	88.6 ± 0.7 a	74.1 ± 1.9 b
	30	92.7 ± 0.5 a	94.8 ± 0.4 a	86.5 ± 0.8 a
100	0	25.2 ± 2.5 j	25.2 ± 2.5 i	25.2 ± 2.5 j
	10	29.9 ± 4.0 ij	30.7 ± 1.8 hi	29.8 ± 2.8 ij
	20	33.2 ± 2.4 hij	34.4 ± 3.4 gh	33.0 ± 2.9 hi
	30	50.3 ± 2.2 ef	53.7 ± 3.7 de	48.9 ± 2.4 ef

[a]Different letters a−j in a column are significantly different ($p < 0.05$), [b]soybean lecithin contents in emulsifier mixture, and [c]liquid oil contents in lipid phase.

Table III-A2. Experimental Factorial Design Factors with Coded Levels/Actual Values and Their Responses in Different Batches of Blank Lipid Nanoparticles

batches	coded levels		actual values		response values			
	SQ[a] (X_1)	SL[b] (X_2)	SQ (wt %) (X_1)	SL (wt %) (X_2)	yield (%)	PS (nm)	ZP (mV)	CI (%)
1	-1	-1	10	50	56.3 ± 1.8	162.5 ± 0.8	-39.5 ± 0.7	72.9 ± 6.8
2	-1	0	10	75	62.9 ± 3.5	157.7 ± 1.5	-43.4 ± 0.2	82.8 ± 1.3
3	-1	1	10	100	30.7 ± 1.8	182.8 ± 1.4	-41.5 ± 1.0	98.1 ± 0.1
4	0	-1	20	50	63.2 ± 1.2	168.8 ± 0.4	-41.9 ± 0.7	71.9 ± 3.6
5	0	0	20	75	88.6 ± 0.7	167.3 ± 1.3	-44.6 ± 0.6	72.7 ± 3.4
6	0	1	20	100	34.4 ± 3.4	166.0 ± 1.6	-48.1 ± 1.3	86.1 ± 2.4
7	1	-1	30	50	93.0 ± 0.5	159.0 ± 2.5	-41.5 ± 1.2	28.7 ± 0.3
8	1	0	30	75	94.8 ± 0.4	158.9 ± 1.6	-44.9 ± 0.7	26.7 ± 0.3
9	1	1	30	100	53.7 ± 3.7	168.4 ± 0.9	-48.3 ± 0.7	60.5 ± 7.6

[a]Squalene contents in lipid phase, [b]soybean lecithin contents in emulsifier mixture. Abbreviations: particle size, PS; ζ potential, ZP; crystallinity index, CI.

III-5-3. Optimization of the Blank Lipid Nanoparticle Formula

As shown in the stability of the blank lipid nanoparticles section, SQ in the lipid phase produced the most stable LNPs, and utilizing the combination of T20 and SL improved the stability. Thus, SQ and SL contents in blank LNPs may be the main factors determining colloidal stability. Therefore, RSM was used to determine the optimum SQ and SL contents for preparing stable blank LNPs. The yield, particle size, ZP, and CI values of the formulations are shown in Table III-A2. The ranges for the two factors (SQ content, X_1; and SL content, X_2) were determined in preliminary experiments (Table III-A1). The analysis of variance (ANOVA) and regression coefficients for the model are shown in Table III-A3 and III-A4, respectively.

As shown in Table III-A3, the R^2 of the yield model was 0.9621 ($p < 0.05$). Thus, the yield model was appropriate and reasonable to analyze yield response trends. The linear and quadratic models significantly affected yield ($p < 0.05$), and X_2 (SL content) was more significant ($p < 0.05$). Additionally, yield was significantly influenced by X_2 and ${X_2}^2$ ($p < 0.05$; Table III-A4), suggesting that SL content could be a major factor for the yield of blank LNPs. This ANOVA result is also depicted in a response surface plot (Figure III-A1a). In the plot, the yield increased with increasing SQ content, and maximum yield was observed at 60–70 wt % SL at constant SQ content. These results are in agreement with those presented in the previous section.

The R^2 of the fitted model for the particle size was 0.8302, but the influence of the linear, quadratic, and crossproduct sources on particle size was not significant (p

= 0.202) (Table III-A3). All regression coefficients were not significant for the particle size ($p > 0.05$). Particle size had a minimum value at 20–25 wt % SQ contents and 60–70 wt % SL content.

The fitted model for ZP was appropriate and reasonable according to Table III-A3 ($R^2 = 0.9581$, $p < 0.05$). Among the model sources, the linear effects significantly influenced ZP ($p < 0.05$), and X_2 (SL content) was significant for the response ($p < 0.05$), suggesting that SL content is a major factor for the ZP value of blank LNPs. The ZP value in Figure III-A1c decreased with increasing SL content and changing the SQ content did not affect ZP. The greater the amount of SL on the particle surfaces, the more the LNPs were charged, contributing to the decrease in ZP (2).

The CI model was appropriate to predict the CI response according to Table III-A3 ($R^2 = 0.9743$, $p < 0.05$). The effect of X_1 (SQ content) was particularly superior to the other effects ($p < 0.05$). Furthermore, the influence of ${X_1}^2$ was significant ($p < 0.05$) (Table III-A4). Thus, changing SQ content affected mainly the CI. The CI was decreased as quadratic function with increasing SQ content (Figure III-A1d), which agrees with my previous study (3). Because SQ content >30 wt % would separate SQ droplets from the LNPs, the minimum CI value was in the LNP prepared with 30 wt % SQ content and ~60 wt % SL content.

Particle size values were not considered as a criterion to optimize stability of the blank LNPs because the submicron values for all samples were sufficient to maintain a high stability of the nonaggregated particles in the aqueous layer (Figure III-A1b).

The ZP for an absolute value > 30 mV was sufficient to maintain a stable system (4) and was applied in all of these experiments (Figure III-A1c). Moreover, the CI is one of many factors that affected LNP stability (3). However, yield is a quantitative criterion for stability of the LNPs. Therefore, the optimum formula (SQ content, 30 wt % and SL content, 67.72 wt %) for preparing stable blank LNPs was determined based on the response surface model for yield. The predicted yield, particle size, ZP, and CI values under an optimum condition were 101.7%, 157.4 nm, −45.8 mV, and 33.6%, respectively, and their values in the actual LNP system were 94.4 ± 0.4%, 155.7 ± 0.4 nm, −41.8 ± 0.5 mV, and 34.7 ± 0.5%, respectively. The response surface models reasonably predicted the effects of SQ and SL contents on yield, particle size, ZP, and CI.

Table III-A3. Analysis of Variance (ANOVA) for the Response Surface Model

response	source	degree of freedom	sum of squares	*F* value	*p* value	R^2	CV
yield	total model	5	4373.51	15.23	0.024	0.9621	11.809
	linear	2	2859.252	24.90	0.014	0.6290	
	quadratic	2	1467.065	12.77	0.034	0.3227	
	crossproduct	1	47.197	0.82	0.431	0.0104	
	residual error	3	172.260				
	X_1	3	1463.637	8.50	0.056		
	X_2	3	2957.074	17.17	0.022		
PS	total model	5	1033.810	2.93	0.202	0.8302	5.137
	linear	2	224.850	1.59	0.338	0.1806	
	quadratic	2	765.860	5.43	0.101	0.6150	
	crossproduct	1	43.099	0.61	0.491	0.0346	
	residual error	3	211.499				
	X_1	3	548.509	2.59	0.227		
	X_2	3	528.400	2.50	0.236		
ZP	total model	5	132.799	13.71	0.028	0.9581	3.045
	linear	2	131.413	33.92	0.009	0.9481	
	quadratic	2	1.288	0.33	0.741	0.0093	
	crossproduct	1	0.099	0.05	0.836	0.0007	
	residual error	3	5.811				
	X_1	3	6.780	1.17	0.451		
	X_2	3	126.119	21.70	0.016		
CI	total model	5	4021.173	22.76	0.014	0.9743	8.773
	linear	2	3503.844	49.57	0.005	0.8490	
	quadratic	2	515.791	7.30	0.070	0.1250	
	crossproduct	1	1.538	0.04	0.848	0.0004	
	residual error	3	106.025				
	X_1	3	3148.875	29.70	0.010		
	X_2	3	873.836	8.24	0.058		

Abbreviations: coefficient of variation, CV; particle size, PS; ζ potential, ZP; crystallinity index, CI.

Table III-A4. Regression Coefficients for the Response Surface Model

response	parameter	degree of freedom	coefficient estimate	standard error	*t* value	*p* value
yield	intercept	1	-153.783	54.409	-2.83	0.066
	X_1	1	1.296	2.446	0.53	0.633
	X_2	1	6.106	1.327	4.60	0.019
	${X_1}^2$	1	0.032	0.054	0.59	0.598
	X_1X_2	1	-0.014	0.015	-0.91	0.431
	${X_2}^2$	1	-0.043	0.009	-5.02	0.015
PS	intercept	1	312.911	60.288	5.19	0.014
	X_1	1	-7.345	2.710	-2.71	0.073
	X_2	1	-2.757	1.470	-1.87	0.158
	${X_1}^2$	1	0.159	0.059	2.68	0.075
	X_1X_2	1	0.013	0.017	0.78	0.491
	${X_2}^2$	1	0.018	0.009	1.92	0.150
ZP	intercept	1	28.727	9.99	2.87	0.064
	X_1	1	-0.195	0.45	-0.43	0.694
	X_2	1	0.294	0.24	1.20	0.315
	${X_1}^2$	1	0.006	0.01	0.63	0.575
	X_1X_2	1	0.001	0.00	0.23	0.836
	${X_2}^2$	1	-0.001	0.00	-0.52	0.638
CI	intercept	1	101.883	42.686	2.39	0.097
	X_1	1	3.225	1.919	1.68	0.191
	X_2	1	-1.539	1.041	-1.48	0.236
	${X_1}^2$	1	-0.139	0.042	-3.30	0.046
	X_1X_2	1	0.002	0.012	0.21	0.848
	${X_2}^2$	1	0.013	0.007	1.92	0.121

Abbreviations: particle size, PS; ζ potential, ZP; crystallinity index, CI.

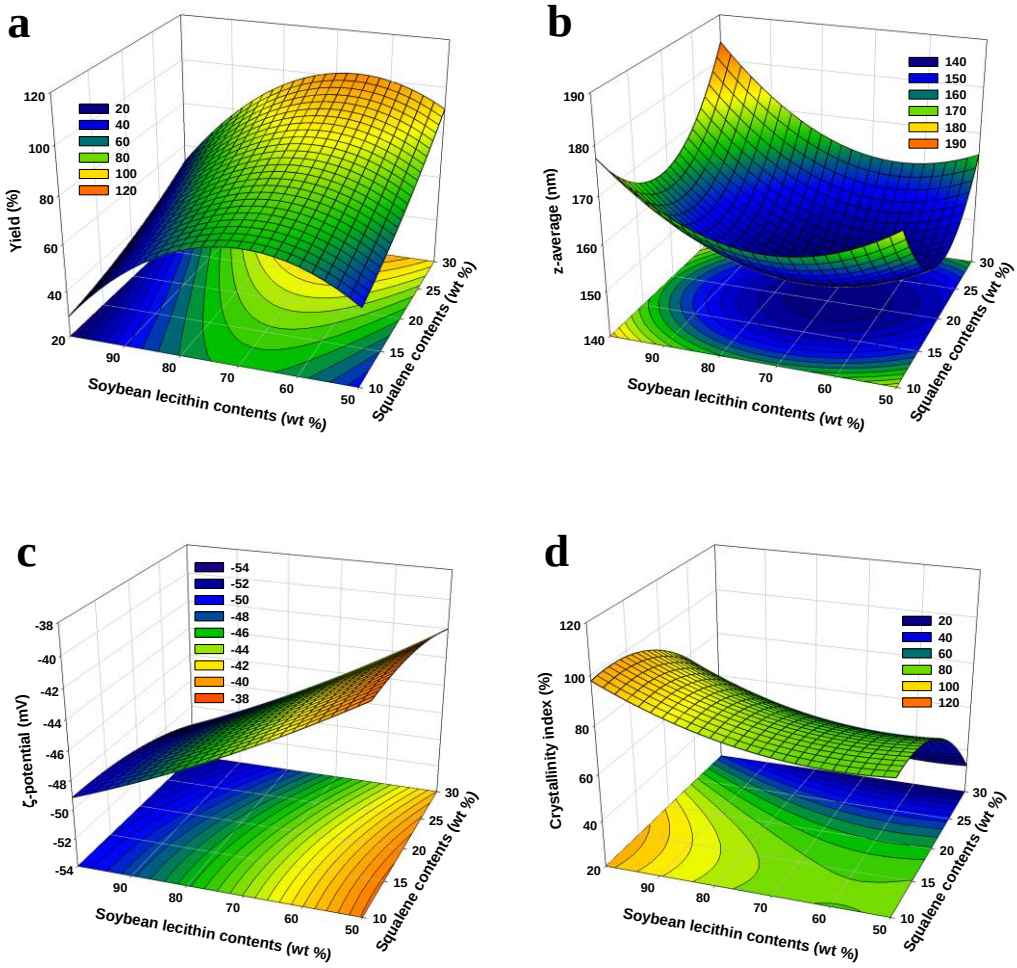

Figure III-A1. Three-dimensional response surface plots and two-dimensional contour plots. Showing the effects of squalene content in the lipid phase and soybean lecithin content in the emulsifier mixture on the (a) yield, (b) particle size (z average), (c) ζ potential, and (d) crystallinity index.

III-5-4. References

(1) Schubert, M. A.; Müller-Goymann, C. C. Characterisation of surface-modified solid lipid nanoparticles (SLN): influence of lecithin and nonionic emulsifier. *Eur. J. Pharm. Biopharm.* **2005,** *61*, 77-86.

(2) Mosqueira, V. C. F.; Legrand, P.; Pinto-Alphandary, H.; Puisieux, F.; Barratt, G. Poly (D, L-lactide) nanocapsules prepared by a solvent displacement process: Influence of the composition on physicochemical and structural properties. *J. Pharm. Sci.* **2000,** *89*, 614-626.

(3) Ban, C.; Lim, S.; Chang, P.; Choi, Y. J. Enhancing the stability of lipid nanoparticle systems by sonication during the cooling step and controlling the liquid oil content. *J. Agric. Food Chem.* **2014,** *62*, 11557-11567.

(4) Levy, M. Y.; Schutze, W.; Fuhrer, C.; Benita, S. Characterization of diazepam submicron emulsion interface: role of oleic acid. *J. Microencapsul.* **1994,** *11*, 79-92.

Chapter IV. Sustained Release of Curcumin Encapsulated in PEGylated Lipid Nanoparticle upon Oral Administration

IV-1. Introduction

Curcumin (CUR), the yellow pigment (polyphenol) found in the spice turmeric extracted from the rhizome of the plant *Curcuma longa*, has been well known for multi-functionality in human health including cancer chemoprevention (1, 2), anti-inflammation (3), etc. In addition to the multiple benefits, CUR is safe to animals or humans according to many researches that have been discovered at the toxicity (4), and has been even utilized as food elements. Therefore, CUR could be a proper material to apply to functional food industry. However, despite the strengths, its low bioavailability due to the insolubility in water (5), autoxidation (6), instability at neutral and alkaline pH (7), and avid metabolism in the body (8) makes difficult to use as a bioactive material for functional foods. Therefore, there are needs of the strategy to overcome the weakness of CUR for the oral ingestion.

Many efforts have been introduced to resolve the CUR low bioavailability problem in terms of several absorption enhancers and formulation strategies. Piperine as an enhancer is a representative example to be proved by both preclinical and clinical studies, which is attributed to the inhibition from CUR metabolizing enzymes (9). However, the enhancement on the CUR bioavailability was not significant to result in satisfactory therapeutic levels. Nanoparticles (10, 11), liposomes (12), and nanoemulsions (13) have been suggested as the formulation strategies for the solution against the CUR weakness. In these suggestions, several

improvements on the bioavailability were informed, but these improvements were not yet enough or sufficiently verified by *in vitro* and *in vivo* results. Additionally, these studies were only interested in the elevation of the CUR bioavailability but indifferent to the controllable CUR absorption into the circulatory system. Recently, some researchers presented for the controllable digestion of carrier oil droplets in gastrointestinal tract (GIT), in order to modulate release patterns of the incorporated materials (14, 15). Unfortunately, the strategy to control the digestion depends on the amount of intake and calcium ions, which are uncontrollable factors. Thus, the necessity for novel strategy still remains to overcome the hurdle for CUR use in the foods.

Lipid nanoparticle (LNP) systems have outstanding advantages as a carrier system for nutraceuticals such as protection of core materials (16) and improvement of the bioavailability (17). Solid lipid matrix of LNPs can provide an immovable condition to core materials and protect the materials from physical and biochemical stressors such as radicals, pH, salts, and metabolizing enzymes during the GIT digestion (18). Orally ingested LNPs are digested by lipases and form micelles mixed with bile salts, phospholipids, and the digestion products, thereby nutraceuticals incorporated in the mixed micelles can be absorbed to the lymph through enterocytes (19). Therefore, the CUR encapsulation using the LNPs is expected to enhance successfully the bioavailability. Meanwhile, polyethylene glycol (PEG) is well known for the nontoxicity in human body, thereby is routinely utilized for medical

purposes (20). PEGylation is defined as the process of both covalent and noncovalent attachment or amalgamation of PEG polymer chains to molecules and macrostructures, which can give an ability to mask the PEGylated agent from digestive enzymes and immune system of the host (21, 22).

In this regard, CUR encapsulated in PEGylated LNP system could be intactly delivered to small intestine tract without the degradation or oxidation, tardily released from the LNPs due to the lipase reaction rate slowed by the PEG effect, loaded within the mixed micelles, and continuously absorbed into the body. In this study, the LNP system prepared with the tristearin and PEGylated surfactants was applied to enhance the bioavailability of CUR. Furthermore, the effect of the molecular and concentration of the surfactants on the bioavailability of CUR was determined using both *in vitro* and *in vivo* models.

IV-2. Materials and Methods

IV-2-1. Chemicals

Glyceryl tristearate (tristearin, TS), polyoxyethylene (10) stearyl ether (PEG10SE, Brij® S10), and polyoxyethylene (100) stearyl ether (PEG100SE, Brij® S100) were purchased from Sigma Aldrich Co. (St. Louis, MO, USA). Liquid canola oil (LCO; 58.3 wt % oleic acid, 20.0 wt % linoleic acid, 8.3 wt % linolenic acid, 4.4 wt % palmitic acid, 1.8 wt % stearic acid, 1.3 erucic acid, 0.6 wt % arachidic acid, and 5.3 wt % other ingredients) were obtained from CJ Cheiljedang Co. (Seoul, Korea). CUR was supplied by Acros Organics (Pittsburg, PA, USA). All other chemicals were of analytical reagent grade.

IV-2-2. Lipid Nanoparticle and Emulsion Fabrication

The LNPs were prepared using an oil-in-water emulsion technique with a high-speed blender and sonication probe as reported previously by me (23), with a little modification. First, the lipid (5 wt %) and aqueous (95 wt %) phases were heated to 85 °C and mixed using a high-speed blender (Ultra-Turrax T25D, Ika Werke GmbH & Co., Staufen, Germany) at 8000 rpm for 1 min and then at 11000 rpm for 1 min, and maintained at 85 °C; the lipid phase (5 wt %) of the blank LNPs was only composed of TS and the lipid phase (5 wt %) of the CUR-loaded LNPs was prepared by blending TS (85 °C, 99 wt % of the lipid phase) and CUR (1 wt % of the lipid phase) dissolved in ethanol (25 mg mL^{-1}) and evaporating the ethanol with stirring for 30 min (85 °C); and the aqueous phase was fabricated by adding an PEG10SE or PEG100SE until reaching each concentration (5.331–46.910 mM of whole LNP system) in double-distilled water (DDW) containing 0.02 wt % sodium azide and mixing for 1 h. After preparing the coarse oil-in-water emulsion, droplet size was further reduced by sonication (VCX 750, Sonics & Materials Inc., Newtown, CT, USA) for 4 min at 60% amplitude, duty cycle of 1 s, and 95 °C. After reducing the droplet size, postsonication for 6 min was applied to the emulsions during cooling to 25 °C in a jacketed beaker, and the samples were maintained at room temperature (25 °C). CUR-loaded emulsion was prepared using the same method for the CUR-loaded LNP emulsified by 5.331 mM PEG10SE, except the utilization of canola oil substituted with TS.

IV-2-3. Quantification of Nonaggregated Lipid Nanoparticles (yield %)

LNPs diluted 10-fold with DDW were passed through a 1 μm pore size glass microfiber filter (GF/B, Whatman Ltd., Loughborough, UK). The aggregated LNPs (> 1 μm) remaining on the filter were weighed after drying in an oven at 60 °C. The difference of filter weight before and after the procedure, which was the weight of the aggregated LNPs, was recorded, and then yield (%) was calculated in the percentage of the difference over the sum of the weight for LNPs.

IV-2-4. Measuring the Size and ζ Potential of Lipid Nanoparticles and Emulsion

The prepared LNPs (4.5 mL) were diluted with 40.5 mL DDW in a vial to separate the layers containing the aggregated and nonaggregated LNPs. The vial containing the diluted samples was sealed tightly with a screw cap and incubated overnight at ambient temperature. The nonaggregated LNPs were collected by filtering with a 1 μm pore size glass microfiber filter (GF/B, Whatman Ltd.), and mean particle size (PS, z average) of the passed portion was measured using a Zetasizer (Nano ZS, Malvern Instruments Ltd., Worcestershire, UK) operated at a 173° angle with a helium-neon laser (λ = 633 nm). In addition, the ζ potential (ZP) was measured using the Zetasizer. The ZP measurement was based on the Smoluchowski equation at 25 °C with electric field strength of 20 V cm^{-1}.

IV-2-5. Determination of Emulsifier Surface Load

In an assumption of the round shape for all LNPs, emulsifier surface load (Γ_s) was calculated as $\Gamma_s = C_a D/6\Phi$, where C_a is the concentration of the emulsifier adsorbed to the surface of LNPs, D is the mean diameter (z average), and Φ is the lipid phase volume fraction (i.e, 0.05 lipid phase) (24). C_a was measured by subtracting the concentration of emulsifiers suspended as single molecules or micelles from the initial concentration of total emulsifiers in the aqueous phase. A total of 2.5 mL of the previously diluted and filtered LNP and emulsion system was injected into the Sephadex G-25 column (GE Healthcare, Chalfont St Giles, UK) filled with DDW. Next, 1 mL of DDW was serially added, and then each fraction passed through the column was collected in a microtube. Then, aliquots of the fractions in the fifth and sixth tubes were selected as samples, in which the emulsifier molecules did not participate in emulsifying activity. Colorimetry for quantification of PEGylated emulsifiers has been reported previously (25). Briefly, each sample was dried at 60 °C in an oven. The sample was then cooled in ambient condition, and 0.6 mL of ammonium cobaltothiocyanate (ACTC) solution and 1.2 mL of dichloromethane were added. The ACTC solution was prepared using 3 g of cobalt nitrate hexahydrate and 18 g of ammonium thiocyanate in 100 mL of DDW. Samples were vortexed for 10 s and centrifuged at 10400 RCF for 10 min (5427R, Eppendorf AG, Hamburg, Germany). After centrifugation, the dichloromethane layer was transferred to a micro quartz cell, and the absorbance at 625 nm was determined using a spectrophotometer

(Pharmaspec UV-1700, Shimadzu Corp., Kyoto, Japan). The amount of emulsifier molecules in samples was calculated using standard curves ranging 62.5–1000 and 31.25–2000 μg mL^{-1} for PEG10SE and PEG100SE (R^2 = 0.9998 and 0.9970), respectively.

IV-2-6. Entrapment Efficiency of the Curcumin-loaded Lipid Nanoparticles and Emulsion

A 0.2 mL portion of each emulsion or LNP system incorporating the CUR was added to 1.8 mL of methanol and acetonitrile mixture (1:1). The mixture was vortexed for 10 s and then centrifuged at 15000 RCF for 20 min (Eppendorf 5427R). After centrifugation, the supernatant was filtered through a 0.22 μm PVDF membrane (Millex-GV 33MM syringe filter, Merck Millipore, Bedford, MA, USA) and used as a sample for CUR quantification. HPLC system equipped with Waters 2695 Separations module (Milford, MA, USA) and analytical C18 column (Venusil XBP C18, 5 μm, 100 Å, 4.6 × 250 mm, Bonna-Agela Technology, Newark, DE, USA) was utilized for quantification. CUR detection was conducted at room temperature using Waters 996 Photodiode Array Detector (Milford, MA, USA). CUR in the sample (20 μL) was isocratically eluted at a flow rate of 0.8 mL min^{-1} using a mixture (35:55:10) of methanol, acetonitrile, and 5% (v/v) acetic acid as the mobile phase. The CUR concentration was calculated using a standard curve ranging 3.125–100 μg mL^{-1} (λ = 426.9 nm, R^2 = 1.0000). CUR entrapment efficiencies (EE (%)) of the CUR-loaded emulsion or LNPs were determined using the equation:

$$\text{EE}\ (\%) = \frac{W_t - W_s}{W_t} \times 100$$

where W_t is the total CUR molecule weight in the entire system, and W_s is the CUR molecule weight in the supernatant after centrifugation.

IV-2-7. Colloidal Stability of Lipid Nanoparticles and Emulsion in High Salt and Acidic Conditions

Prior to determining colloidal stability of LNPs and emulsion in harsh conditions, LNPs and emulsion were diluted 10-fold, then the aggregated particles and droplets eliminated by the filtration (1 μm). To make high salt condition, 5 mL of the diluted and filtered LNP and emulsion systems was blended with 3.8 mL of the mixture of all media and juices except HCl solution, proteins, bile, and enzymes in Table IV-1, and then adjusted to pH 7 using 1 M NaOH or 1 M HCl solution with monitoring on pH meter (Professional Meter PP-15, Sartorius AG, Goettingen, Germany). For acidic condition experiments, the pH of the diluted and filtered dispersions was adjusted to pH 3 using 50 mM HCl solution with monitoring on the pH meter. After the treatment of high salt and acidic conditions, LNP and emulsion samples were incubated in a shaking water bath (BS-31, JEIO Tech., Seoul, Korea) for 2 h at 37 ℃ with shaking (100 rpm). Next, 1 mL of the samples was used to measure the size and ZP of particles and droplets in the samples using the Zetasizer (Malvern Nano ZS).

IV-2-8. Determining the *in Vitro* Digestion Patterns of the Lipid Nanoparticles and Emulsion

The digestion patterns of CUR-loaded LNPs and emulsion during or after the *in vitro* digestion were determined as monitoring the particle characteristics (PS and ZP), quantifying the bioaccessible CUR, analyzing the CUR release patterns from particles, and profiling the particle lipolysis. First, for determining the effects of pancreatic lipase and bile acids on the characteristics of LNPs and emulsion, each 5 mL of the LNPs and emulsion previously diluted (10-fold) and filtered (1 μm) were treated with pancreatic lipase solution (3.965 mg mL^{-1}), bile extract solution (41.32 mg mL^{-1}), and the mixture of the lipase and bile solutions, which were incubated for 2 h at 37 °C with shaking (100 rpm). After the incubation, 2 mL of the samples was centrifuged for 10 min at 25000 RCF (Eppendorf 5427R), and the PS and ZP of LNPs and emulsion in the supernatant were measured using the Zetasizer (Malvern Nano ZS).

The mimicked *in vitro* digestion test model was modified from the version described by Hur et al (26):

I. preingestion: LNPs and emulsion were passed through a 1 μm pore sized filter
II. mouth (pH 7; 5 min): 5 mL of filtered systems was mixed with 6 mL simulated salivary medium
III. stomach (pH 3; 2 h): 12 mL of simulated gastric juice were added

IV. small intestine (pH 6.5–7; 2 h): simulated duodenal juice (12 mL), bile juice (6 mL), and $NaHCO_3$ solution (2 mL) were added.

The formulations of the simulated saliva medium, gastric, duodenal, and bile juices are shown in Table IV-1. All samples were shaken (100 rpm) in the water bath (JEIO Tech BS-31) during the *in vitro* digestion test and maintained at 37 °C to mimic GIT motility. After the digestion for 4 h 5 min and centrifugation for 10 min at 25000 RCF, the PS and ZP of supernatant samples were measured using the Zetasizer (Malvern Nano ZS).

After all digestion steps, the relative bioaccessibility of CUR was determined as described earlier (17), with modifications. Briefly, the whole digesta (43 mL) was firstly centrifuged to gravitate the insoluble CUR part and proteins for 30 min at 1500 RCF (Supra 22K, Hanil Science Industrial Co., Seoul, Korea), and their whole supernatant was secondly centrifuged to gravitate the insoluble CUR and protein residues for 20 min at 16000 RCF. Each pellet firstly and secondly gravitated was carefully washed twice with DDW, then 43 mL of the mixture (45:45:10) of methanol, acetonitrile, and DDW was added prior to the sonication treatment to dissolve CUR in the mixture solvent and the centrifugation for 20 min at 16000 RCF. The mixture of each supernatant for two pellets was collected to quantify the insoluble CUR part after the digestion. Meanwhile, after the second centrifugation of the digesta, a 0.2 mL aliquot the supernatant was diluted 10-fold with 1.8 mL of the mixture (1:1) of methanol and acetonitrile prior to centrifugation for 20 min at 16000 RCF, and the

supernatant was collected to quantify the soluble CUR part after the digestion. After collecting supernatants containing the insoluble and soluble parts of CUR, each supernatant was filtered through the 0.22 μm PVDF membrane (Millipore Millex-GV). The concentration of CUR in the supernatant was quantified using a same method in the EE (%) determination section and calculated using standard curves ranging 3.125–100 μg mL^{-1} (λ = 426.9 nm, R^2 = 1.0000). The relative bioaccessibility of the flavonoids in the digested micellar fraction was determined using the equation:

$$\text{bioaccesibility (\%)} = \frac{W_s}{W_p + W_s} \times 100$$

where W_s is the weight of the CUR in the supernatant collected as the soluble CUR part, and W_p is the weight of the CUR in the supernatant mixture for two pellet collected as the insoluble CUR part. In addition to the CUR-encapsulated LNPs, equivalent quantities (500 μg mL^{-1}) of CUR in their native form and the diluted form with ethanol, LCO, and tristearin were also investigated.

The release patterns of the CUR from the LNPs and emulsion were studied using dialysis bags with a 12 kDa molecular weight cut-off. The bags were immersed in DDW for 12 h before use. They were filled with 5 mL of the CUR-loaded LNP and emulsion sample, tightly sealed, suspended in 45 mL of the mixture (1:1) of the enzyme-free *in vitro* digestion medium mixture and methanol, which were rotated at 100 rpm in a 37 °C water bath. At predetermined time intervals, a 1 mL aliquot was withdrawn from the medium mixture, and 1 mL of fresh medium was replaced

immediately. Next, the absorbance of the aliquot was measured with a spectrophotometer. The concentrations of CUR in the aliquots were calculated using standard curves ranging 2.5–40 μg mL^{-1} (λ = 426.9 nm, R^2 = 0.9996).

Determining lipolysis patterns of CUR-loaded LNPs and emulsion were carried out for 2 h at 37 °C using the previously introduced titration method (27) with little modification. The simulated intestine fluid used in this analysis was prepared by dissolving sodium chloride, calcium chloride, bile extract, and pancreatic lipase in 10 mM sodium phosphate buffer (pH 7) as the concentrations at 43.83, 11.098, 100, and 12 mg mL^{-1}, respectively, which was adjusted to the pH 7 using 1 M NaOH solution as necessary. Prior to titration, the LNPs and emulsion were diluted 10-fold with 10 mM sodium phosphate buffer (pH 7), which was adjusted to the pH 7 using 0.1 M NaOH solution as necessary. Lipid digestion was monitored by measuring the free fatty acid (FFA) release from the samples after the fluid addition. Lipase hydrolyzes one triacylglycerol (TAG) into one monoacylglycerol (MAG) and two FFAs. The released amount of FFAs was quantified by adding 50 mM NaOH solution to the reaction vessel to maintain the pH 3 using an automatic titration unit (842 Titrando, Metrohm AG, Herisau, Switzerland). The added amount of NaOH is proportional to the produced amount of FFAs. Blank experiments were also conducted without the enzyme to eliminate any pH decrease due to other factors. All the samples were diluted with the phosphate buffer and the fluid so that the final lipid content in the reaction beaker was 0.4 wt %.

Table IV-1. Formulations and Concentrations of the Various Media and Juices for the Simulated *in Vitro* Digestion Test of Blank Lipid Nanoparticles

	saliva medium	gastric juice	duodenal juice	bile juice
inorganic solution	20 mL $NaHCO_3$ 84.7 g L^{-1}	15.7 mL NaCl 175.3 g L^{-1}	40 mL NaCl 175.3 g L^{-1}	30 mL NaCl 175.3 g L^{-1}
	10 mL KCl 89.6 g L^{-1}	9.2 mL KCl 89.6 g L^{-1}	40 mL $NaHCO_3$ 84.7 g L^{-1}	60.3 mL $NaHCO_3$ 84.7 g L^{-1}
	10 mL NaH_2PO_4 88.8 g L^{-1}	18 mL $CaCl_2{\cdot}2H_2O$ 22.2 g L^{-1}	6.3 mL KCl 89.6 g L^{-1}	4.2 mL KCl 89.6 g L^{-1}
	1.7 mL NaCl 175.3 g L^{-1}	3.0 mL NaH_2PO_4 88.8 g L^{-1}	9 mL $CaCl_2{\cdot}2H_2O$ 22.2 g L^{-1}	10 mL $CaCl_2{\cdot}2H_2O$ 22.2 g L^{-1}
	10 mL Na_2SO_4 57 g L^{-1}	10 mL NH_4Cl 30.6 g L^{-1}	10 mL KH_2PO_4 8 g L^{-1}	150 µL HCl 35% g g^{-1}
	10 mL KSCN 20 g L^{-1}	6.5 mL HCl 35% g g^{-1}	10 mL $MgCl_2$ 5 g L^{-1}	
			180 µL HCl 35% g g^{-1}	
organic solution	8 mL urea 25 g L^{-1}	34 mL urea 25 g L^{-1}	4 mL urea 25 g L^{-1}	10 mL urea 25 g L^{-1}
		10 mL glucose 65 g L^{-1}		
		10 mL glucosamine hydrochloride 33 g L^{-1}		
		10 mL glucuronic acid 2 g L^{-1}		
add to mixture	15 mg uric acid	1 g BSA	1 g BSA	1.8 g BSA
inorganic + organic	25 mg mucin	3 g mucin	9 g pancreatin	30 g bile
solution	290 mg α-amylase	2.5 g pepsin	1.5 g lipase	
pH	6.8	1.3	8.1	8.2

IV-2-9. Pharmacokinetic Study

Male Sprague Dawley (SD) rats (250–300 g) were sacrificed for *in vivo* pharmacokinetic studies. The pharmacokinetic procedure was duly permitted by the Institutional Animal Care and Use Committee of the Seoul National University, Seoul, Korea (Registration number, SNU-160316-1, Korea). The rats were divided into nine groups (n = 5). Group 1 was administered with 50 mg kg^{-1} body weight (BW) of CUR dissolved in ethanol; group 2 with 50 mg kg^{-1} BW of CUR dissolved in LCO; group 3 with as 25 mg kg^{-1} BW of CUR incorporated in LCO emulsion; group 4 and 5 were respectively administered with 25 mg kg^{-1} BW of CUR encapsulated in LNPs emulsified by 17.058 and 40.000 mM PEG10SE; and group 6 was administered 25 mg kg^{-1} BW of CUR encapsulated in LNPs emulsified by 17.058 mM PEG100SE using oral gavage. After the administration, 0.4 mL of the blood sample was collected from the tail vein into the tubes with K_2EDTA. After sampling, 0.5 mL of dextrose normal saline was administered to prevent changes in the central compartment volume and electrolytes. Plasma was obtained by the blood sample centrifugation at 4000 RCF for 10 min (4 °C). The 25 μL of 2.8% acetic acid was added to 200 μL of the plasma for CUR stabilization; 50 μL of β-estradiol 17-acetate (100 μg mL^{-1} of ethanol) as internal standard was added, vortexed for 20 s; then the extraction was conducted by adding 1 mL of ethyl acetate and vortexing for 10 min. After the extraction, it was finally centrifuged at 10000 RCF for 10 min (4 °C). The organic layer containing CUR and β-estradiol 17-acetate was collected and evaporated for 40 min using a

centrifugal evaporator (CVE-2200, Tokyo Rikakiki Co., Ltd., Tokyo, Japan), which was reconstituted in the 200 μL mixture (45:45:10) of methanol, acetonitrile, and DDW and analyzed using the HPLC method introduced in the EE (%) determination section.

IV-2-10. Data Analysis

Pharmacokinetic parameters were calculated based on the curcumin plasma concentration profiles under pharmacokinetic study. AUC_{0-t}, which was the area under the profile from time 0 to time t, was determined using a trapezoidal method. Peak concentration ($C_{\max}$) and time of peak concentration ($t_{\max}$) were obtained from the individual profiles. $AUC_{0-\infty}$, which was the area under the profile from time 0 to infinity, was determined as:

$$AUC_{0-\infty} = AUC_{0-t} + C_t/K_e$$

where C_t is the curcumin concentration observed at last time, and K_e is the apparent elimination rate constant obtained from the terminal slope of the individual profiles. All results from the pharmacokinetic study were analyzed using Tukey's significant difference test using the IBM SPSS Statistics version 21.0 software (IBM Co., Armonk, NY, USA). Data represent means of at least three independent experiments or measurements. A p value <0.05 was considered to indicate a significant difference.

IV-3. Results and Discussion

IV-3-1. Characteristics of Lipid Nanoparticles

Blank and CUR-loaded LNPs emulsified by PEG10SE and PEG100SE in various concentrations were shown in Figure IV-1. All LNPs stabilized by 46.910 mM emulsifiers were translucent whereas others were opaque despite the same content of lipid phase, which means that PS of LNPs covered by 46.910 mM emulsifiers is smaller than that of other systems. In addition, LNPs prepared using PEG100SE at the concentration above 25.588 mM were thicker than other LNPs using PEG100SE. Particularly, LNPs emulsified by 46.910 mM PEG100SE looked like a non-fluidic gel, which resulted from the characteristic of long-chained PEG. However, their high viscosity was disappeared after the 10-fold dilution.

In the cooling stage among serial procedures for the LNP preparation, the melted TS molecules in droplets were crystallized to the solid TS, which may generate some partially coalesced (28) or aggregated LNPs (29). These unstable particles were eliminated after the dilution and filtration procedures of the yield (%) determination because of their large PS in a micron scale. Therefore, the yield (%) value means the amount of nonaggregated LNPs and is the criterion for colloidal stability of the prepared LNP system. The yield (%) of the produced LNPs was quantified as shown in Figure IV-2a. In emulsifier concentrations $\leq$ 34.117 mM, the yield (%) values of LNPs emulsified by PEG10SE was lower than those for PEG100SE while the values

were similar to each other at 46.910 mM, which was attributed to the difference between PEG10SE and PEG100SE on the length of hydrophilic part, i.e. PEG part. This result suggests that longer PEG molecules at the interface between water and lipid phases could better hinder the collision among LNPs as a steric effect. Moreover, in all LNP samples, the yield (%) was elevated with increasing the surfactant concentration, which resulted from the elevation of the amount of emulsifiers participating in the lipid stabilization at the interface. Meanwhile, the difference between the blank and CUR-loaded LNPs in the yield (%) was not observed, which suggest that encapsulating CUR at 1 wt % of lipid phase could not affect the colloidal stability of LNP system.

It is well known that the quantitative increase of emulsifiers used for preparing emulsion affects the droplet size decrease, because more emulsifiers can stabilize the droplet surface more widened by the size decrease (30). This effect was also observed in this result (Figure IV-2b). PS of all LNPs was decreased with the elevation of PEG10SE and PEG100SE concentrations. In a general trend, the PS of LNPs emulsified by PEG10SE were more sensitive to the emulsifier concentration change than that of PEG100SE-LNPs, which might be influenced by the deference in the diffusion coefficient from the aqueous phase to particle surfaces (31). On the one hand, it seemed that there was no relationship between CUR loading and unloading to the LNP size, which was in accordance with the yield (%) result.

Because both PEG10SE and PEG100SE are nonionic surfactants, their electrical charge is near to zero. According to this reason, it can be inferred that the increased contents of these emulsifiers used for LNP preparation influenced the neutralization of the LNP surface charge (Figure IV-2c), resulting from an effect of PEG covering the TS surface of LNPs. However, almost of the LNPs still had the negative surface charge except the samples emulsified by 34.117 and 46.910 mM PEG100SE. In particular, the surface charge of all LNPs emulsified by PEG10SE was negative even in high level PEG10SE, which could imply that the hydrophilic part (10 molecules of ethylene glycols) is insufficient to cover the TS surface of LNPs. Additionally, the surface charge of CUR-loaded LNPs was lower than that of the blank LNPs, because of CUR molecules present in the TS matrix.

The surface load value of LNPs indicates the amount of emulsifier molecules adsorbed on a unit surface of the LNPs (32). Therefore, larger surface load value means denser emulsifiers on the LNP surface and more stable LNPs as a colloid system. In this study, the surface load results were measured as shown in Figure IV-2d. Surface load values of all LNPs were enlarged with the growth of the emulsifier concentration below 34.117 mM. However in 34.117 and 46.910 mM samples, the values were maintained at ~3 nm^{-2}, which allude to the quantitative limit of the emulsifiers (PEG10SE and PEG100SE) that can occupy the LNP surface. In Figure IV-2c, ZP values of LNPs prepared using PEG10SE or PEG100SE at 34.117 and 46.910 mM were similar, which might be attributed to this surface load limit.

Meanwhile, results in Figure IV-2 was more detailedly discussed in the Appendix section.

EE (%) of CUR incorporated in LNP matrix was determined as shown in Figure IV-2e. All CUR-loaded LNPs had values above 90%, which means that the almost of the CUR utilized for preparing CUR-loaded LNPs was well encapsulated in TS matrix. There were no trend relating to the concentration and molecular weight of emulsifiers. Meanwhile, the CUR-loaded LCO emulsion fabricated using 46.910 mM PEG10SE had a similar EE (%) value (91.04%) to all CUR-loaded LNPs. Moreover, in other physicochemical characteristics (PS, ZP, and surface load), this emulsion was similar to the CUR-loaded LNP emulsified by 46.910 mM PEG10SE.

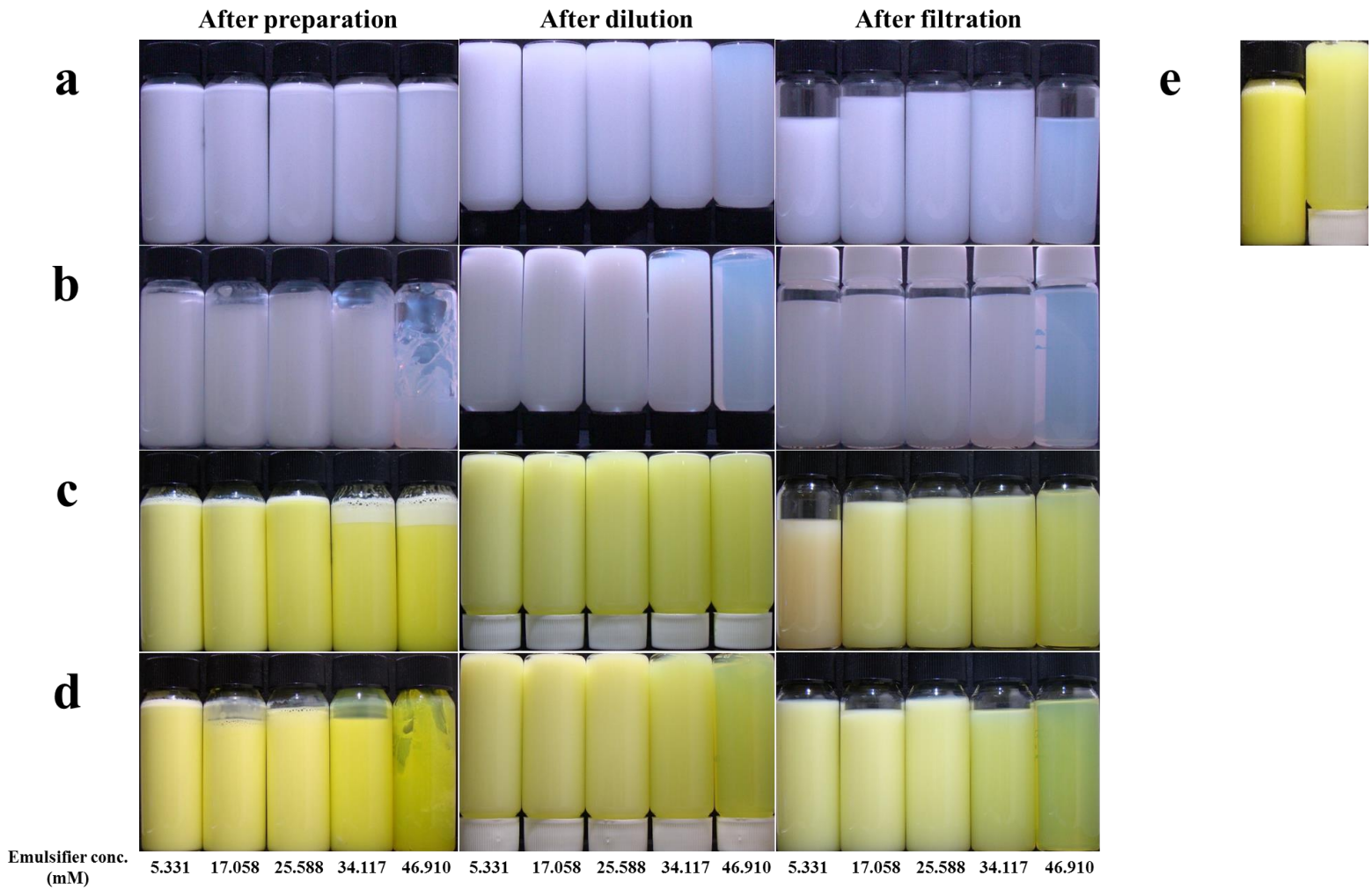
After preparation
After dilution
After filtration
a
b
c
d
e
Emulsifier conc. (mM)
5.331 17.058 25.588 34.117 46.910 5.331 17.058 25.588 34.117 46.910 5.331 17.058 25.588 34.117 46.910

Figure IV-1. Lipid nanoparticle systems after preparation, dilution (10-fold), and subsequent filtration (1 μm). Blank tristearin nanoparticles emulsified by (a) polyoxyethylene (10) stearyl ether and (b) polyoxyethylene (100) stearyl ether; curcumin-loaded tristearin nanoparticles emulsified by (c) polyoxyethylene (10) stearyl ether and (d) polyoxyethylene (100) stearyl ether; and (e) curcumin-loaded canola oil emulsion emulsified by polyoxyethylene (10) stearyl ether.

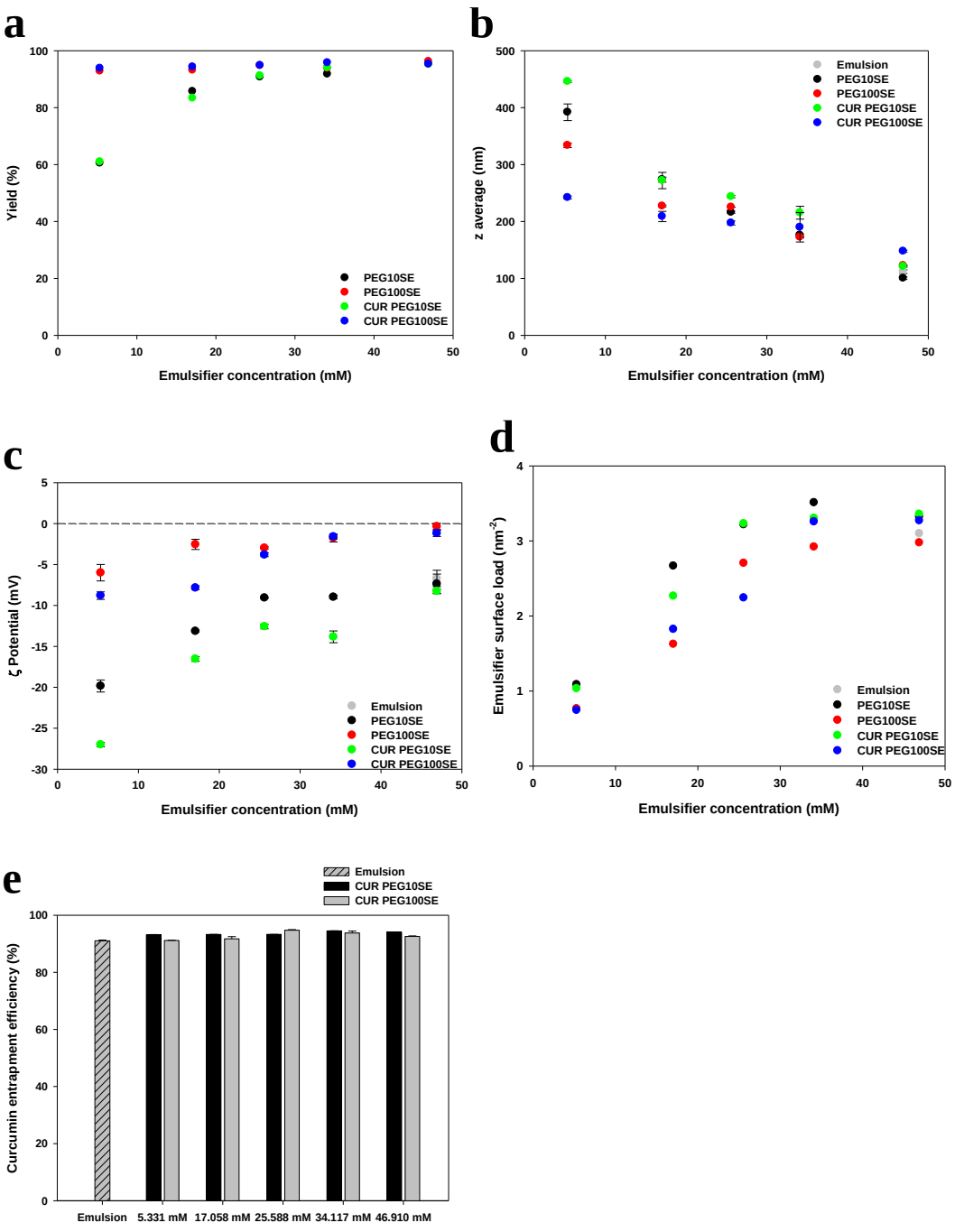
a
Yield (%)
Emulsifier concentration (mM)
PEG10SE
PEG100SE
CUR PEG10SE
CUR PEG100SE
b
z average (nm)
Emulsifier concentration (mM)
Emulsion
PEG10SE
PEG100SE
CUR PEG10SE
CUR PEG100SE
c
ζ Potential (mV)
Emulsifier concentration (mM)
Emulsion
PEG10SE
PEG100SE
CUR PEG10SE
CUR PEG100SE
d
Emulsifier surface load (nm-2)
Emulsifier concentration (mM)
Emulsion
PEG10SE
PEG100SE
CUR PEG10SE
CUR PEG100SE
e
Curcumin entrapment efficiency (%)
Emulsion
CUR PEG10SE
CUR PEG100SE
Emulsion
5.331 mM
17.058 mM
25.588 mM
34.117 mM
46.910 mM

Figure IV-2. Physicochemical characteristics of blank and curcumin-loaded tristearin nanoparticles and curcumin-loaded canola oil emulsion. (a) Yield (%), (b) particle size (z average), (c) ζ potential, (d) emulsifier surface load, and (e) entrapment efficiency of blank and curcumin-loaded lipid nanoparticles and curcumin-loaded emulsion as the increase of emulsifier concentration. Emulsion, curcumin-loaded canola oil emulsion; CUR PEG10SE and CUR PEG100SE, curcumin-loaded tristearin nanoparticle emulsified by polyoxyethylene (10) stearyl ether and polyoxyethylene (100) stearyl ether, respectively.

IV-3-2. Effects of Incubation Condition on Colloidal Stability of the Curcumin-loaded Lipid Nanoparticles

Colloid system is easy to be influenced by conditions of its continuous phase such as pH, ions, etc. Particularly, the pH changes and the high concentration of various ions during the GIT digestion of ingested colloids can cause undesirable results like a colloid aggregation (33), which might induce the unpredictable LNP digestion opposed to the purpose in this research. In this regard, the LNP stability was determined in high salt and low pH conditions (Figure IV-3). As observed in Figure IV-3a and b, only some minor aggregations were identified in LNP samples except a sample emulsified by 5.331 mM PEG10SE. In previous research, it was observed that oil droplets stabilized by nonionic surfactant were relatively stable in the similar conditions (high salts and low pH) (34). According to the data in Figure IV-3c and d, the surface charge of all samples was near to zero in the salty and pH 3 conditions. Thus, a mechanism to prevent the LNP collision is just a steric hindrance by surfactants (PEG10SE or PEG100SE) at the interface of LNPs. Fortunately, LNPs would be not aggregated by the intermediation of positive-charged divalent ions (35), because the net charge of the surfactants is zero. Consequently, the orally administered CUR-loaded LNPs are expected to reach the small intestine without the unexpected aggregation.

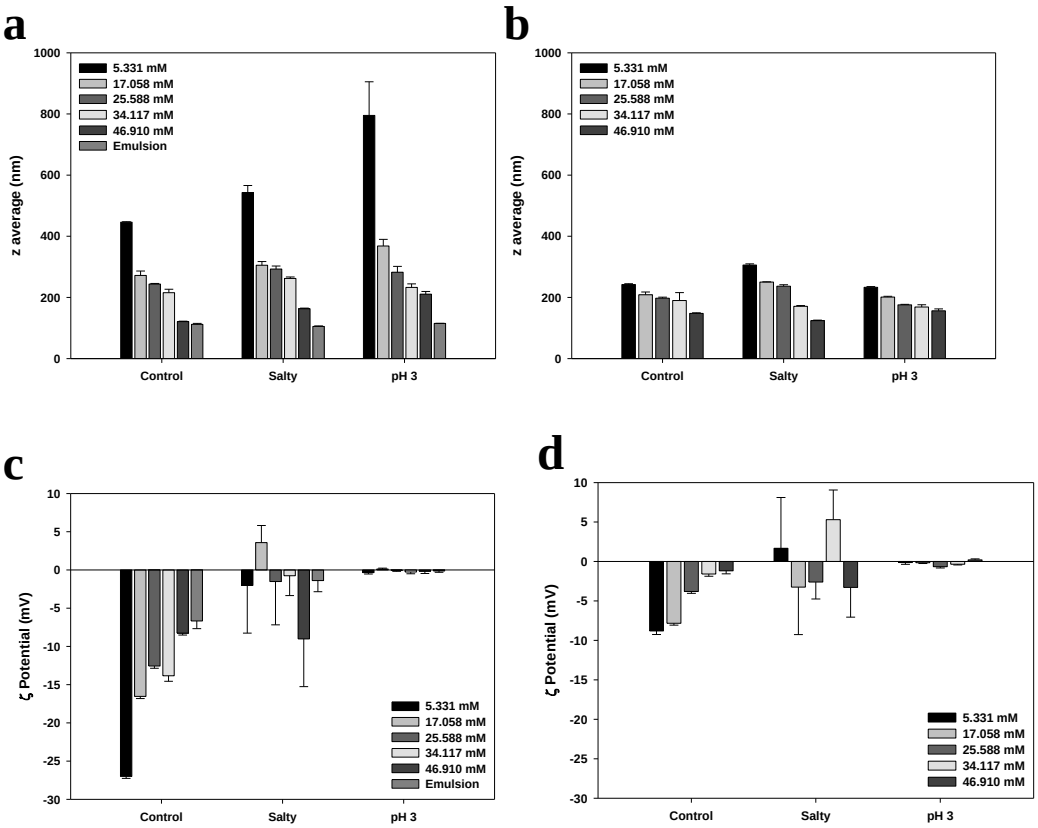

Figure IV-3. Colloidal stability of curcumin-loaded tristearin nanoparticles and canola oil emulsion after the incubation (2 h) in high salty and acidic (pH 3) conditions. Particle size (z average) of curcumin-loaded tristearin nanoparticles and canola oil emulsion emulsified by (a) polyoxyethylene (10) stearyl ether or (b) polyoxyethylene (100) stearyl ether; and ζ potential of curcumin-loaded tristearin nanoparticles and canola oil emulsion emulsified by (c) polyoxyethylene (10) stearyl ether or (d) polyoxyethylene (100) stearyl ether.

IV-3-3. *In Vitro* Digestion and Absorption of the Curcumin-loaded Lipid Nanoparticles

In small intestine, one triacylglycerol composed of long chain fatty acids is hydrolyzed to one monoglycerol and two fatty acids by pancreatic lipase; aggregates with the hydrolyzed molecules, phospholipids, and bile acids; forms the mixed micelles; and is finally absorbed into the circulatory system through enterocytes (36). In this study, the strategy for CUR uptake is to be incorporated within the mixed micelles and to be delivered into the circulatory system. Therefore, the lipolysis of CUR-loaded LNPs by the lipase is the key point to control the CUR uptake. For the lipolysis of LNPs, the lipases need the bald lipid surface of LNPs to adsorb. Lipases can firstly hydrolyze tristearin molecules from the bald surfaces, if there are some bald surfaces. Otherwise, lipases should adhere to the LNP surface after elimination of the hindrance by PEG, if there are no bald surfaces to adsorb. Bile acids play a role for the hindrance elimination by means of the surfactant displacement from the lipid surface (37). In this regard, the results in Figure IV-4 can explain the lipase adsorption and the substitution of bile acids. A slight change in LNP sizes was observed under the lipase adding condition in LNP samples emulsified by both PEG10SE and PEG100SE (Figure IV-4a and b). However, ZP of samples emulsified by PEG10SE was more decreased than samples for PEG100SE after the lipase addition (Figure IV-4c and d). This result implies that all LNP samples were not degraded by lipase alone but lipase can more adhere to PEG part of PEG10SE compared to the part of

PEG100SE. Under the bile extract addition, a little PS change was also observed in all samples. However, all ZP values of PEG10SE-LNP samples were similar to each other (~40 mV) while a slight ZP decrease was observed in PEG100SE-LNP samples. This result suggest that PEG10SE molecules can be easily replaced by bile acids (ZP: ~52 mV) but PEG100SE molecules can relatively well prevent bile acids from adsorbing on the LNP surface. Under each condition of the bile/lipase mixture and the digestion juice, PS values of all LNP samples were significantly changed, which indicates the LNP lipolysis. Meanwhile, results in Figure IV-4 was more detailedly discussed in the Appendix section.

CUR has many health benefits but has limited bioavailability due to its low permeability across the apical surface of intestinal epithelial cells (38). A LNP system was adopted to overcome this hurdle, which was expected to improve the CUR bioaccessibility. In this regard, the relative quantity of bioaccessible CUR was measured as shown in Figure IV-5. According to this result, the bioaccessibility (%) of the native-formed CUR sample was just 14.13%. In contrast, the values of CUR dissolved in ethanol, LCO, and TS were 92.35, 66.28, and 70.29%, respectively. In particular, the values of CUR incorporated in emulsion and LNP systems were near to 94%. These results means that the bioaccessibility (%) was already determined by the ingestion form of CUR. As discussed earlier, the LNP system is hydrolyzed in small intestine by the action of bile acids and lipases, which induces the formation of mixed micelles. Therefore, CUR molecules encapsulated in LNPs would solubilize

well in the micelles unlike a native-formed CUR. Comparatively large bioaccessibility (%) of the CUR sample dissolved in LCO and TS can be also understood in the same context, i.e. incorporation in the micelles. However, the CUR sample dissolved in ethanol did not have the large bioaccessibility (%) from the same reason but from the instantaneously increased solubility of CUR due to ethanol. Because only this instantaneous increase by ethanol cannot confirm the quantitative increase of the CUR absorbed by enterocytes, the bioavailability of this sample would be still low level. Meanwhile, in all LNP samples, CUR molecules encapsulated in the LNP matrix were only released <40% for 2 h into the medium despite its sink condition accelerated by 50% ethanol (Figure IV-6). In addition, it can be estimated that the CUR molecules would not be concentrically positioned at the outer shell of LNPs but evenly distributed into the lipid matrix, because there was no burst release phenomenon of CUR from LNPs. In this regard, the CUR molecules in lipid matrix could not be unintensionally released unless CUR-loaded LNPs are hydrolyzed by lipase. Consequently, the LNP system promised the high level bioaccessibility of CUR at least.

The mixed micelles produced by lipid digestion in small intestine are absorbed into enterocytes (19), where fatty acids and monoacylglycerols composing the micelles are recombined into triacylglycerols, are transformed into the chylomicrons with the recombined triacylglycerols, cholesterols, and apoproteins, then are finally taken into the lymphatic system through lacteals (36). Therefore, the uptake of CUR

incorporated in the mixed micelles into the circulatory system depends on the micelle production in small intestine, the micelle absorption into enterocytes, and the chylomicron synthesis in enterocytes. In an assumption of the steady rate of the micelle absorption and the chylomicron synthesis, the CUR uptake rate is governed by the producing rate of the mixed micelles, which was affected by the lipolyzing rate of CUR-loaded LNPs. For this connection, the amount of free fatty acids produced from TS molecules of the LNPs was profiled as shown in Figure IV-7. In the CUR-loaded LNP samples emulsified by PEG10SE (Figure IV-7a), the lipid digestion was quicken with increasing the amount of PEG10SE utilized for LNP production. This result corresponds to the specific surface area widened by the PS decrease, due to the increase of PEG10SE concentration. However, this trend was not observed in the LNP samples emulsified by PEG100SE, but rather the extent of the lipid digestion within 2 h was become smaller with the increase of PEG100SE concentration (Figure IV-7b), which might be due to the PEG100SE action for preventing the emulsifier replacement by bile acids. In a LCO emulsion sample stabilized by 46.910 mM PEG10SE, ~50% of lipid droplets was digested within 10 min, because the digestion of liquid oil, as usual, is rapider than that of solid lipid. In summary, these results suggest that the digestion rate and extent of the particulate lipid can be modulated by the designs in the lipid composition and the molecular weight/concentration of PEGylated surfactants. Furthermore, it was hypothesized that the bioavailability of CUR encapsulated in the designed particulate lipids could be controllable in this

manner. Meanwhile, results in Figure IV-7 was more detailedly discussed in the Appendix section.

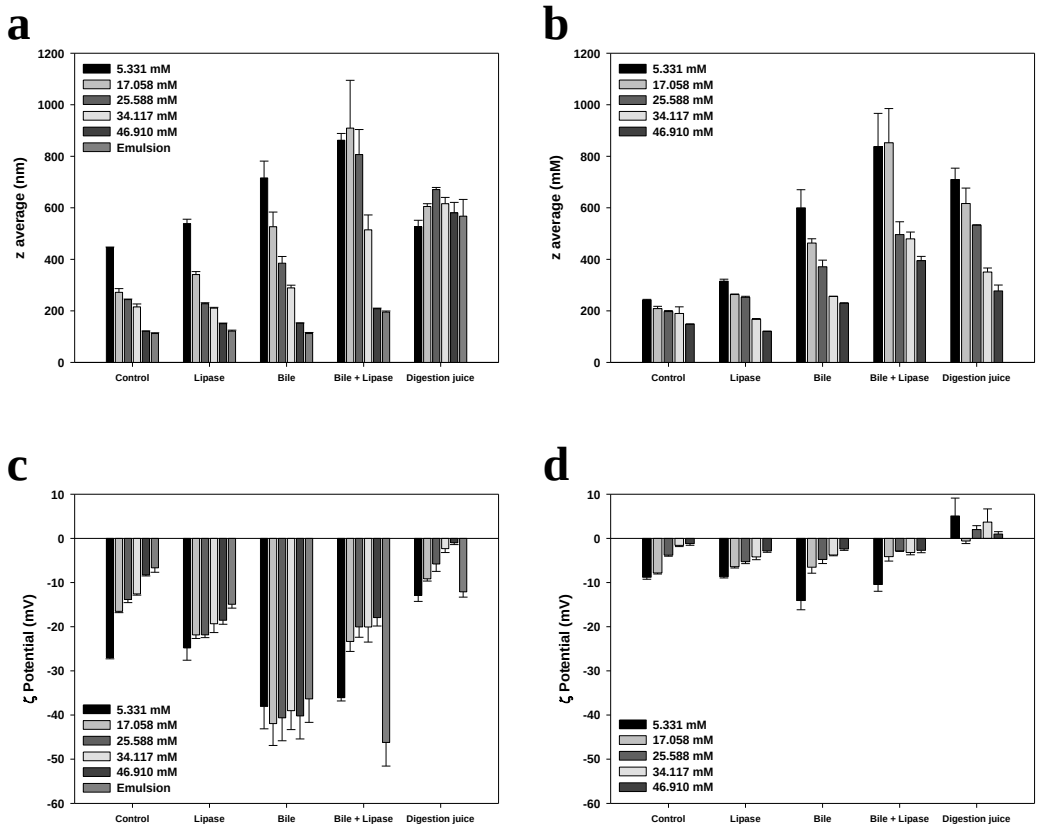

Figure IV-4. Particle size (z average) and ζ potential for curcumin-loaded tristearin nanoparticles and canola oil emulsion after the treatment (2 h) of lipase, bile extract, the mixture of lipase and bile extract, and the simulated digestion juice. Particle size (z average) of curcumin-loaded tristearin nanoparticles and canola oil emulsion emulsified by (a) polyoxyethylene (10) stearyl ether or (b) polyoxyethylene (100) stearyl ether; and ζ potential of curcumin-loaded tristearin nanoparticles and canola oil emulsion emulsified by (c) polyoxyethylene (10) stearyl ether or (d) polyoxyethylene (100) stearyl ether.

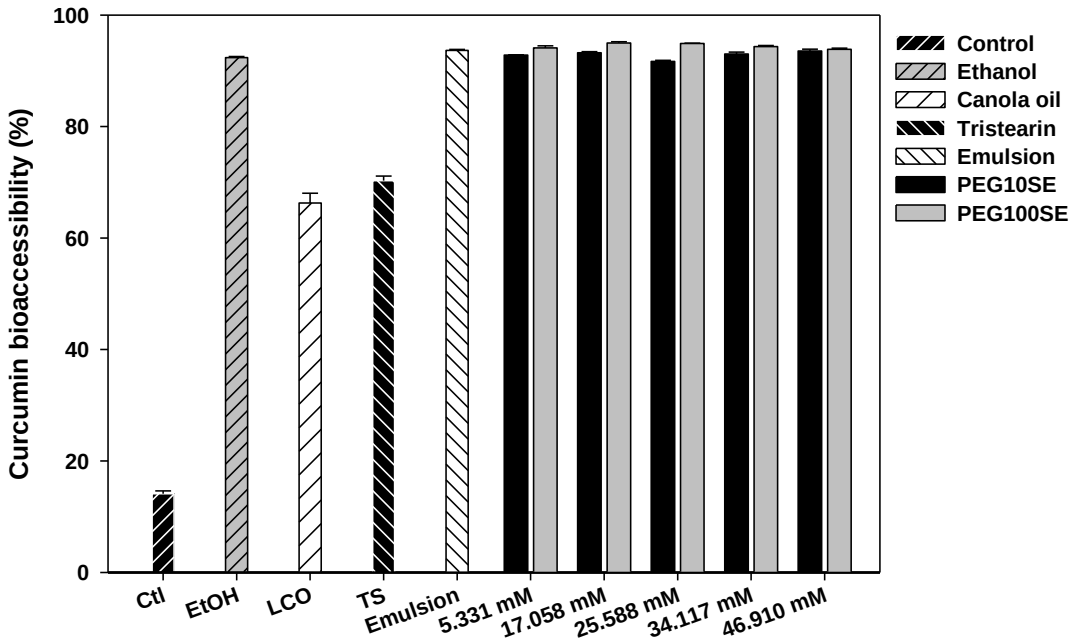

Figure IV-5. Curcumin contents in the digested micellar fraction, bioaccessibility (%), after the simulated digestion was completed. Control (Ctl), powdered curcumin; Ethanol (EtOH), curcumin dissolved in ethanol; canola oil (LCO), curcumin in canola oil; Tristearin (TS), curcumin in tristearin; Emulsion, curcumin-loaded canola oil emulsion; PEG10SE and PEG100SE, curcumin-loaded tristearin nanoparticles emulsified by polyoxyethylene (10) stearyl ether and polyoxyethylene (100) stearyl ether, respectively.

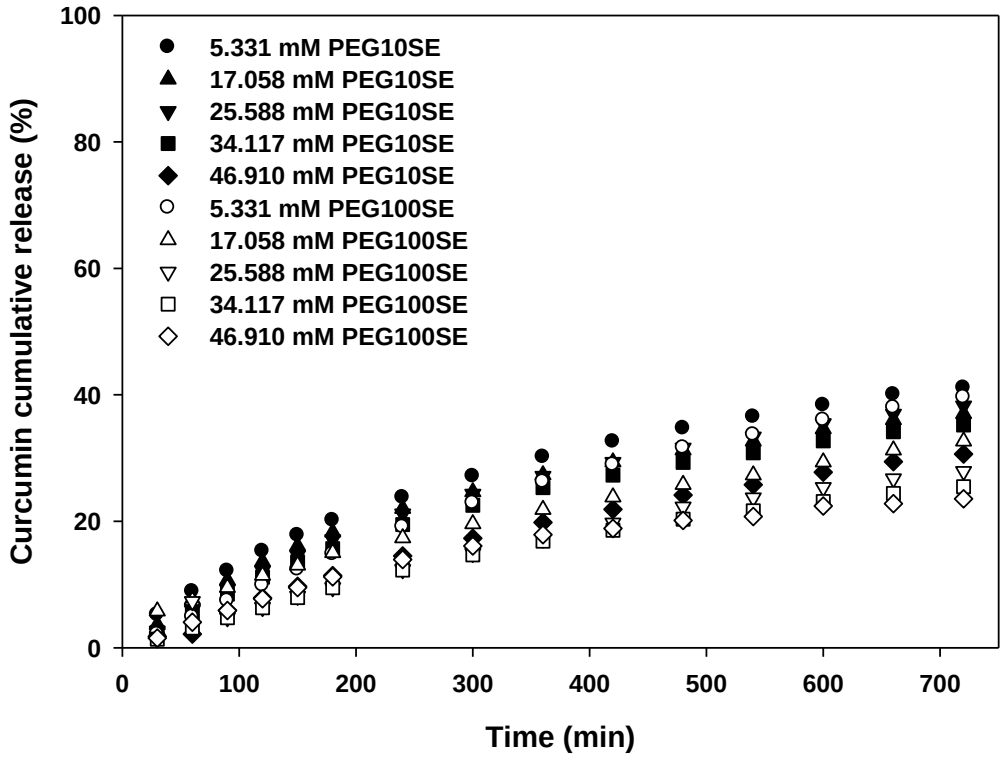

Figure IV-6. ***In vitro*** **cumulative release profiles of curcumin from tristearin nanoparticles and canola oil emulsion in the enzyme-free simulated digestion medium using a dialysis membrane under sink conditions (50% v/v ethanol).** PEG10SE and PEG100SE, tristearin nanoparticle samples emulsified by polyoxyethylene (10) stearyl ether and polyoxyethylene (100) stearyl ether, respectively.

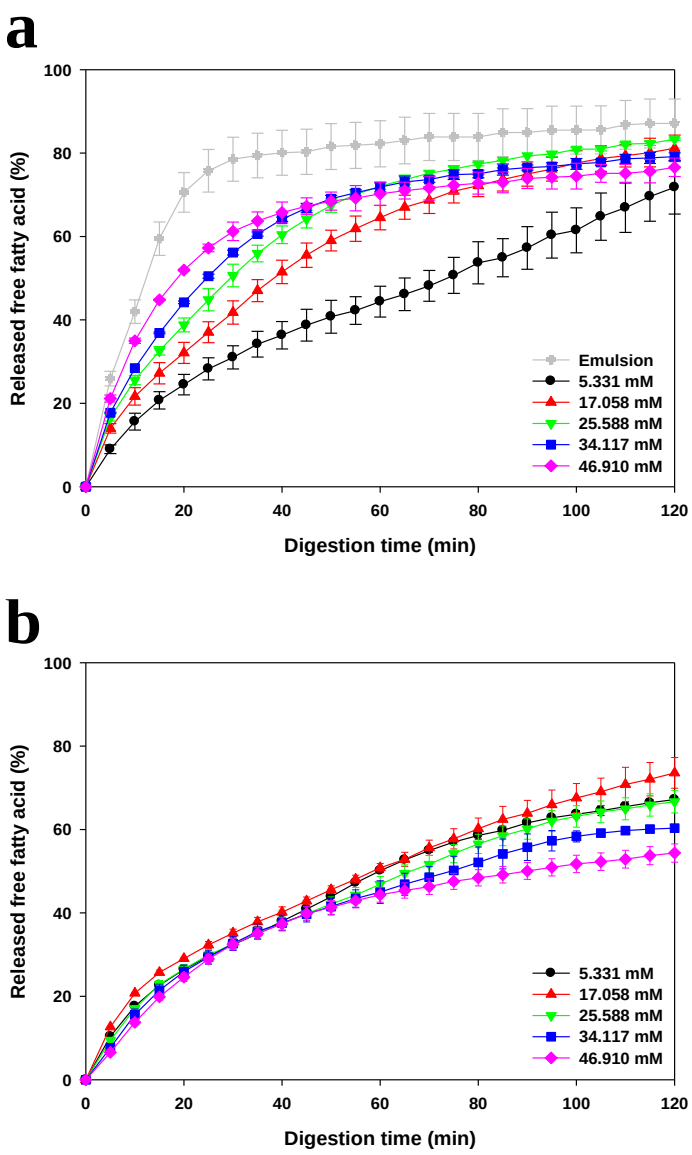

Figure IV-7. Lipolysis profiles of curcumin-loaded tristearin nanoparticles and canola oil emulsion (Emulsion) in the simulative small intestine condition as the changes of emulsifier concentration. Samples emulsified by (a) polyoxyethylene (10) stearyl ether and (b) polyoxyethylene (100) stearyl ether.

IV-3-4. *In Vivo* Pharmacokinetics and Bioavailability of the Curcumin Encapsulated in Lipid Nanoparticles

CUR-loaded LNPs were designated to enhance the oral bioavailability of CUR. CUR levels in the plama of model rat blood were determined as CUR concentration-time profiles observed in Figure IV-8, and then pharmacokinetics parameters including peak concentration ($C_{\max}$), time at the peak ($t_{\max}$), and area under curve ($AUC_{0-\infty}$) were evaluated from the profiles (Table IV-2). As observed in Figure IV-8, all groups for 9 h had low CUR concentration (<35 ng mL^{-1}) except CUR LNP group prepared with 17.058 mM PEG100SE, and a group for CUR LNP fabricated with 17.058 mM PEG100SE had also high concentration (>35 ng mL^{-1}) only for ~1 h nearby the initiation of pharmacokinetic study. This result might be attributed to the liquid state of orally administered samples unlike the lyophilized and nanoparticulated samples in the study of J. Shaikh group (11). A group administered for CUR LNP prepared with 17.058 mM PEG100SE had the highest values in $C_{\max}$ and $AUC_{0-\infty}$ as 115.66 ng mL^{-1} and 622.13 h*ng mL^{-1} (Table IV-2), which values were 7.06 and 5.32 times of those for a group administered for CUR desolved in ethanol (CUR in EtOH), respectively, despite the lower dose (25 mg kg^{-1}) than that of the CUR in EtOH (50 mg kg^{-1}). Obviously, since blood collection in this pharmacokinetic study was conducted as frequent as just 1 time for 0.5 h nearby the initiation, it was hard to tell that all pharmacokinetics parameters including $C_{\max}$, $t_{\max}$, and $AUC_{0-\infty}$ were correct. Thereby realistic $t_{\max}$ for all groups may be appeared in 0−0.5 or 0.5−1 and realistic

$C_{\max}$ and $AUC_{0-\infty}$ values for all groups could be higher than those in Table IV-2. Nonethless, according to the obtained $C_{\max}$ and $AUC_{0-\infty}$ values, it was true that bioavailability of CUR encapsulated in LNP stabilized with 17.058 mM PEG100SE was the best. This result suggest that the prolonged gastrointestinal digestion of CUR-loaded LNPs by PEG100SE could contributed to the elevation in terms of bioavailability of orally administered CUR.

In summary, the expected absorption mechanisms of the native or encapsulated CUR through the GIT were illustrated in Figure IV-9. The CUR ingested as raw materials was extremely easy to autoxidize in the GIT (mouth and small intestine circumstance) because of its chemical instability at neutral and slightly alkaline pH (Figure IV-9a) (8). Moreover, the raw CUR poorly permeates from the intestinal lumen to the portal blood, and almost of the raw CUR is excreted with feces regardless of its incorporation in the carriers comprised of bile salts and phospholipids (8), which ensures the low level of CUR in blood plasma. On the other hand, the CUR delivered using the lipid carrier systems such as the emulsion and LNP could be protected from the GIT environment and absorbed with chylomicrons to the circulatory system through the lacteal of intestinal villus. As shown in Figure 8b, the CUR incorporated in the emulsion could be merely oxidized a little during the digestion due to the mass exchangeable interface between oil and water phases, resulting from the liquidity of oil droplets (16). In case of the LNP system, which was prepared using a solid lipid, the CUR oxidation could be prevented due to the

substantial solid matrix (Figure IV-9c and d). Besides, as discussed relavant to the CUR bioaccessibility, the CUR uptake rate into the circulatory system could be controllable on the basis of the purpose, because the lypolysis of the lipid carrier systems loading CUR molecules was controlled by the selection of the lipid and emulsifier types. Consequently, the bioavailability of the CUR would be successfully improved and controlled using the LNP models.

The CUR encapsulated in LNP system, which was produced using TS as a lipid and PEG10SE/PEG100SE as a surfactant, was solubilized well into micelles mixed with the LNP digesta (stearic acids, glyceryl monostearates, etc.), bile acids, and phospholipids in the end of the mimicked GIT digestion. Moreover, it is expected to modulate the GIT digestion fate of the ingested CUR-loaded emulsion and LNP systems by designing their components, compositions, and contents. Consequently, my LNP system for oral administration would enhance and control the CUR absorption into the blood successfully. In conclusion, this work may serve as a basis for further studies to develop an oral delivery system for non-bioavailable molecules for functional foods or drugs.

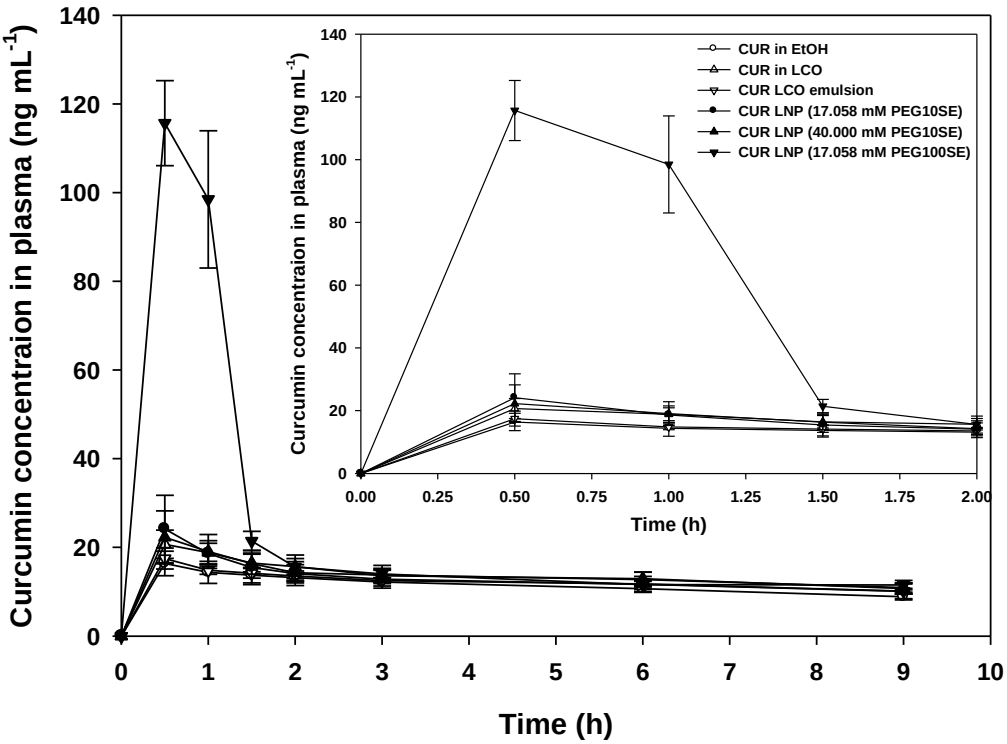

Figure IV-8. ***In vivo*** **plasma concentration profiles of different curcumin formulations.**

Table IV-2. Pharmacokinetics parameters of different curcumin formulations[a]

Formulation	Dose (mg kg^{-1})	$C_{\max}$ (ng mL^{-1})	$t_{\max}$ (h)	$AUC_{0-\infty}$ (h*ng mL^{-1})
CUR in EtOH	50	16.39 ± 2.76b	0.5	116.87 ± 4.44b
CUR in LCO	50	20.70 ± 3.19b	0.5	136.95 ± 12.02b
CUR LCO emulsion	25	17.48 ± 2.38b	0.5	128.05 ± 5.38b
CUR LNP (17.058 mM PEG10SE)	25	24.15 ± 7.61b	0.5	136.23 ± 19.32b
CUR LNP (40.000 mM PEG10SE)	25	22.27 ± 5.97b	0.5	145.16 ± 19.94b
CUR LNP (17.058 mM PEG100SE)	25	115.66 ± 9.57a	0.5	622.13 ± 5.42a

[a]Different letters a and b in a column are significantly different ($p < 0.05$).

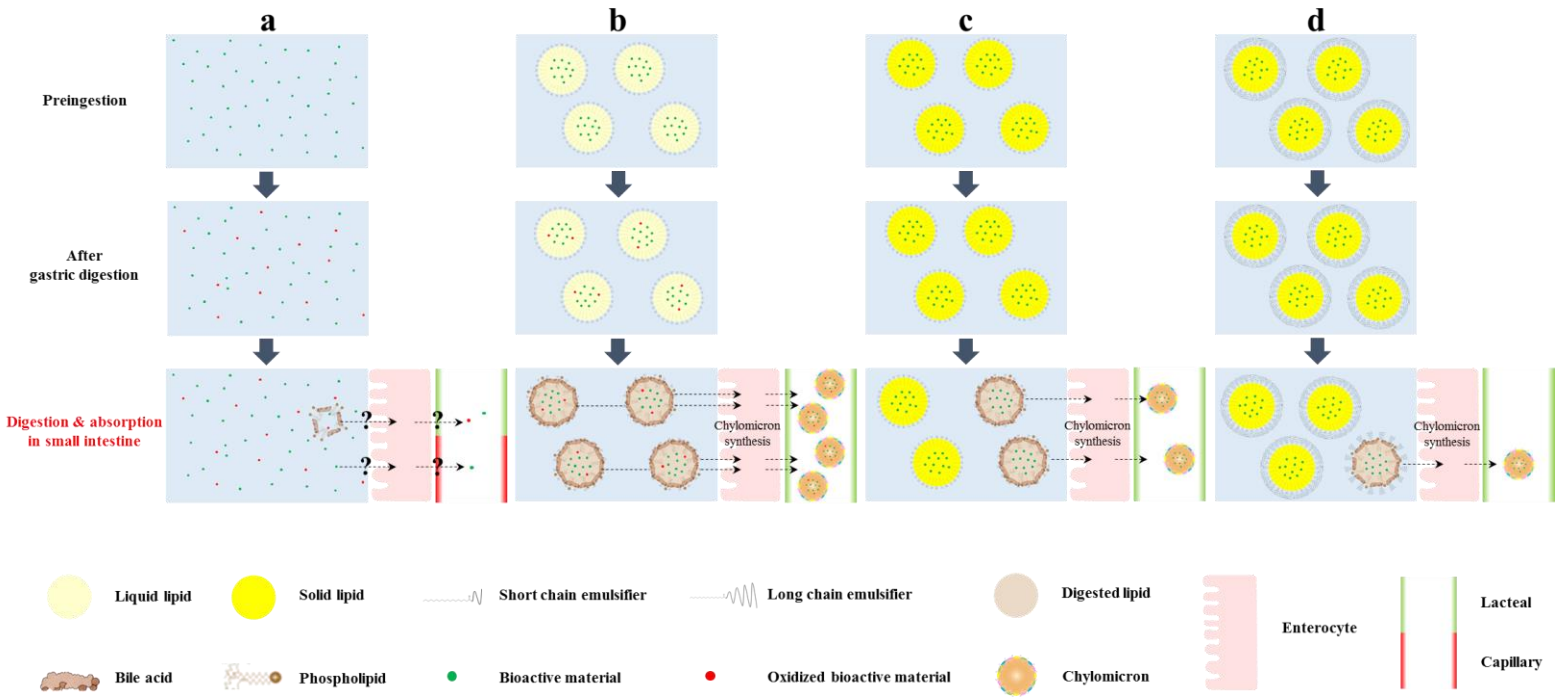

Figure IV-9. Schematic representation of the digestion in gastrointestinal tract and the absorption to the circulating system. The ingested curcumin molecules in (a) native form and the encapsulated form in (b) emulsion and lipid nanoparticles emulsified by (c) short or (d) long chain emulsifier.

IV-4. References

(1) Strimpakos, A. S.; Sharma, R. A. Curcumin: preventive and therapeutic properties in laboratory studies and clinical trials. *Antioxid. Redox Signaling* **2008,** *10*, 511-546.

(2) Shehzad, A.; Wahid, F.; Lee, Y. S. Curcumin in cancer chemoprevention: molecular targets, pharmacokinetics, bioavailability, and clinical trials. *Arch. Pharm. (Weinheim, Ger.)* **2010,** *343*, 489-499.

(3) Julie, S.; Jurenka, M. T. Anti-inflammatory properties of curcumin, a major constituent. *Altern. Med. Rev.* **2009,** *14*.

(4) Sharma, R. A.; Euden, S. A.; Platton, S. L.; Cooke, D. N.; Shafayat, A.; Hewitt, H. R.; Marczylo, T. H.; Morgan, B.; Hemingway, D.; Plummer, S. M. Phase I clinical trial of oral curcumin biomarkers of systemic activity and compliance. *Clin. Cancer Res.* **2004,** *10*, 6847-6854.

(5) Anand, P.; Kunnumakkara, A. B.; Newman, R. A.; Aggarwal, B. B. Bioavailability of curcumin: problems and promises. *Mol. Pharm.* **2007,** *4*, 807-818.

(6) Schneider, C.; Gordon, O. N.; Edwards, R. L.; Luis, P. B. Degradation of curcumin: From mechanism to biological implications. *J. Agric. Food Chem.* **2015,** *63*, 7606-7614.

(7) Wang, Y. J.; Pan, M. H.; Cheng, A. L.; Lin, L. I.; Ho, Y. S.; Hsieh, C. Y.; Lin, J. K. Stability of curcumin in buffer solutions and characterization of its degradation products. *J. Pharm. Biomed. Anal.* **1997,** *15,* 1867-1876.

(8) Metzler, M.; Pfeiffer, E.; Schulz, S. I.; Dempe, J. S. Curcumin uptake and metabolism. *Biofactors* **2013,** *39,* 14-20.

(9) Shoba, G.; Joy, D.; Joseph, T.; Majeed, M.; Rajendran, R.; Srinivas, P. S. Influence of piperine on the pharmacokinetics of curcumin in animals and human volunteers. *Planta Med.* **1998,** *64,* 353-356.

(10) Bisht, S.; Feldmann, G.; Soni, S.; Ravi, R.; Karikar, C.; Maitra, A.; Maitra, A. Polymeric nanoparticle-encapsulated curcumin ("nanocurcumin"): a novel strategy for human cancer therapy. *J. Nanobiotechnol.* **2007,** *5,* 1-18.

(11) Shaikh, J.; Ankola, D. D.; Beniwal, V.; Singh, D.; Kumar, M. N. V. R. Nanoparticle encapsulation improves oral bioavailability of curcumin by at least 9-fold when compared to curcumin administered with piperine as absorption enhancer. *Eur. J. Pharm. Sci.* **2009,** *37,* 223-230.

(12) Maiti, K.; Mukherjee, K.; Gantait, A.; Saha, B. P.; Mukherjee, P. K. Curcumin–phospholipid complex: preparation, therapeutic evaluation and pharmacokinetic study in rats. *Int. J. Pharm.* **2007,** *330,* 155-163.

(13) Ahmed, K.; Li, Y.; McClements, D. J.; Xiao, H. Nanoemulsion-and emulsion-based delivery systems for curcumin: encapsulation and release properties. *Food Chem.* **2012,** *132,* 799-807.

(14) Zhang, R.; Zhang, Z.; Zhang, H.; Decker, E. A.; McClements, D. J. Influence of emulsifier type on gastrointestinal fate of oil-in-water emulsions containing anionic dietary fiber (pectin). *Food Hydrocolloids* **2015,** *45,* 175-185.

(15) Zeeb, B.; Lopez-Pena, C. L.; Weiss, J.; McClements, D. J. Controlling lipid digestion using enzyme-induced crosslinking of biopolymer interfacial layers in multilayer emulsions. *Food Hydrocolloids* **2015,** *46,* 125-133.

(16) Müller, R. H.; Radtke, M.; Wissing, S. A. Solid lipid nanoparticles (SLN) and nanostructured lipid carriers (NLC) in cosmetic and dermatological preparations. *Adv. Drug Deliv. Rev.* **2002,** *54,* S131-S155.

(17) Aditya, N. P.; Shim, M.; Lee, I.; Lee, Y. S.; Im, M.; Ko, S. Curcumin and genistein coloaded nanostructured lipid carriers: *in vitro* digestion and antiprostate cancer activity. *J. Agric. Food Chem.* **2013,** *61*, 1878-1883.

(18) Ban, C.; Park, S. J.; Lim, S.; Choi, S. J.; Choi, Y. J. Improving flavonoid bioaccessibility using an edible oil-based lipid nanoparticle for oral delivery. *J. Agric. Food Chem.* **2015,** *63*, 5266-5272.

(19) McClements, D. J.; Xiao, H. Potential biological fate of ingested nanoemulsions: influence of particle characteristics. *Food Funct.* **2012,** *3*, 202-220.

(20) Molineux, G. Pegylation: engineering improved pharmaceuticals for enhanced therapy. *Cancer Treat. Rev.* **2002,** *28*, 13-16.

(21) Jeong, J. H.; Park, T. G.; Kim, S. H. Self-assembled and nanostructured siRNA delivery systems. *Pharm. Res.* **2011,** *28*, 2072-2085.

(22) Gursahani, H.; Riggs-Sauthier, J.; Pfeiffer, J.; Lechuga-Ballesteros, D.; Fishburn, C. S. Absorption of polyethylene glycol (PEG) polymers: the effect of PEG size on permeability. *J. Pharm. Sci.* **2009,** *98*, 2847-2856.

(23) Ban, C.; Lim, S.; Chang, P.; Choi, Y. J. Enhancing the stability of lipid nanoparticle systems by sonication during the cooling step and controlling the liquid oil content. *J. Agric. Food Chem.* **2014,** *62*, 11557-11567.

(24) McClements, D. J. Critical review of techniques and methodologies for characterization of emulsion stability. *Crit. Rev. Food Sci. Nutr.* **2007,** *47*, 611-649.

(25) Khossravi, M.; Kao, Y. H.; Mrsny, R. J.; Sweeney, T. D. Analysis methods of polysorbate 20: A new method to assess the stability of polysorbate 20 and established methods that may overlook degraded polysorbate 20. *Pharm. Res.* **2002,** *19*, 634-639.

(26) Hur, S. J.; Joo, S. T.; Lim, B. O.; Decker, E. A.; McClements, J. D. Impact of salt and lipid type on *in vitro* digestion of emulsified lipids. *Food Chem.* **2011,** *126*, 1559-1564.

(27) Li, Y.; McClements, D. J. Modulating lipid droplet intestinal lipolysis by electrostatic complexation with anionic polysaccharides: Influence of cosurfactants. *Food Hydrocolloids* **2014,** *35*, 367-374.

(28) Vanapalli, S. A.; Coupland, J. N. Emulsions under shear—the formation and properties of partially coalesced lipid structures. *Food Hydrocolloids* **2001,** *15*, 507-512.

(29) Helgason, T.; Awad, T. S.; Kristbergsson, K.; McClements, D. J.; Weiss, J. Effect of surfactant surface coverage on formation of solid lipid nanoparticles (SLN). *J. Colloid Interface Sci.* **2009,** *334*, 75-81.

(30) Qian, C.; McClements, D. J. Formation of nanoemulsions stabilized by model food-grade emulsifiers using high-pressure homogenization: factors affecting particle size. *Food Hydrocolloids* **2011,** *25*, 1000-1008.

(31) Tadros, T.; Izquierdo, P.; Esquena, J.; Solans, C. Formation and stability of nano-emulsions. *Adv. Colloid Interface Sci.* **2004,** *108*, 303-318.

(32) McClements, D. J. Protein-stabilized emulsions. *Curr. Opin. Colloid Interface Sci.* **2004,** *9*, 305-313.

(33) McClements, D. J.; Li, Y. Structured emulsion-based delivery systems: controlling the digestion and release of lipophilic food components. *Adv. Colloid Interface Sci.* **2010,** *159*, 213-228.

(34) Mun, S.; Decker, E. A.; McClements, D. J. Influence of emulsifier type on *in vitro* digestibility of lipid droplets by pancreatic lipase. *Food Res. Int.* **2007,** *40*, 770-781.

(35) Golding, M.; Wooster, T. J. The influence of emulsion structure and stability on lipid digestion. *Curr. Opin. Colloid Interface Sci.* **2010,** *15*, 90-101.

(36) Shi, Y.; Burn, P. Lipid metabolic enzymes: emerging drug targets for the treatment of obesity. *Nat. Rev. Drug Discov.* **2004,** *3*, 695-710.

(37) Maldonado-Valderrama, J.; Wilde, P.; Macierzanka, A.; Mackie, A. The role of bile salts in digestion. *Adv. Colloid Interface Sci.* **2011,** *165*, 36-46.

(38) Wahlang, B.; Pawar, Y. B.; Bansal, A. K. Identification of permeability-related hurdles in oral delivery of curcumin using the Caco-2 cell model. *Eur. J. Pharm. Biopharm.* **2011,** *77*, 275-282.

IV-5. Appendix: Controlling the Digestibility of Lipid Nanoparticles Stabilized by PEGylated Emulsifiers

IV-5-1. Introduction

Controllable digestion of lipid carrier system in the gastrointestinal (GI) tract has been one of big issues to successfully develop the functional foods fortified in aspects of biological activities such as bioavailability and controlled release of bioactive materials incorporated in the carriers (1, 2). Ingested lipid carrier systems should travel from mouth to intestine along the lumen and undergo various environmental changes; e.g. mouth: neutral pH, many ions, mucin, amylase, lingual lipase, etc.; stomach: highly acidic condition, many ions, mucin, pepsin, gastric lipase, etc.; and small intestine: neutral pH, high ion strength, pancreatic lipase, colipase, bile salts, phospholipids, etc. (3, 4) During the retention time, the highly acidic condition in stomach brings unwanted aggregation of the carriers and lingual/gastric/pancreatic lipases hydrolyze the lipid molecules in the carriers. Particularly, lipid digestion occurs in the small intestine (70–90%) by pancreatic lipases with helps of calcium ions, bile salts, and colipase (5). Therefore, the controllable digestion of the lipid carriers can be accomplished with preventing the collision among the carriers and the adsorption of various lipases, colipase, and bile salts onto the lipid-water interface. In this regard, understanding the interface of lipid carrier systems would be a key point to modulate their digestion rate/extent.

Many researchers have striven to control the lipid hydrolysis by means of modulating the interfacial properties. Maldonado-Valderrama et al. examined the compositional changes of the β-lactoglobulin-stabilized lipid surface by ionic surfactants (Tween 20) and biological surfactants (bile salts) during the digestion process (6−8). Chu et al. studied the interfacial changes induced by bile salts and the adsorption of colipase and pancreatic lipase onto the interface, then suggested that galactolipids on the lipid surface could retard the rate and extent of lipid digestion within the GI tract (9, 10). Furthermore, Torcello-Gómez et al. introduced the controllable digestion method of oil droplets under the *in vitro* small intestinal condition using the Poloxamer 188 as a nonionic emulsifier (11). These literatures would be representative instances to convince the possibility of the controllable lipid digestion using the design of the interfacial composition. However, it is still unclear how large or many emulsifiers onto the interface can effectively hinder the adsorption of biological surface active components such as bile salts, colipase, and lipase.

Lipid nanoparticle (LNP) system, including solid lipid nanoparticle and nanostructured lipid carrier, has regarded as an attractive lipid carrier system due to the use of solid-stated lipid at room/body temperatures. The solid lipid in LNPs can give some merits for delivering bioactive materials, i.e. the rigid matrix capable of protection from the outside condition and the possibility for the controlled release of the bioactives (12). Polyethylene glycol (PEG) is a synthetic polymer approved of the safety in the body (13), which has universally been used in pharmaceutics and

cosmetics, even in foods. Particularly, PEGs long-chained above a certain level (~2 kDa) can sterically repulse the approach of proteins and enzymes and have an ability to avoid the detection against the immune system in the body (14). In this manner, many molecules or macrostructures are covalently/non-covalently attached with PEGs to have a stealth function in the body, which is called as PEGylation (15, 16). Müller and coworkers achieved the modulation of the lipolysis of PEGylated LNPs under the simulated GI condition using Poloxamer 188 (17) and Poloxamer 407/cholic acid (18), respectively. However, it was also unclear for the colipase/lipase adsorption and the surfactant displacement on the lipid surface. Therefore, the curiosity relating mechanisms of the LNP digestion should be verified to control by considering the compositional changes of the interface in a molecular level.

Model LNPs prepared using tristearin (TS) and various PEGylated emulsifiers were utilized in this research, and the number of the emulsifiers participating in the LNP surface covering was quantitatively determined for the consideration in a molecular level. Moreover, the digestion patterns of the PEGylated LNPs under the mimicked *in vitro* GI environment were measured to study the effects of the type/density of various PEGylated emulsifiers at the lipid-water interface on the LNP hydrolysis followed by the adsorption of bile acids, colipase, and pancreatic lipase. On the basis of all results, it was intended to suggest the digestion mechanism of PEGylated LNPs in a molecular level and the controllable hydrolysis methods of the LNPs.

IV-5-2. Materials and Methods

IV-5-2-1. Chemicals

Glyceryl tristearate (tristearin), polyoxyethylene (10) stearyl ether (PEG10SE, Brij® S10), polyoxyethylene (100) stearyl ether (PEG100SE, Brij® S100), polyoxyethylene (10) oleyl ether (PEG10OE, Brij® O10), polyoxyethylene (10) lauryl ether (PEG10LE), and polyoxyethylene sorbitan monostearate (PEG20SS, Tween® 60) were purchased from Sigma Aldrich Co. (St. Louis, MO, USA). Polyoxyethylene (10) stearate (PEG10S) and polyoxyethylene (100) stearate (PEG100S, Myrj® S100) were obtained from TCI (Tokyo, Japan) and Croda (Parsippany, NJ, USA), respectively. All other chemicals were of analytical reagent grade.

IV-5-3. Results and Discussion

IV-5-3-1. Physicochemical Characteristics of Lipid Nanoparticles

Emulsifiers are comprised of two groups, which are the hydrophilic group (head) and the hydrophobic group (tail). The head and tail of each emulsifier used in this study were chosen by regarding changes of molecular weight and structure. As shown in Figure IV-A1, the heads were PEG polymer chains that ethylene glycols repeated from 10 to 100 times and the tails were fatty acids (stearic acids) or fatty alcohols (lauryl, stearyl, or oleyl alcohols). In other words, the emulsifiers used for LNP preparation were the PEGylated emulsifiers, in which PEG polymer chains are covalently attached to the tails. Appearance of LNP systems prepared with the PEGylated emulsifiers was picturized as observed in Figure IV-A2. According to the appearance after dilution, at same concentration of the PEGylated emulsifiers, LNPs stabilized using PEG100S, PEG100SE, and PEG20SS were more stable than those stabilized using PEG10S, PEG10SE, PEG10OE, and PEG10LE, i.e. the former had larger PEG polymers than the latter. Even in the latter samples except a PEG10SE-LNP sample, the creamed or sedimentary aggregators of LNPs were observed with the naked eye. However, elevation of concentration of the used emulsifiers enhanced the stability of LNPs regardless of emulsifiers. This result suggests that a lot of large PEG chains at the interface between lipid and water phases might improve colloidal stability of LNPs.

The yield (%) value means the quantity of submicron lipid particles in a whole

LNP dispersion system, without the partial coalescence (19) and aggregation (20). In this regard, the apparent colloidal stability picturized in Figure IV-A2 can be converted to numerical value using the yield (%), and Figure IV-A3a is the yield (%) result. Of course, the yield (%) of all samples was increased with a growth of emulsifier concentration because more emulsifiers can better stabilize the interface of LNPs. Similarly to the apparent results in Figure IV-A2, LNP samples prepared using PEG100S, PEG100SE, and PEG20SS had large values than those of LNPs using PEG10S, PEG10SE, PEG10OE, and PEG10LE. Among PEGylated samples using 10 ethylene glycols, PEG10SE-LNPs peculiarly had the largest yield (%) close to the values of PEG100S-, PEG100SE-, and PEG20SS-samples at a same emulsifier concentration, and a reason for the peculiarity would be further verified.

Particle size (PS, z average) of all LNPs was reduced with increasing emulsifier concentration (Figure IV-A3b), which is attributed to the emulsifier capability of holding the surface tension increased by the droplet size reduction during producing process (20). On the other hand, ZP of all LNPs was elevated with an increase of emulsifier concentration due to the negative ZP values of all LNP samples, which means that more PEGylated emulsifiers can more neutralize the surface of LNPs because of electrostatic neutrality of PEG chains, (Figure IV-A3c). LNPs emulsified using PEG10S and PEG100SE had lower ZP values than PEG10SE- and PEG100SE-LNPs despite the same PEG chain length, respectively, which is due to an double-bonded oxygen atom in a carbonyl group (C=O) of PEG10S and

PEG100SE. Meanwhile, PEG10SE-, PEG10OE-, PEG10LE-LNPs had a similar ZP values each other. These results in terms of the physicochemical stability of LNP samples would correlate with the PEGylated emulsifier covering on the LNP surface and this is discussed in the following section.

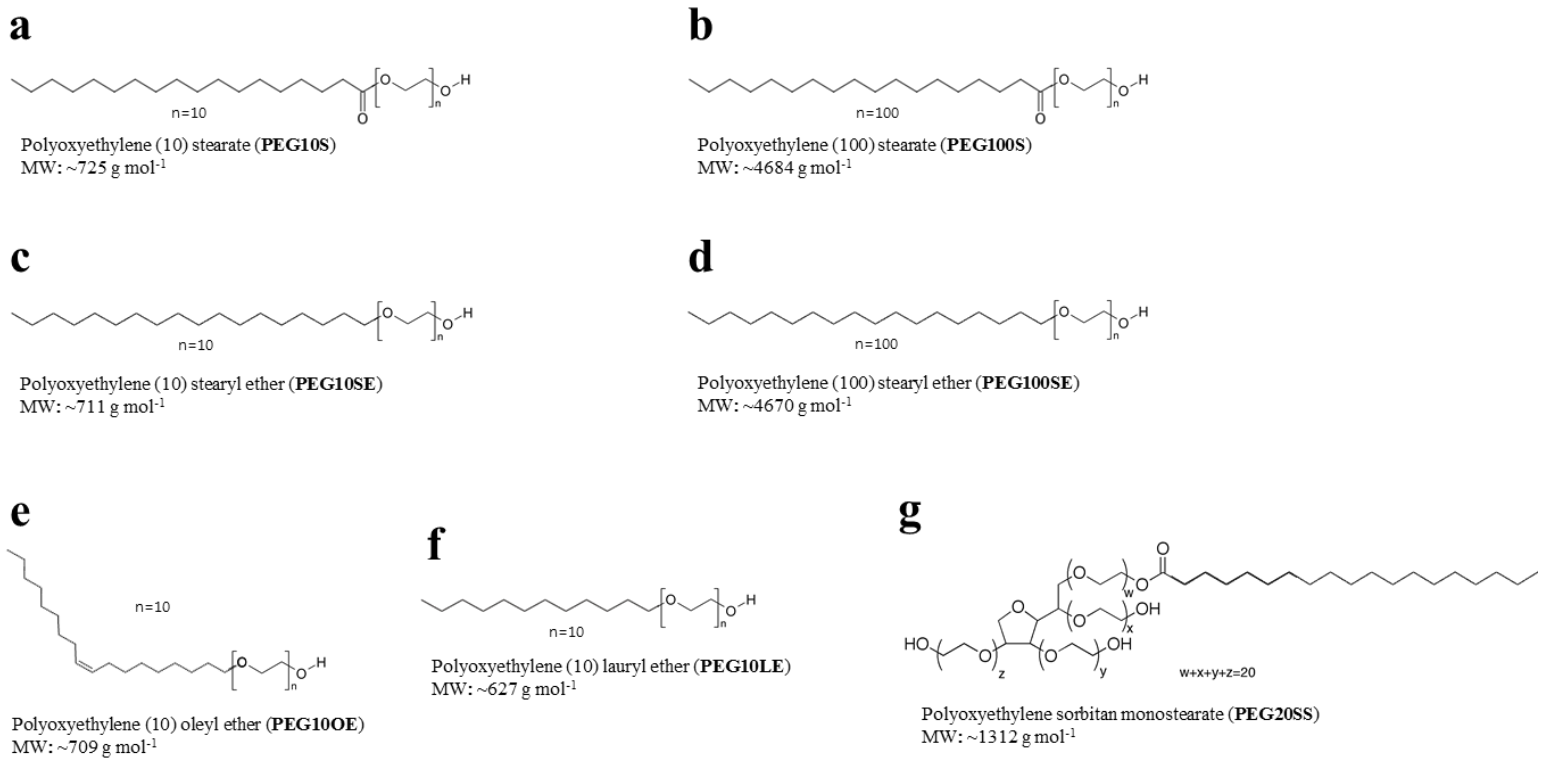

Figure IV-A1. Structure and molecular weight (MW) of PEGylated emulsifiers used to emulsify tristearin nanoparticles.

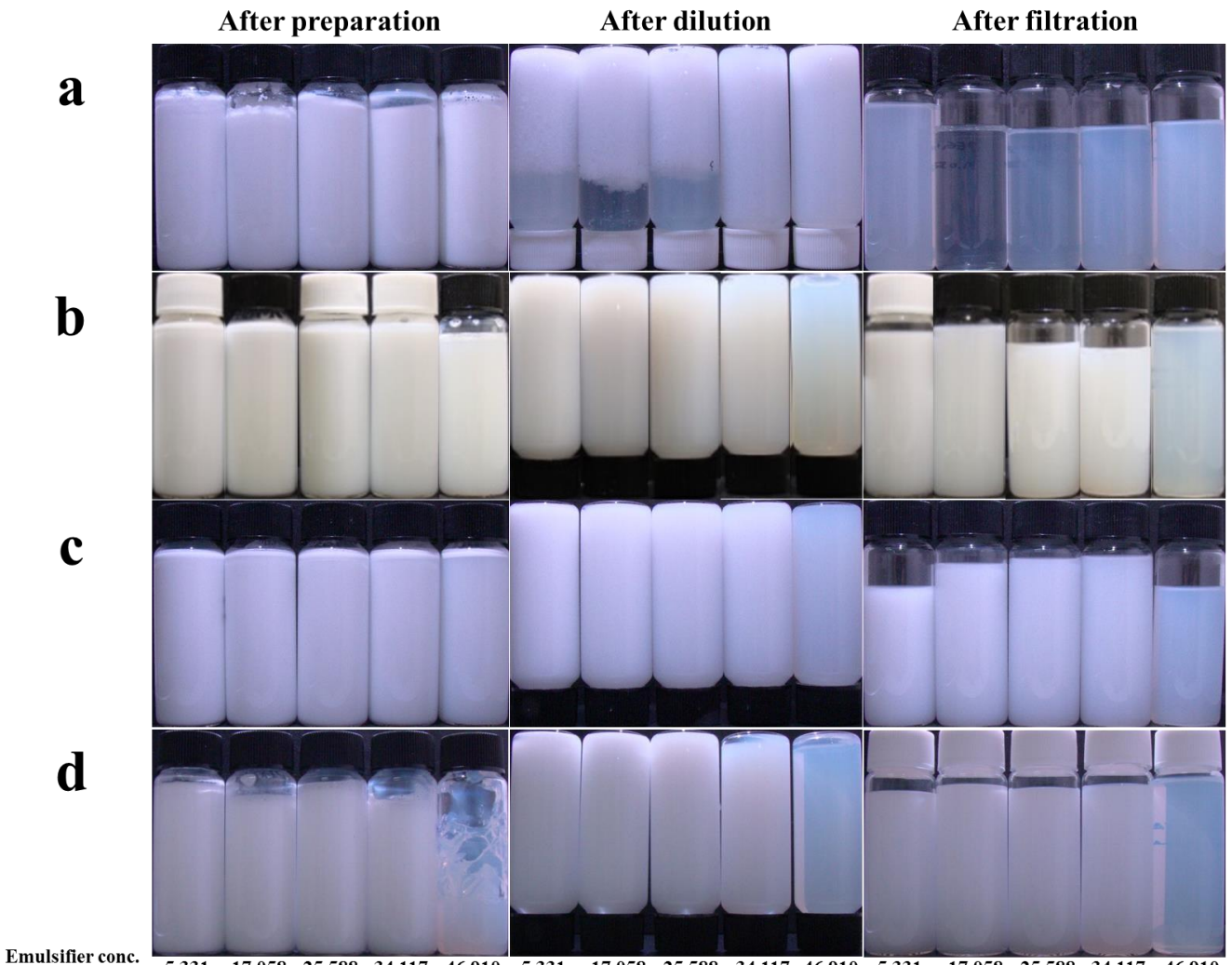
After preparation
After dilution
After filtration
a
b
c
d
Emulsifier conc. (mM)
5.331 17.058 25.588 34.117 46.910
5.331 17.058 25.588 34.117 46.910
5.331 17.058 25.588 34.117 46.910

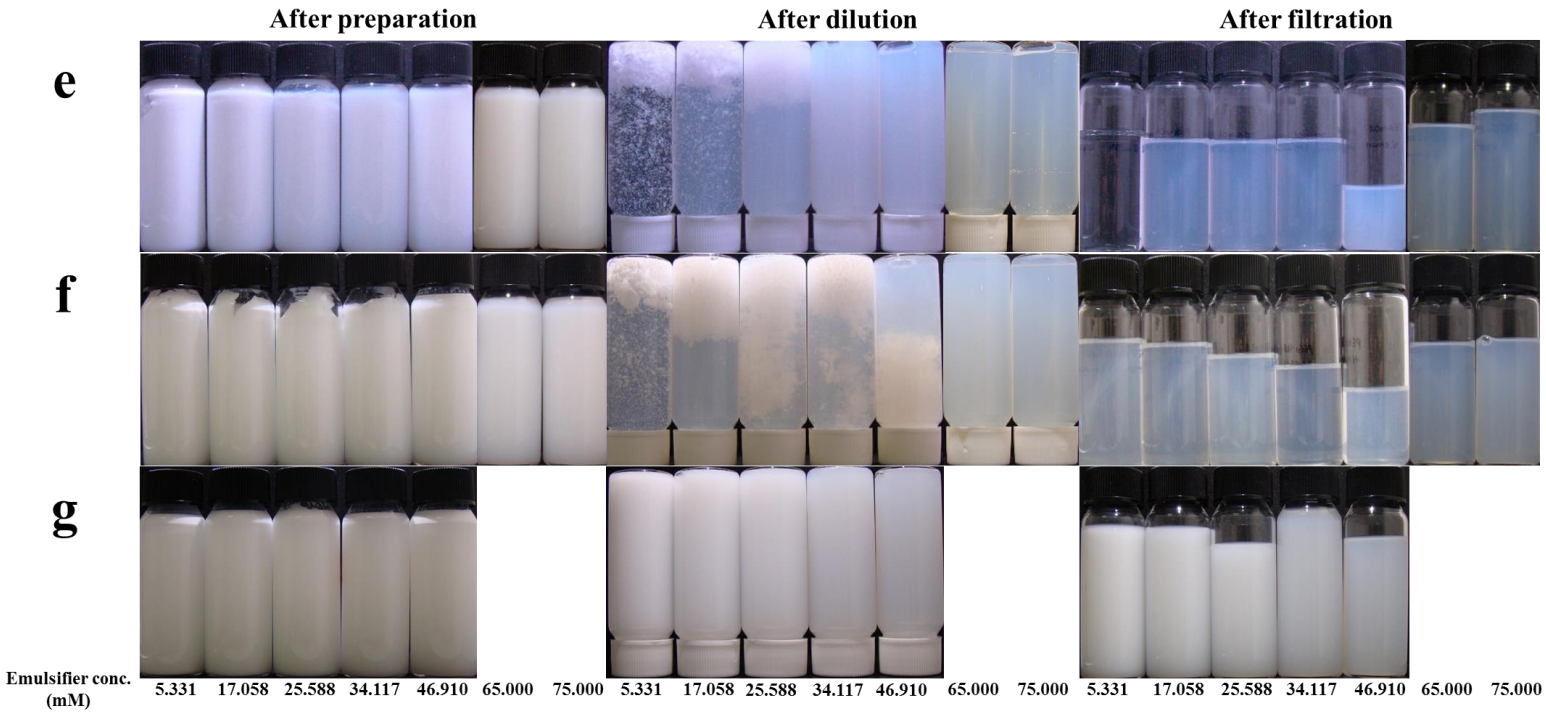

Figure IV-A2. Lipid nanoparticle systems after preparation, dilution (10-fold), and subsequent filtration (1 μm). Tristearin nanoparticles emulsified by (a) PEG10S, (b) PEG100S, (c) PEG10SE, (d) PEG100S, (e) PEG10OE, (f) PEG10LE, and (g) PEG20SS.

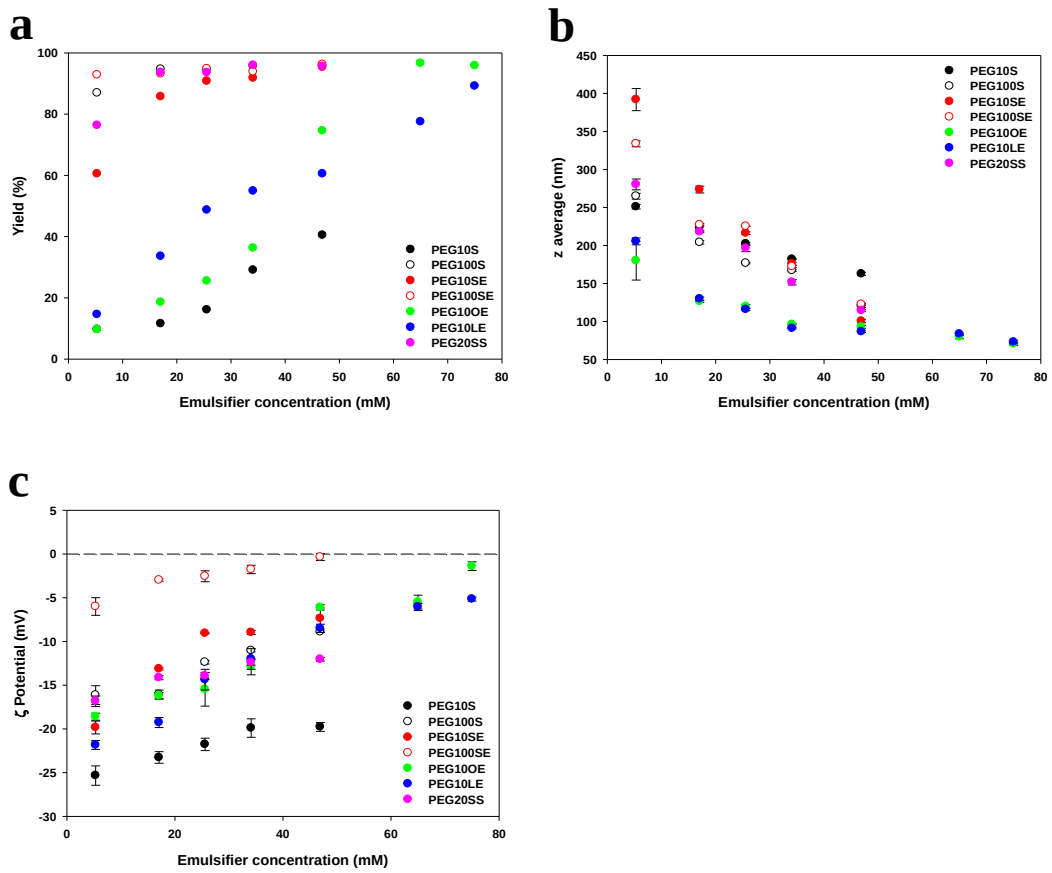

Figure IV-A3. Physicochemical characteristics of tristearin nanoparticles. (a) Yield (%), (b) particle size (z average), and (c) ζ potential of tristearin nanoparticles emulsified by PEGylated emulsifiers.

IV-5-3-2. Emulsifier Covering on the Surface of Lipid Nanoparticles

In many previous studies, the surface load value was generally expressed as weights per a unit area. However in this research, to examine emulsifiers covering on LNP surface in a molecular level, the unit of the surface load was converted as the number of emulsifiers per nm^2 (nm^{-2}). In this regard, the converted surface load of LNP samples was determined as observed in Figure IV-A4a, applying the Avogadro's number and the molecular weight of each emulsifier. According to this result, in all PEGylated emulsifiers, the surface load was increased with increasing the emulsifier concentration below a certain level but maintained in a relatively constant level over the certain level. This phenomenon could indicate the saturation of PEGylated emulsifiers covering on the LNP surface. Surprisingly, the relatively constant level of all samples was similar each other as ~3 nm^{-2}. In addition, whereas each certain level of PEG10S-, PEG100S-, PEG10SE-, PEG100SE-, and PEG20SS-LNPs (i.e. their tail groups were comprised of stearic acid or stearyl alcohol) was similar, the certain levels of PEG10OE- and PEG10LE-LNP samples were larger than those of the rest of samples. This result appears that the tail group in PEGylated emulsifier molecule would determine the certain level.

Surface load values in Figure IV-A4a were converted into their reciprocal number versions as shown in Figure IV-A4b, which means the area occupied by one emulsifier molecule. In an assumption of a square arrayal of emulsifiers on the LNP surface, the distance between the nearest emulsifiers was calculated as observed in

Figure IV-A4c (> 0.5 nm), using the square root of the area value in Figure IV-A4b. In addition, for examining the ratio between TS molecules and emulsifiers at the LNP interface, the molecular weight of TS and the thickness of a β-formed TS lamellar were regarded as 891.45 g mol^{-1} (22) and 4.5 nm (23, 24), respectively. Figure IV-A4d is a result of the ratio (< 1.4). These results would be regarded in a section of the *in vitro* digestion of LNPs, in order to assume the molecular-level interaction among TS, emulsifier, bile salt, pancreatic lipase, and colipase at the interface in a molecular level.

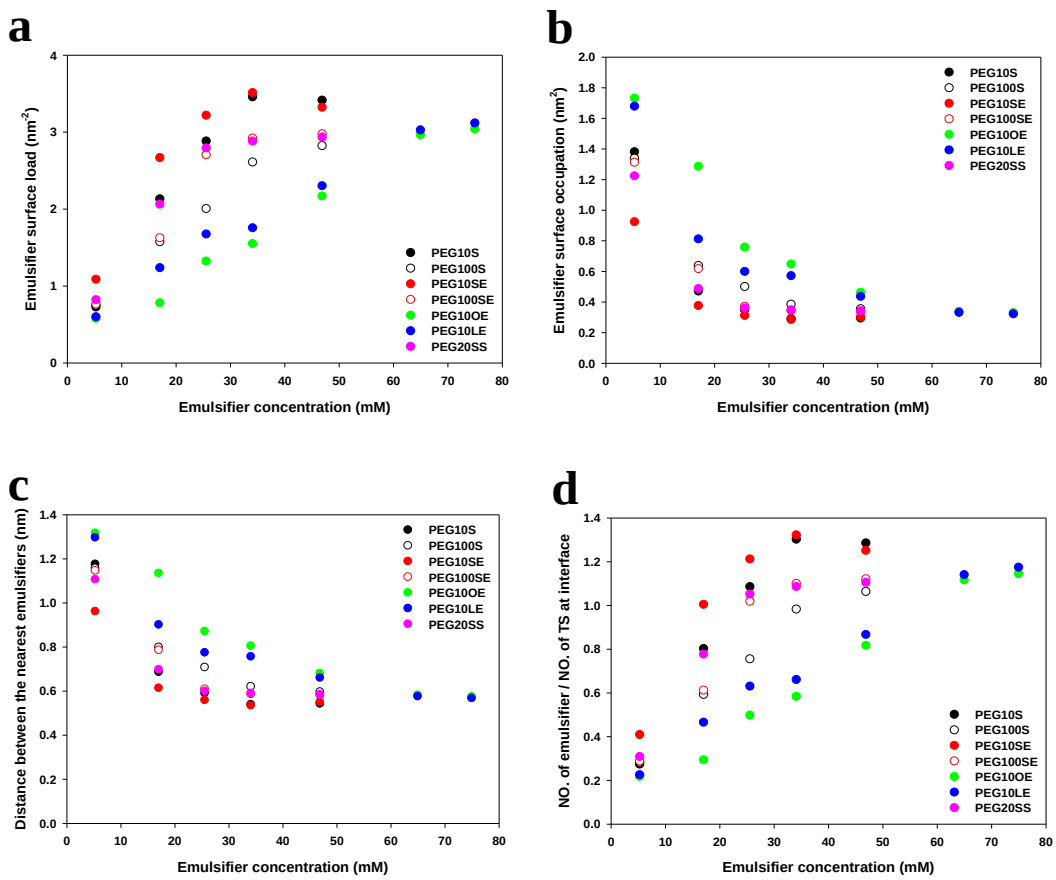

Figure IV-A4. Surface load values of tristearin nanoparticles emulsified by PEGylated emulsifiers. (a) The number of emulsifiers adsorbing on the unit surface (1 nm^2) of tristearin matrix, (b) Occupying area of an emulsifier adsorbing on the surface of tristearin matrix, (c) the distance between the nearest emulsifiers, and (d) the numerical ratio of emulsifier molecules versus tristearin molecules at their interface.

IV-5-3-3. Effects of Incubation Condition on Colloidal Stability of Lipid Nanoparticles

Colloidal system including LNP is usually influenced by the condition of its dispersion medium. Particularly, pH and ion strength principally affect the aggregation of LNP system. In this regard, the LNPs were incubated in high salt (containing various salts in Table IV-1, e.g. $NaHCO_3$, NaCl, KCl, $CaCl_2$, etc.) and pH 3 conditions for 2 h, and their PS and ZP were measured as shown in Figure IV-A5 and A6, respectively. In LNP samples prepared with 5.331 mM emulsifiers repeated of 10 ethylene glycols (PEG10-; i.e. PEG10S, PEG10SE, PEG10OE, and PEG10LE), their PS values were increased in the pH 3 and high ionic strength conditions, which indicate the aggregation of LNPs. However, there was no aggregation in PEG100S-, PEG100SE-, PEG20SS-LNP samples. According to ZP results in Figure IV-A6, since there was no surface charge of all LNPs under the pH 3 and high salts, this result suggests that even low content of emulsifiers having $\geq$ 20 ethylene glycols can effectively prevent the LNP aggregation induced by acidic and high ionic environments, by using a steric hindrance effect. Moreover, even in samples using PEG10-emulsifiers, the heavy aggregation of LNPs using the emulsifiers over 17.058 mM was not observed, which could be attributed to the growth of the surface load as the increase of emulsifier concentration. Therefore, increases of the PEG chain length and the surface load can successfully enhance the colloidal stability of LNPs under acidic and high ionic circumstances.

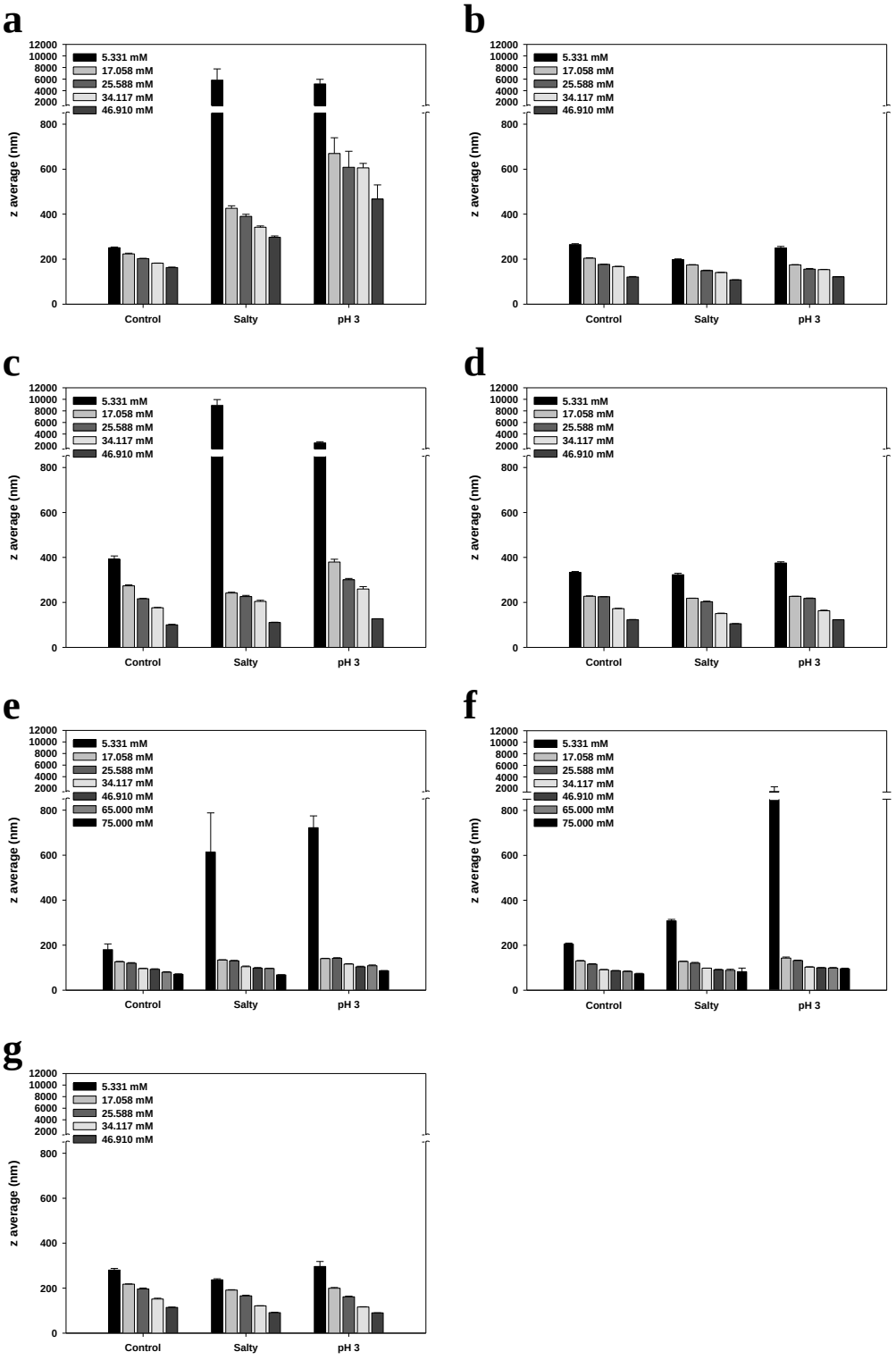
a
b
c
d
e
f
g
z average (nm)
5.331 mM
17.058 mM
25.588 mM
34.117 mM
46.910 mM
65.000 mM
75.000 mM
Control
Salty
pH 3

Figure IV-A5. Particle size (z average) of tristearin nanoparticles emulsified by PEGylated emulsifiers. (a) PEG10S, (b) PEG100S, (c) PEG10SE, (d) PEG100SE, (e) PEG10OE, (f) PEG10LE, and (g) PEG20SS after the incubation (2 h) in high salty and acidic (pH 3) conditions.

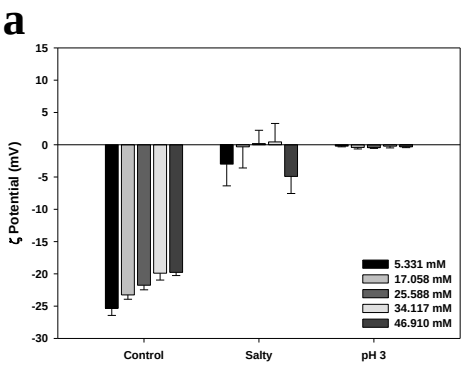
a
ζ Potential (mV)
15
10
5
0
-5
-10
-15
-20
-25
-30
Control
Salty
pH 3
5.331 mM
17.058 mM
25.588 mM
34.117 mM
46.910 mM

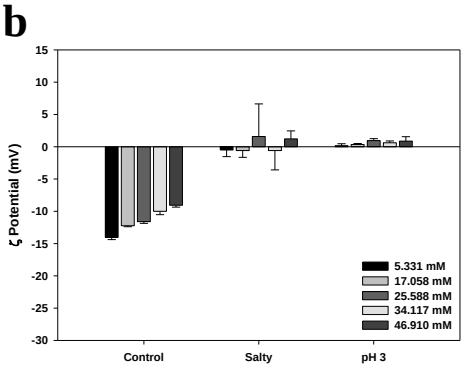
b
ζ Potential (mV)
15
10
5
0
-5
-10
-15
-20
-25
-30
Control
Salty
pH 3
5.331 mM
17.058 mM
25.588 mM
34.117 mM
46.910 mM

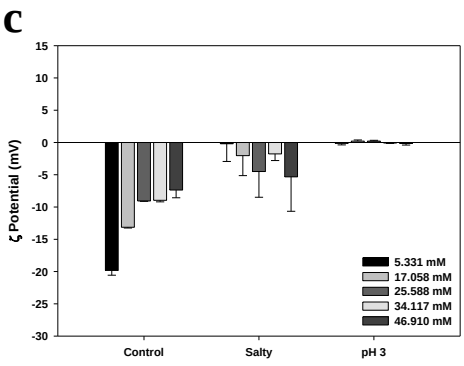
c
ζ Potential (mV)
15
10
5
0
-5
-10
-15
-20
-25
-30
Control
Salty
pH 3
5.331 mM
17.058 mM
25.588 mM
34.117 mM
46.910 mM

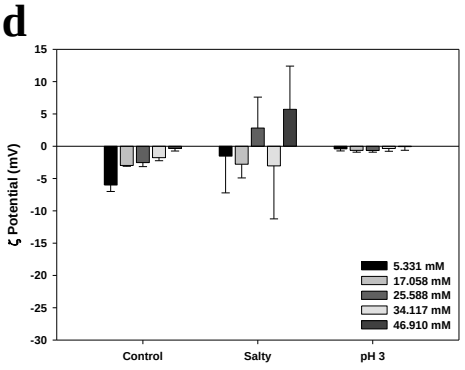
d
ζ Potential (mV)
15
10
5
0
-5
-10
-15
-20
-25
-30
Control
Salty
pH 3
5.331 mM
17.058 mM
25.588 mM
34.117 mM
46.910 mM

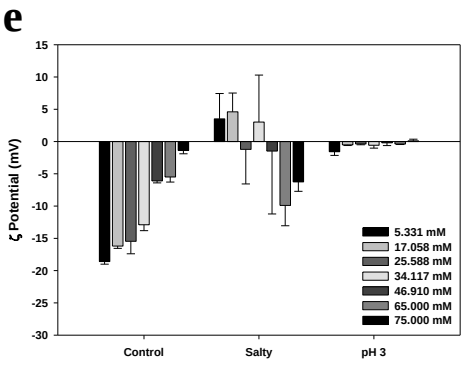
e
ζ Potential (mV)
15
10
5
0
-5
-10
-15
-20
-25
-30
Control
Salty
pH 3
5.331 mM
17.058 mM
25.588 mM
34.117 mM
46.910 mM
65.000 mM
75.000 mM

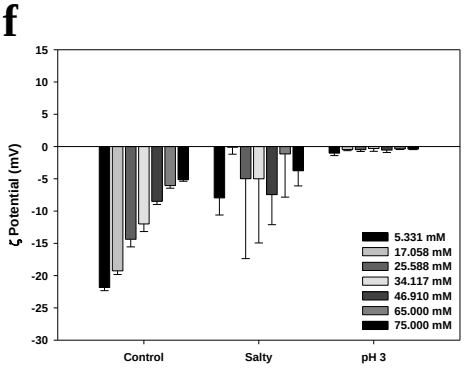
f
ζ Potential (mV)
15
10
5
0
-5
-10
-15
-20
-25
-30
Control
Salty
pH 3
5.331 mM
17.058 mM
25.588 mM
34.117 mM
46.910 mM
65.000 mM
75.000 mM

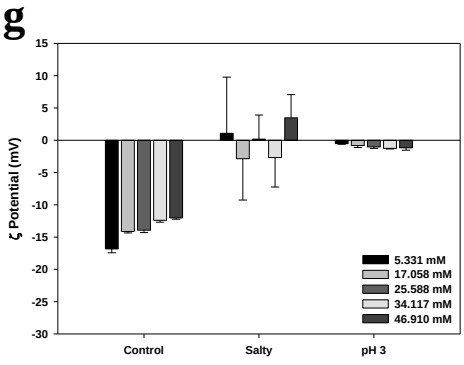
g
ζ Potential (mV)
15
10
5
0
-5
-10
-15
-20
-25
-30
Control
Salty
pH 3
5.331 mM
17.058 mM
25.588 mM
34.117 mM
46.910 mM

Figure IV-A6. ζ potential of tristearin nanoparticles emulsified by PEGylated emulsifiers. (a) PEG10S, (b) PEG100S, (c) PEG10SE, (d) PEG100SE, (e) PEG10OE, (f) PEG10LE, and (g) PEG20SS after the incubation (2 h) in high salty and acidic (pH 3) conditions.

IV-5-3-4. *In Vitro* Digestion of Lipid Nanoparticles

Small intestine, particularly duodenum, unlike mouth and stomach serves an environment to hydrolyze the almost of orally administrated lipids by secretion of pancreatic lipase, colipase, and bile salt (25, 26). Pancreatic lipase hydrolyzes a triacylglyceride to a monoglyceride and two fatty acids, colipase as a cofactor of pancreatic lipase forms the complex with pancreatic lipase and helps the lipase to adsorb well the lipid surface (27). Bile salt as a biosurfactant eliminates alien substances (such as proteins, emulsifiers, etc.) from the lipid surface in order to prepare the naked lipid surface where can be adsorbed by the lipase (5). In order to understand whether lipases and bile salts can adsorb the surface of LNPs or not, PS and ZP changes of LNPs were monitored under the lipase solution, the bile solution, the mixture solution of lipase and bile, and the mixture of digestion juice (Figure IV-A7 and A8). Nevertheless all LNPs were not hydrolyzed in pancreatic lipase solution, PS and ZP of some LNPs were slightly changed except PEG100S- and PEG100SE-LNP samples. Therefore, these changes in PS and ZP indicate just adherence of the lipase on PEG chains of emulsifier, and PEG100S and PEG100SE on LNPs can effectively prevent the lipase adhering.

Bile extract used in this study was composed of 5 wt % phosphatidylcholine and 49 wt % bile salts (with 10–15% glycodeoxycholic acid, 3–9% tauro-deoxycholic acid, 0.5–7% deoxycholic acid, etc.) (11). Conventional surfactants have a linear conformational structure comprised of hydrophilic head and hydrophobic tail, but bile

salts have a flat conformation (planar structure) composed of hydrophilic and hydrophobic faces (5). This flat conformation causes higher diffusivity on lipid surface and lower surface pressure than the linear conformation of conventional emulsifiers (28). In this manner, adsorption of bile salts into the LNP interfaces occupied by PEGylated emulsifiers is mainly driven by competition for available interfacial area (9, 10). On the one hand, the larger PEG chains and their hydrogen bonding with water (hydration) will promote better interfacial packing of the PEG chains on LNPs, and prevent better the adsorption of bile salts (29). On the other hand, the hydration of PEG chains is considerably reduced with slight increase of temperature from room temperature (25 °C) body temperature (37 °C) (30). According to the results in Figure IV-A7, PS of all LNPs treated with bile extract was unchanged except LNPs using 5.331 mM emulsifiers, i.e. nonaggregation. However, ZP values were steeply decreased after the bile extract treatment except LNPs emulsified by PEG100S and PEG100SE over 17.058 mM (Figure IV-A8), which was attributed to the LNP-interfacial absorption of bile salts or phosphatidyl choline in bile extracts (ZP: ~52 mV). In addition, all LNP samples were hydrolyzed after treating both of the lipase and bile extract. These results suggest that long PEG chains of PEG100S and PEG100SE at the LNP interface cannot fully prevent the LNP hydrolysis initiated by the adsorption of bile acids and lipases but can be hydrated enough to delay the bile acid adsorption even at 37 °C. This tendency was continued after the treatment of the digestion juice containing colipase and was in accordance

with the previously reported literatures (9, 10).

The amount of free fatty acids generated from TS molecules in the LNPs was recorded as shown in Figure IV-A9. For LNP samples emulsified by PEG10SE (Figure IV-A9a), the hydrolysis rate was increased with growing the concentration of PEG10SE. However, in LNPs stabilized by PEG100SE (Figure IV-A9b), the increase of the LNP hydrolyzing rate was not observed but the extent of the free fatty acid releasing became smaller with the increase of emulsifier concentration, which could be attributed to the action of a long PEG chain in PEG100SE for delaying the emulsifier displacement by bile acids. Therefore, these results imply that the hydrolysis rate and extent of the LNPs can be controlled by the molecular weight/concentration of PEGylated emulsifiers.

As mentioned previously, bile acid has a peculiar planar amphiphilic structure, which brings higher affinity with the TS surface of LNPs as compared with nonionic emulsifiers. Despite the high affinity, bile acids also require the minimum hydrophobic area to adsorb on LNP surface. Cholic acid as one of the bile acids has the bottom dimensions (hydrophobic face) of 2.6 nm^2 and the height of 0.8 nm (31). According to the dimensions of cholic acid and the ZP results in Figure IV-A8, the absorption of bile acids was effectively hindered by only PEG100S and PEG100SE among the PEGylated emulsifiers, because all values in Figure IV-A4b were much smaller than the 2.6 nm^2. Colipase as a cofactor of pancreatic lipase (~50000 kDa) is an amphiphilic wedge-shaped protein with a three-finger having hydrophobic tip (17,

32), which becomes a complex with the lipase and anchors the lipase onto the triacylglyceride surface (33). As following previous studies, colipase binds to the noncatalytic C-terminal domain of the lipase, and the hydrophobic tips adhere a lipid–water interface and help to bring the catalytic N-terminal domain of the lipase into close contact with the interface (32, 34). In addition, colipase requires about 1.45–5.00 nm^2 of hydrophobic area for the adsorption and colipase/lipase complex requires ~9.00 nm^2 (≤1.8 nm by ≥5.0 nm) to form a lipid–water interface binding site (33). Therefore, it is impossible that the lipase or lipase/colipase complex adsorb to the LNP surface alone and hydrolyze TS molecules of LNPs without a help of bile acids. As a result, the digestion of LNPs in small intestine environment should be governed by the adsorption of bile acids onto the interface.

As summarizing previous discussion under a consideration for sizes of TS, emulsifiers, bile acids, colipase, and the lipase, the digestion mechanism of LNPs covered PEGylated emulsifiers was presented as pictorial diagrams in Figure IV-A10. LNPs at low surface load of emulsifiers containing a short PEG chain such as PEG10S, PEG10SE, PEG10OE, PEG10LE, and PEG20SS are digested rapidly due to the free adsorption of bile acids on the TS surface. LNPs at high surface load of the short-chained emulsifiers are also digested relatively quickly because of the fast displacement of the emulsifiers by bile acids. Thus, the digestion rate of LNP samples covered by the short-chained emulsifiers could mainly depend on their PS. In contrast, LNPs stabilized by the long-chained emulsifiers such as PEG100S and PEG100SE

are hydrolyzed slowly due to the hindrance effect by long PEG chains. This effect of the large emulsifiers is in a good accordance with previously reported literatures, e.g. the effect by digalactosyldiacylglycerol (10), Poloxamer 188 (17), and Poloxamer 407 (18).

In this research, colloidal stability and digestion of TS LNPs stabilized with various PEGylated emulsifiers were examined in molecular level. Particularly, lipolysis of the LNPs by bile salts, colipase, and pancreatic lipase in small intestinal tract was minutely studied under the *in vitro* simulated condition. According to results of the study, LNPs coated with short chain PEGylated emulsifiers was digested rapider than LNPs covered with long chain PEGylated one. In addition, the former were increased with the PS reduction of LNPs, but the latter was influenced by the surface load of LNPs rather than the PS. This result suggests that short (10 or 20) PEGylated emulsifiers cannot hinder the adsorption of bile salts, colipase, and pancreatic lipase while long (100) PEGylated emulsifiers are more resistant to lipolysis resulted from the adsorption. Consequently, it was demonstrated that digestion fate of the orally administered LNPs can be controlled by rational design in terms of choosing type and concentration of emulsifiers. In conclusion, this research could serve as a basis for further studies to develop an oral lipid carrier system for functional foods or drugs.

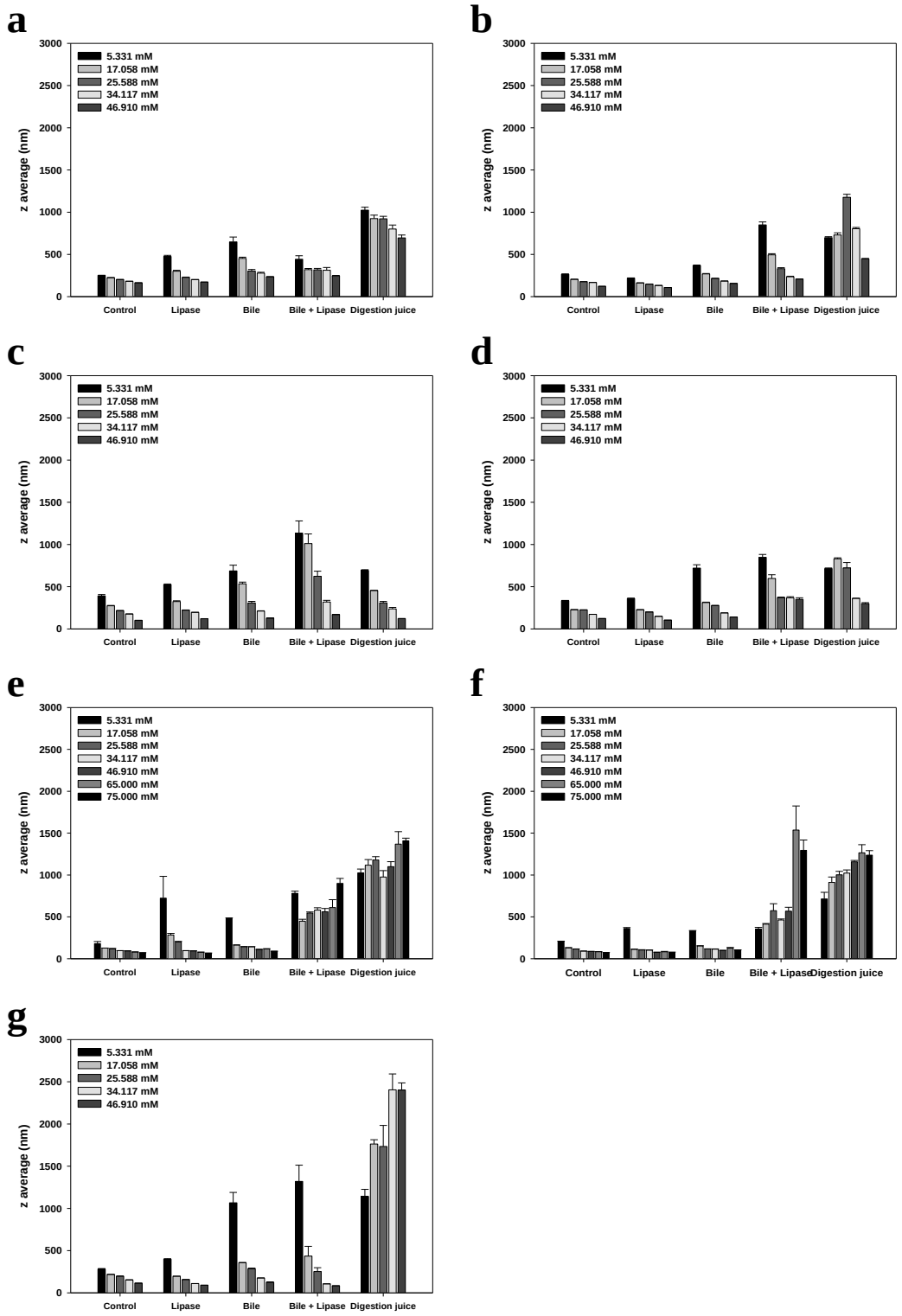
a
b
c
d
e
f
g
z average (nm)
0
500
1000
1500
2000
2500
3000
5.331 mM
17.058 mM
25.588 mM
34.117 mM
46.910 mM
65.000 mM
75.000 mM
Control
Lipase
Bile
Bile + Lipase
Digestion juice

Figure IV-A7. Particle size (z average) of tristearin nanoparticles emulsified by PEGylated emulsifiers. (a) PEG10S, (b) PEG100S, (c) PEG10SE, (d) PEG100SE, (e) PEG10OE, (f) PEG10LE, and (g) PEG20SS after the treatment (2 h) of lipase, bile extract, the mixture of lipase and bile extract, and the simulated digestion juice.

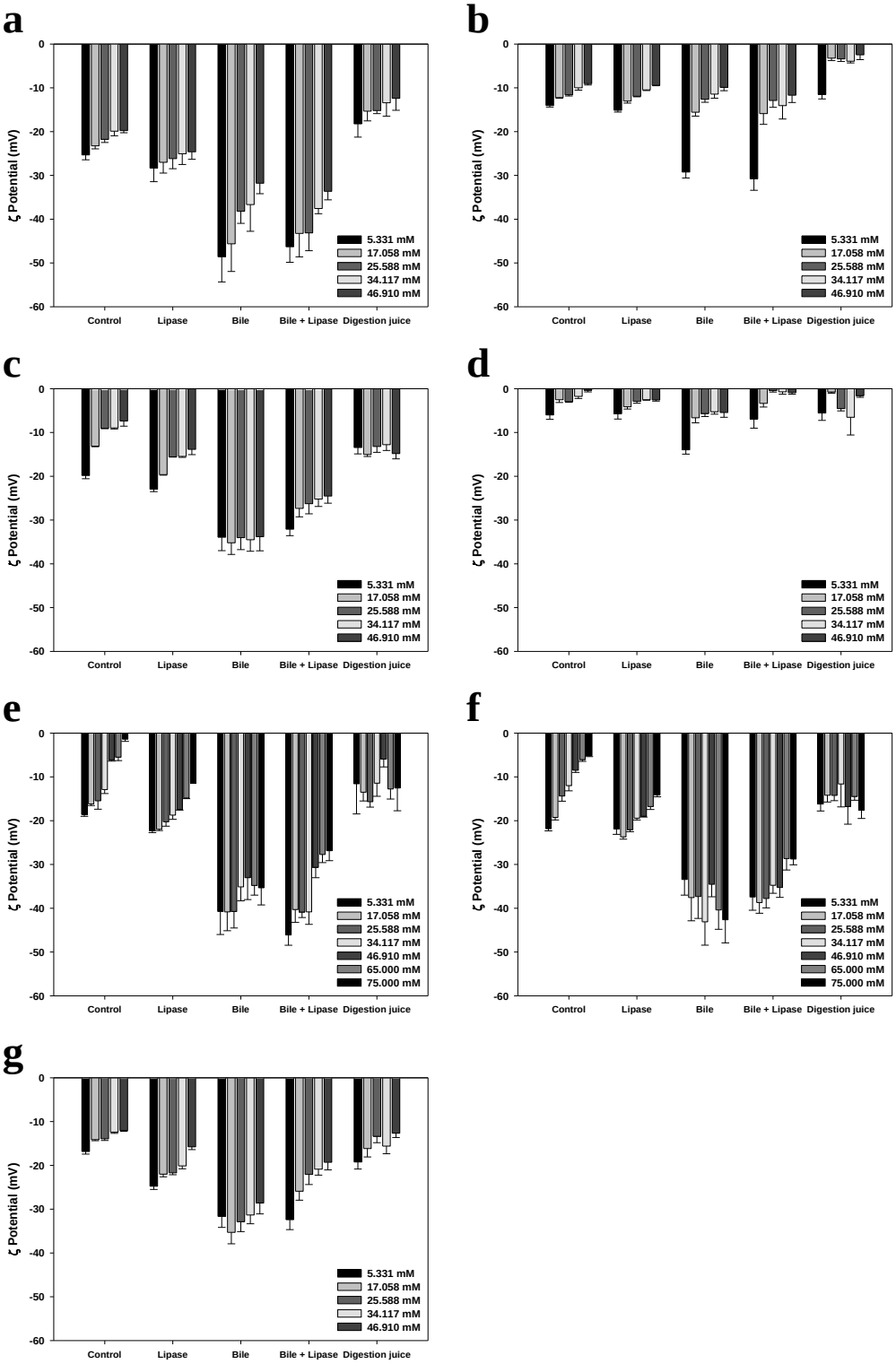
a
b
c
d
e
f
g
ζ Potential (mV)
0
-10
-20
-30
-40
-50
-60
Control
Lipase
Bile
Bile + Lipase
Digestion juice
5.331 mM
17.058 mM
25.588 mM
34.117 mM
46.910 mM
65.000 mM
75.000 mM

Figure IV-A8. ζ potential of tristearin nanoparticles emulsified by PEGylated emulsifiers. (a) PEG10S, (b) PEG100S, (c) PEG10SE, (d) PEG100SE, (e) PEG10OE, (f) PEG10LE, and (g) PEG20SS after the treatment (2 h) of lipase, bile extract, the mixture of lipase and bile extract, and the simulated digestion juice.

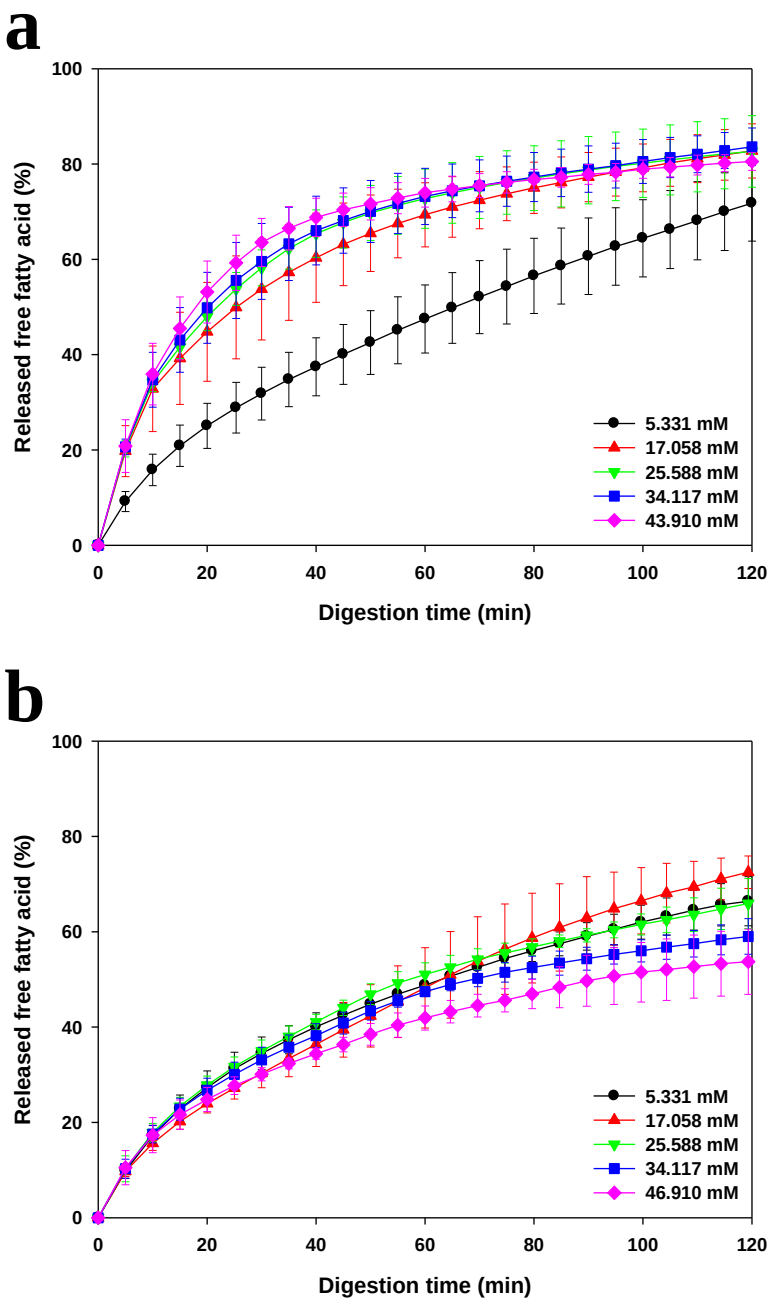

Figure IV-A9. Lipolysis profiles of tristearin nanoparticles emulsified by (a) PEG10SE and (b) PEG100SE in the simulative small intestine condition as the changes of emulsifier concentration.

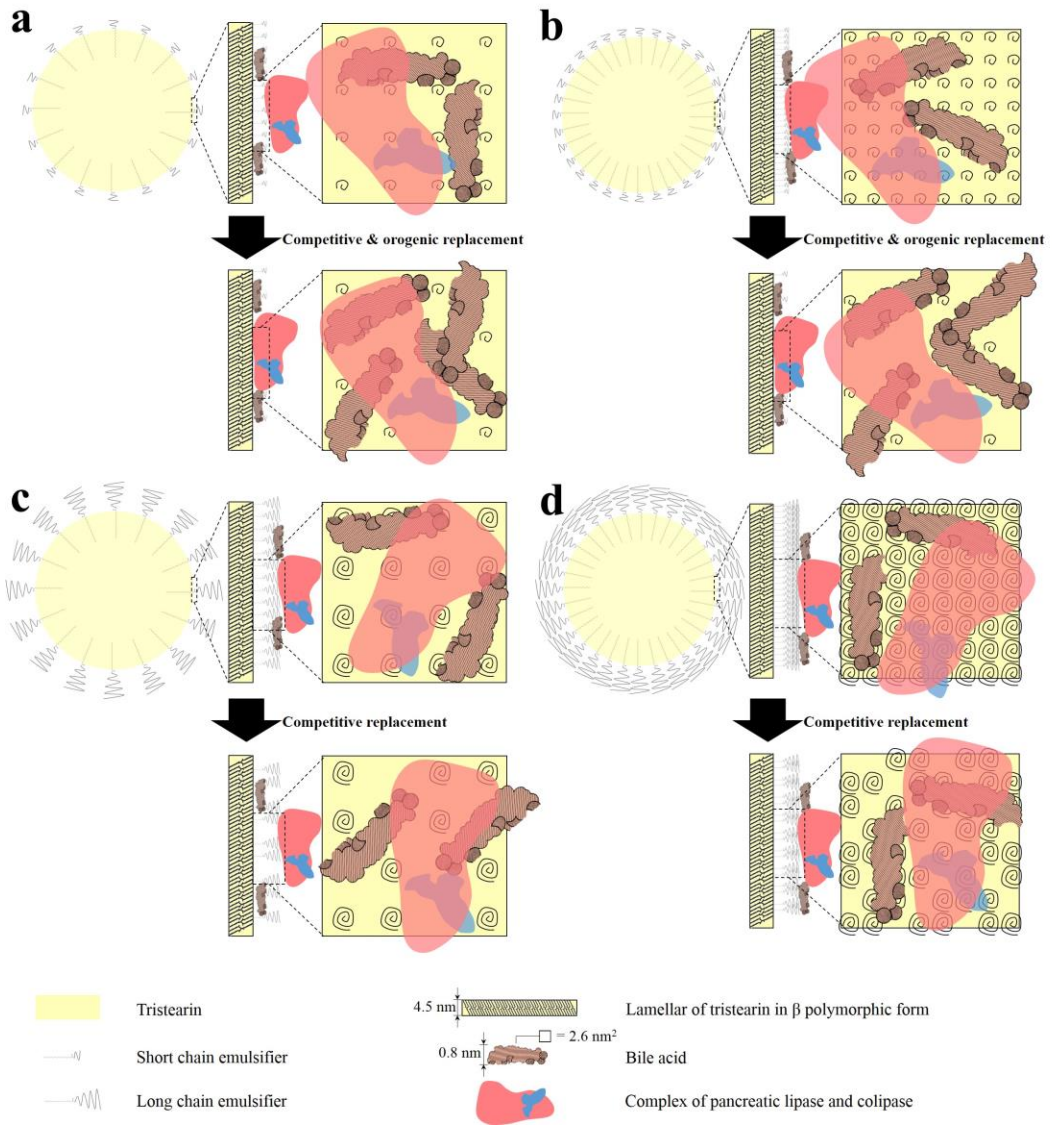

Figure IV-A10. Schematic representation for the adsorption mechanism of bile acids and pancreatic lipases on tristearin nanoparticles. (a and c) Sparsely and (b and d) densely stabilized by short- and long-PEGylated-emulsifiers in small intestinal tract, respectively.

IV-5-4. Reference

(1) Porter, C. J. H.; Pouton, C. W.; Cuine, J. F.; Charman, W. N. Enhancing intestinal drug solubilisation using lipid-based delivery systems. *Adv. Drug Deliv. Rev.* **2008,** *60*, 673-691.

(2) McClements, D. J.; Decker, E. A.; Park, Y. Controlling lipid bioavailability through physicochemical and structural approaches. *Crit. Rev. Food Sci. Nutr.* **2008,** *49*, 48-67.

(3) Kong, F.; Singh, R. P. Disintegration of solid foods in human stomach. *J. Food Sci.* **2008,** *73*, R67-R80.

(4) McClements, D. J.; Xiao, H. Potential biological fate of ingested nanoemulsions: influence of particle characteristics. *Food Funct.* **2012,** *3*, 202-220.

(5) Maldonado-Valderrama, J.; Wilde, P.; Macierzanka, A.; Mackie, A. The role of bile salts in digestion. *Adv. Colloid Interface Sci.* **2011,** *165*, 36-46.

(6) Maldonado-Valderrama, J.; Gunning, A. P.; Ridout, M. J.; Wilde, P. J.; Morris, V. J. The effect of physiological conditions on the surface structure of proteins: setting the scene for human digestion of emulsions. *Eur. Phys. J. E* **2009,** *30*, 165-174.

(7) Maldonado-Valderrama, J.; Gunning, A. P.; Wilde, P. J.; Morris, V. J. *In vitro* gastric digestion of interfacial protein structures: visualisation by AFM. *Soft Matter* **2010,** *6*, 4908-4915.

(8) Maldonado-Valderrama, J.; Woodward, N. C.; Gunning, A. P.; Ridout, M. J.; Husband, F. A.; Mackie, A. R.; Morris, V. J.; Wilde, P. J. Interfacial characterization of β-lactoglobulin networks: displacement by bile salts. *Langmuir* **2008,** *24*, 6759-6767.

(9) Chu, B.; Rich, G. T.; Ridout, M. J.; Faulks, R. M.; Wickham, M. S. J.; Wilde, P. J. Modulating pancreatic lipase activity with galactolipids: effects of emulsion interfacial composition. *Langmuir* **2009,** *25*, 9352-9360.

(10) Chu, B.; Gunning, A. P.; Rich, G. T.; Ridout, M. J.; Faulks, R. M.; Wickham, M. S. J.; Morris, V. J.; Wilde, P. J. Adsorption of bile salts and pancreatic colipase and lipase onto digalactosyldiacylglycerol and dipalmitoyl-phosphatidylcholine monolayers. *Langmuir* **2010,** *26*, 9782-9793.

(11) Torcello-Gómez, A.; Maldonado-Valderrama, J.; Martín-Rodríguez, A.; McClements, D. J. Physicochemical properties and digestibility of emulsified lipids in simulated intestinal fluids: influence of interfacial characteristics. *Soft Matter* **2011,** *7*, 6167-6177.

(12) Müller, R. H.; Mäder, K.; Gohla, S. Solid lipid nanoparticles (SLN) for controlled drug delivery–a review of the state of the art. *Eur. J. Pharm. Biopharm.* **2000,** *50*, 161-177.

(13) Nagaoka, S.; Nakao, A. Clinical application of antithrombogenic hydrogel with long poly (ethylene oxide) chains. *Biomaterials* **1990,** *11*, 119-121.

(14) Jeong, J. H.; Park, T. G.; Kim, S. H. Self-assembled and nanostructured siRNA delivery systems. *Pharm. Res.* **2011,** *28*, 2072-2085.

(15) Gref, R.; Lück, M.; Quellec, P.; Marchand, M.; Dellacherie, E.; Harnisch, S.; Blunk, T.; Müller, R. H. 'Stealth'corona-core nanoparticles surface modified by polyethylene glycol (PEG): influences of the corona (PEG chain length and surface density) and of the core composition on phagocytic uptake and plasma protein adsorption. *Colloid Surf. B-Biointerfaces* **2000,** *18*, 301-313.

(16) Niidome, T.; Yamagata, M.; Okamoto, Y.; Akiyama, Y.; Takahashi, H.; Kawano, T.; Katayama, Y.; Niidome, Y. PEG-modified gold nanorods with a stealth character for *in vivo* applications. *J. Control. Release* **2006,** *114*, 343-347.

(17) Müller, R. H.; Rühl, D.; Runge, S. A. Biodegradation of solid lipid nanoparticles as a function of lipase incubation time. *Int. J. Pharm.* **1996,** *144*, 115-121.

(18) Olbrich, C.; Müller, R. H. Enzymatic degradation of SLN—effect of surfactant and surfactant mixtures. *Int. J. Pharm.* **1999,** *180*, 31-39.

(19) Vanapalli, S. A.; Coupland, J. N. Emulsions under shear—the formation and properties of partially coalesced lipid structures. *Food Hydrocolloids* **2001,** *15*, 507-512.

(20) Helgason, T.; Awad, T. S.; Kristbergsson, K.; McClements, D. J.; Weiss, J. Effect of surfactant surface coverage on formation of solid lipid nanoparticles (SLN). *J. Colloid Interface Sci.* **2009,** *334*, 75-81.

(21) Aveyard, R.; Binks, B. P.; Clint, J. H. Emulsions stabilised solely by colloidal particles. *Adv. Colloid Interface Sci.* **2003,** *100*, 503-546.

(22) Rocha, S. A.; Guirardello, R. An approach to calculate solid–liquid phase equilibrium for binary mixtures. *Fluid Phase Equilib.* **2009,** *281*, 12-21.

(23) Mayama, H. Blooming theory of tristearin. *Soft Matter* **2009,** *5*, 856-859.

(24) Hughes, Z. E.; Walsh, T. R. Tristearin bilayers: structure of the aqueous interface and stability in the presence of surfactants. *RSC Adv.* **2015,** *5*, 49933-49943.

(25) Whitcomb, D. C.; Lowe, M. E. Human pancreatic digestive enzymes. *Dig. Dis. Sci.* **2007,** *52*, 1-17.

(26) Larsen, A. T.; Sassene, P.; Müllertz, A. *In vitro* lipolysis models as a tool for the characterization of oral lipid and surfactant based drug delivery systems. *Int. J. Pharm.* **2011,** *417*, 245-255.

(27) Lowe, M. E. The triglyceride lipases of the pancreas. *J. Lipid Res.* **2002,** *43*, 2007-2016.

(28) O'Connor, C. J.; Ch'ng, B. T.; Wallace, R. G. Studies in bile salt solutions: 1. Surface tension evidence for a stepwise aggregation model. *J. Colloid Interface Sci.* **1983,** *95*, 410-419.

(29) Mannock, D. A.; Harper, P. E.; Gruner, S. M.; McElhaney, R. N. The physical properties of glycosyl diacylglycerols. Calorimetric, X-ray diffraction and Fourier transform spectroscopic studies of a homologous series of 1, 2-di-O-

acyl-3-O-(β-d-galactopyranosyl)-sn-glycerols. *Chem. Phys. Lipids* **2001,** *111*, 139-161.

(30) Mehnert, W.; Mäder, K. Solid lipid nanoparticles: production, characterization and applications. *Adv. Drug Deliv. Rev.* **2001,** *47*, 165-196.

(31) Despa, F.; Luo, J. T.; Li, J.; Duan, Y.; Lam, K. S. Cholic acid micelles—controlling the size of the aqueous cavity by PEGylation. *Phys. Chem. Chem. Phys.* **2010,** *12*, 1589-1594.

(32) Egloff, M.; Marguet, F.; Buono, G.; Verger, R.; Cambillau, C.; van Tilbeurgh, H. The 2.46 Å Resolution structure of the pancreatic lipase-colipase complex inhibited by a C11 alkyl phosphonate. *Biochemistry* **1995,** *34*, 2751-2762.

(33) Sugar, I. P.; Mizuno, N. K.; Momsen, M. M.; Brockman, H. L. Lipid lateral organization in fluid interfaces controls the rate of colipase association. *Biophys. J.* **2001,** *81*, 3387-3397.

(34) van Tilbeurgh, H.; Egloff, M.; Martinez, C.; Rugani, N.; Verger, R.; Cambillau, C. Interfacial activation of the lipase–procolipase complex by mixed micelles revealed by X-ray crystallography. *Nature* **1993**, *362*, 814-820.

국문 초록

캡슐화된 생리활성물질의 방출 조절이 가능한 지질 운송체는 생체이용률 증가와 생리활성물질의 표적운반을 원하는 많은 산업현장(식품, 화장품, 약품)에서 오랫동안 관심을 끌어왔다. 하지만, 아직까지 적절한 기능성과 경제성을 동시에 가지는 성공적인 사례를 찾아보기 힘들다. 고체 지질 나노입자와 나노구조 지질 운송체을 포함하는 지질 나노입자(LNP)는 에멀션이나 리포좀 같은 기존의 지질 운송체를 대체하는 새로운 전략으로서 에멀션으로부터 약간의 변형(고체 지질의 이용)을 가하여 발명되었다. LNP 는 생리적 지질을 사용, 외부 스트레스로부터의 보호, 경구 생체이용률의 향상, 심재료의 방출 조절, 대량생산의 가능화 같은 다양한 장점을 가지고 있다. 하지만, 식품에 적용하기 위해 식품과학자들의 많은 노력에도 불구하고 교질 또는 저장 안정성 측면에서 해결되지 않은 문제들 때문에 식품에는 아직 채택되지 못했다. 본 연구에서는, 안정성 향상을 위해 LNP 생산 공정이 최적화되었고, 플라보노이드의 생체접근률 개선을 위해 앞선 최적 공정에 기초하여 플라보노이드를 실은 LNP 가 개발되었으며, 그리고 지질-물 계면의 특성 조절에 기초하여 LNP 에 담긴 커큐민의 혈액 내 흡수패턴이 조절되었다. 세부적으로, 녹은 지질 방울의 크기 감소 공정 이후의 냉각공정 동안 6 분 차후초음파처리는 자체 조립된/단독의 유화제를 LNP 표면위로 확산시킬 수

있었고, 고체 지질상 내로의 30 무게%(wt %) 액체 지질 첨가는 고체 지질체의 결정도 감소를 야기하여 LNP 교질 안정성을 개선하였다. 게다가, 모방 체외 위장관 환경 하에서, 극도경화카놀라유 3.5 wt %, 스쿠알렌 1.5 wt %, 대두 레시틴 1.083 wt %, Tween 20 0.583 wt %를 이용해 제조된 LNP 내로 캡슐화된 쿼세틴, 나린제닌, 헤스페레틴의 생체접근률 수치는 원 형태 플라보노이드의 수치보다 각각 11.71, 5.03, 4.76 배 증가되었다. 마지막으로, 페길레이션된 (PEGylated) 다양한 유화제로 뒤덮힌 LNP 의 체외 위장관 가수분해는 폴리에틸렌글리콜(PEG) 길이, 유화제 농도, 지질 유형 측면에서의 LNP 설계에 의해 조절되었기 때문에, PEGylated LNP 내에 캡슐화된 커큐민의 혈장 체류는 경구 투여를 위한 체내 쥐 모델 하에서 앞선 LNP 설계들을 통해 성공적으로 연장되거나 단축될 것이다. 요컨대, 이 결과들은 본 연구에서 개발된 LNP 가 식품 수준 지질 운반체로서 생산자와 소비자의 기대를 충분히 만족시킬 수 있다는 것을 시사한다. 결론적으로, 본 연구는 식품과 약품용 운반체 개발을 지향하는 진보된 연구에 기초 역할을 할 수 있을 것이다.

핵심어: 지질 나노입자(LNP), 생리활성물질, 교질 안정성, 생체이용률, 방출 조절

학 번: 2011-23529